**UNIVERSIDADE FEDERAL DE MINAS GERAIS**
Escola de Engenharia
Programa de Pós-Graduação em Saneamento, Meio Ambiente e Recursos Hídricos

Clara Demattos Nogueira

# QUANTIFICATION AND PROPAGATION OF RATING CURVE UNCERTAINTIES IN HYDROLOGICAL AND HYDRODYNAMIC MODELING

Belo Horizonte
2026

Clara Demattos Nogueira

# QUANTIFICATION AND PROPAGATION OF RATING CURVE UNCERTAINTIES IN HYDROLOGICAL AND HYDRODYNAMIC MODELING

Dissertação apresentada ao Programa de Pós-graduação em Saneamento, Meio Ambiente e Recursos Hídricos da Universidade Federal de Minas Gerais, como requisito parcial à obtenção do título de Mestre em Saneamento, Meio Ambiente e Recursos Hídricos.

Área de concentração: Recursos Hídricos

Linha de pesquisa: Modelagem de Processos Hidrológicos

Orientador: Veber Afonso Figueiredo Costa

Coorientador: Francisco Eustáquio Oliveira e Silva

Belo Horizonte
2026

Nogueira, Clara Demattos.
N778q Quantification and Propagation of Rating Curve Uncertainties in Hydrological and Hydrodynamic Modeling [recurso eletrônico] / Clara Demattos Nogueira. - 2026.
1 recurso online (148 f.: il., color.): pdf.

Orientador: Veber Afonso Figueiredo Costa.
Coorientador: Francisco Eustáquio Oliveira e Silva.

Dissertação (mestrado) Universidade Federal de Minas Gerais, Escola de Engenharia.

Inclui Bibliografia.
Exigências do sistema: Adobe Acrobat Reader.

1. Engenharia Sanitária – Teses. 2. - Teoria bayesiana de decisão estatística-Teses. 3. Incerteza – Teses. 4.Hidrodinâmica – Teses. I. Costa, Veber Afonso Figueiredo. II. Silva, Francisco Eustáquio Oliveira e. III. Universidade Federal de Minas Gerais. Escola de Engenharia. IV. Título.

CDU: 628(043)

Ficha catalográfica elaborada pela Bibliotecária Letícia Alves Vieira CRB/6 2337
Biblioteca Prof. Mário Werneck, Escola de Engenharia da UFMG

UNIVERSIDADE FEDERAL DE MINAS GERAIS
Escola de Engenharia
Programa de Pós-Graduação em Saneamento, Meio Ambiente e Recursos Hídricos

# FOLHA DE APROVAÇÃO

## Quantification and Propagation of Rating Curve Uncertainties in Hydrological and Hydrodynamic Modeling

## CLARA DEMATTOS NOGUEIRA

Dissertação defendida e aprovada pela banca examinadora constituída pelos Senhores:

Prof. Veber Afonso Figueiredo Costa
Prof. Francisco Eustáquio Oliveira e Silva
Prof. Wilson dos Santos Fernandes
Profa Viviane Borda Pinheiro Rocha
Prof. Dirceu Silveira Reis Júnior

Coordenação do PPG-SMARH

Veber Afonso Figueiredo Costa
Orientador

Belo Horizonte, 27 de fevereiro de 2026.

Documento assinado eletronicamente por **Veber Afonso Figueiredo Costa**, **Professor do Magistério Superior**, em 27/02/2026, às 12:28, conforme horário oficial de Brasília, com fundamento no art. 5º do Decreto nº 10.543, de 13 de novembro de 2020.

Documento assinado eletronicamente por **Francisco Eustaquio Oliveira e Silva**, **Professor do Magistério Superior**, em 02/03/2026, às 14:45, conforme horário oficial de Brasília, com fundamento no art. 5º do Decreto nº 10.543, de 13 de novembro de 2020.

Documento assinado eletronicamente por **Dirceu Silveira Reis Junior**, **Usuário Externo**, em 11/03/2026, às 12:11, conforme horário oficial de Brasília, com fundamento no art. 5º do Decreto nº 10.543, de 13 de novembro de 2020.

Documento assinado eletronicamente por **Wilson dos Santos Fernandes**, **Professor do Magistério Superior**, em 15/03/2026, às 10:56, conforme horário oficial de Brasília, com fundamento no art. 5º do Decreto nº 10.543, de 13 de novembro de 2020.

Documento assinado eletronicamente por **Viviane Borda Pinheiro Rocha**, **Professora do Magistério Superior**, em 20/03/2026, às 16:28, conforme horário oficial de Brasília, com fundamento no art. 5º do Decreto nº 10.543, de 13 de novembro de 2020.

Documento assinado eletronicamente por **Eduardo Coutinho de Paula**, **Coordenador(a) de curso de pós-graduação**, em 25/03/2026, às 12:06, conforme horário oficial de Brasília, com fundamento no art. 5º do Decreto nº 10.543, de 13 de novembro de 2020.

A autenticidade deste documento pode ser conferida no site https://sei.ufmg.br/sei/controlador_externo.php?acao=documento_conferir&id_orgao_acesso_externo=0, informando o código verificador **4967526** e o código CRC **FCB9A222**.

**Referência:** Processo nº 23072.209643/2026-16 SEI nº 4967526

## AGRADECIMENTOS

O desenvolvimento desse trabalho só foi possível graças ao apoio de diversas pessoas, às quais sou imensamente grata. Assim, agradeço:

Aos meus pais, pelo amor incondicional e por sempre incentivarem a mim e aos meus irmãos na busca por uma educação de qualidade. Obrigada por nos incentivarem a sonhar e por serem um porto seguro sempre que necessário. Aos meus irmãos, por serem bons companheiros nessa vida. Agradeço por me despertarem o interesse pela ciência, pela visão sempre crítica e pelo bom humor. Sou muito feliz por fazer parte dessa família.

Ao Vitor, a quem não tenho palavras para agradecer pelo apoio e pelo carinho diários. Seu olhar gentil torna tudo mais leve, e é uma grande alegria poder partilhar a vida com você.

Ao resto da família, por todo o carinho e o incentivo.

Aos professores Veber e Chico, orientador e coorientador dessa pesquisa, pela orientação presente, paciência e disposição de sempre para ensinar; e por confiarem em mim para o desenvolvimento desse trabalho.

Ao Alan, que foi um grande companheiro nessa pesquisa e me ensinou muito.

Ao professor Palmier, por todos os conhecimentos sobre hidráulica.

À banca avaliadora, pela leitura atenciosa e sugestões pertinentes.

Aos demais professores com quem tive contato ao longo das disciplinas necessárias para minha formação.

Aos funcionários da secretaria do programa e do EHR, pelo apoio nas burocracias necessárias. Aos funcionários da Escola de Engenharia e da UFMG.

Aos amigos da salinha 4504, pelos cafés, almoços, dicas e conversas. Aos amigos e colegas do mestrado, por todas as trocas.

Aos colegas do trabalho, pelo suporte durante o período em que conciliei as duas jornadas.

Aos amigos além do mestrado, pelos momentos de descontração tão necessários, pelo apoio das mais diversas formas e por darem mais cor à minha vida. Essa empreitada foi mais agradável e divertida graças ao apoio de vocês.

À UFMG e ao CNPq pelo amparo concedido para o desenvolvimento da pesquisa. À CAPES pela concessão da bolsa de estudos.

*“Lembro-me ainda do temor de minha mãe nos dias de fortes chuvas. Em cima da cama, agarrada a nós, ela nos protegia com seu abraço. E com os olhos alagados de prantos balbuciava rezas a Santa Bárbara, temendo que o nosso frágil barraco desabasse sobre nós. E eu não sei se o lamento-pranto de minha mãe, se o barulho da chuva... Sei que tudo me causava a sensação de que a nossa casa balançava ao vento. Nesses momentos os olhos de minha mãe se confundiam com os olhos da natureza. Chovia, chorava! Chorava, chovia!”*

(Conceição Evaristo)

## RESUMO

Inundações provocam impactos sociais e econômicos significativos, incluindo a perda de vidas humanas. Sistemas de alerta, quando bem operados, apresentam potencial para mitigar esses impactos e salvar vidas. Entretanto, a tomada de decisão quanto ao acionamento desses sistemas é dificultada por diversas incertezas, incluindo aquelas associadas às cotas de inundações preditas obtidas a partir de modelagens hidrológicas e hidrodinâmicas. Modelos chuva-vazão, frequentemente utilizados para subsidiar decisões, são afetados por diversas incertezas que devem ser explicitamente consideradas. Dentre elas, destacam-se as incertezas associadas aos dados de saída, uma vez que as vazões são comumente obtidas por meio de curvas-chave, as quais apresentam incertezas frequentemente negligenciadas. Essa situação é particularmente crítica em pequenas bacias, nas quais dados de vazão muitas vezes não estão disponíveis para construção das curvas-chave. Nesse contexto, o presente trabalho utilizou estatística Bayesiana para o desenvolvimento de um modelo hidrológico do tipo chuva-nível, que permite a consideração explícita das incertezas paramétricas e estruturais da curva-chave e do modelo hidrológico. Além disso, o modelo possibilita a predição de vazões mesmo em casos em que não há descargas medidas, a partir da utilização de uma curva-chave *a priori*, construída com base em características geométricas e hidráulicas. Posteriormente, as vazões simuladas foram propagadas em um modelo hidrodinâmico com o objetivo de avaliar o impacto da consideração explícita das incertezas da curva-chave na predição das cotas de inundação. A aplicação do método foi realizada na estação fluviométrica Jardim, posicionada no córrego Juatuba, na bacia hidrográfica do rio Paraopeba; selecionada por se tratar de uma estação telemétrica com dados horários previamente consistidos e com disponibilidade de informações para o estudo. As incertezas da curva-chave foram quantificadas por meio do método BaRatin, que se baseia na análise Bayesiana e permite a incorporação do conhecimento físico na definição da relação entre nível e vazão. Foram desenvolvidas duas curvas-chave: uma utilizando os dados de vazão disponíveis e outra desconsiderando esses dados, simulando um cenário sem observação de vazões. Em seguida, foi desenvolvido o modelo chuva-nível, também sob uma abordagem Bayesiana, adotando-se o modelo hidrológico GR4H. Por fim, as vazões estimadas foram propagadas em modelo hidrodinâmico unidimensional utilizando o *software* HEC-RAS. Os resultados do modelo chuva-nível utilizando a curva-chave calibrada indicaram predominância da incerteza estrutural do modelo hidrológico, com contribuições variando de 43% a 99% e valor médio de 66%. A incerteza estrutural da curva-chave também se mostrou relevante na incerteza preditiva total, com contribuição média de 30% e valor máximo de 54%. Para o modelo que utilizou a curva-chave *a priori*, observou-se aumento da incerteza estrutural da curva-chave, com valor médio de 37%, além de significativa piora nas métricas de desempenho. A propagação dos resultados do modelo chuva-nível com curva-chave estimada no modelo hidrodinâmico evidenciou o impacto da consideração explícita da incerteza da curva-chave ao longo de todas as seções. Os resultados reforçam a necessidade da observação de dados de vazão para construção de curvas-chave, da consideração explícita da incerteza da curva-chave e do aprimoramento do entendimento de processos hidrológicos visando à redução da incerteza estrutural.



Palavras-chave: Inferência Bayesiana, modelagem chuva-nível, análise de incerteza, modelagem hidrodinâmica 1D.

## ABSTRACT

Floods cause significant social and economic impacts, including loss of human life. Flood alert systems, when properly operated, have the potential to mitigate these impacts and save lives. However, decision-making regarding alert system activation is often challenging due to multiple uncertainties, including those related to predicted flood levels obtained through hydrological and hydrodynamic modeling. Rainfall-runoff models, frequently used to support decision-making, are affected by multiple sources of uncertainties that should be explicitly considered. Among these, uncertainties associated with output data are particularly relevant, since discharge is commonly obtained from rating curves, which are themselves subject to substantial uncertainty that is often neglected. This issue is especially critical in small catchments, in which discharge measurements are frequently unavailable for rating curve constructions. In this context, this study develops a rainfall-stage hydrological model based on Bayesian statistics, allowing explicit representation of parametric and structural uncertainties associated with both the rating curve and the hydrological model. By incorporating a prior rating curve constructed from hydraulic and geometric characteristics, the proposed model enables discharge estimation even in cases where no discharge measurement data are available. The simulated discharges are subsequently routed through a hydrodynamic model to assess the impact of the explicit consideration of rating curve uncertainty on water level predictions. The method was applied to Jardim streamflow gauging station, inserted on the Juatuba stream, on the Paraopeba river basin; selected due to its telemetric nature and the availability of previously quality-controlled hourly data. Rating curve uncertainty was quantified using the BaRatin method, which relies on Bayesian inference and enables the incorporation of physical knowledge in defining the stage-discharge relationship. Two rating curves were constructed, one using available discharge data and another neglecting these data, simulating a scenario without discharge observations. Subsequently, a rainfall-stage model was implemented within a Bayesian framework using the GR4H hydrological model. Finally, discharge outputs were routed through a one-dimensional hydrodynamic model using the HEC-RAS software. Results from the rainfall-stage model using the estimated rating curve indicated that structural uncertainty associated with the hydrological model was dominant, with contributions ranging from 43% to 99%, and an average contribution of 66%. Structural uncertainty related to the rating curve was also significant, with an average contribution of 30% and maximum values reaching 54%. For the model utilizing the prior rating curve, the mean structural uncertainty associated with the rating curve increased to 37%, and performance metrics were substantially deteriorated. The propagation of results through the hydrodynamic model highlighted the importance of accounting for rating curve uncertainty across all sections. Overall, the results emphasize the need for discharge measurement for rating curve construction, explicit consideration of rating curve uncertainty, and improved understanding of hydrological processes to reduce structural uncertainty.



Keywords: Bayesian inference, rainfall-stage model, uncertainty analysis, 1D hydrodynamic modeling.

## LIST OF FIGURES

## LIST OF TABLES

## LIST OF ACRONYMS AND ABBREVIATIONS

ABNT - Associação Brasileira de Normas Técnicas

AR – Autoregressive

ARMA - Autoregressive Moving Average

BATEA - Bayesian Total Error Analysis

BFMI - Bayes Fraction of Missing Information

CNPq - Conselho Nacional de Desenvolvimento Científico e Tecnológico

COPASA - Companhia de Saneamento de Minas Gerais

CPRM - Companhia de Pesquisa em Recursos Mineirais

ESS - Effective sample size

GLUE - Generalized Likelihood Uncertainty Estimation

GR4H – Génie Rural à 4 paramètres Horaires

HEC-RAS - Hydrologic Engineering Center - River Analysis System

HMC - Hamiltonian Monte Carlo

KGE - Kling-Gupta Efficiency

lp – logposterior distribution

MCMC - Markov Chain Monte Carlo

NSE - Nash-Sutcliffe Efficiency

NUTS - No-U-Turn Sampler

PACF - Partial autocorrelation function

sd – Standard deviation

SGB - Serviço Geológico Brasileiro

UH – Unit hydrograph

## LIST OF SYMBOLS

| | |
|---|---|
| 1D, 2D, 3D | number of dimensions in which the characteristic variables of flows are considered in a hydraulic/hydrodynamic model |
| $A$ | cross-sectional flow area |
| $a, b, c$ | rating curve parameters |
| $B$ | cross-section top width |
| $B_t$ | hydrological model error term |
| $D$ | diagonal matrix |
| $E$ | evaporation |
| $E_n$ | net evaporation |
| $E_s$ | evaporation rate |
| $e_M$ | discharge measurement error |
| $F$ | groundwater exchange term in the GRH4 model |
| $I$ | input from a hydrological model |
| $i, k, j$ | indices |
| $h$ | water stage at a cross-section |
| $J$ | friction slope |
| $k_{1,2}$ | average bed level and floodplain elevation parameters from the rating curve model |
| $n$ | Manning roughness coefficient |

| | |
|---|---|
| $n_c$ | Manning roughness coefficient for the channel |
| $n_p$ | Manning roughness coefficient for the floodplain |
| $P$ | precipitation |
| $P_n$ | net precipitation |
| $P_s$ | fractions of $P_n$ directed to the production store in the GR4H model |
| $P_r$ | fractions of $P_n$ routed through $UH_1$ and $UH_2$ in the GR4H model |
| $Perc$ | percolation leakage from production store in the GR4H model |
| $Q$ | discharge output from a hydrological model |
| $q$ | modeled discharges |
| $R$ | routing store reservoir in the GR4H model |
| $R_h$ | hydraulic radius |
| $\hat{R}$ | convergence diagnostic based on between and within chain variance |
| $S$ | riverbed slope |
| $St$ | production store reservoir in the GR4H |
| $SH_1, SH_2$ | S-curves associated with unit hydrographs $UH_1$ and $UH_1$ in the GR4H |
| $t$ | time |
| $UH$ | unit hydrograph |
| $v$ | flow velocity |
| $x$ | longitudinal spatial coordinate |

| | |
|---|---|
| $x_1, x_2, x_3, x_4$ | GRH4 hydrological model parameters |
| $y$ | flow depth |
| $\beta_0, \beta_1$ | heteroscedasticity error model parameters (intercept and slope) |
| $\Delta$ | finite difference operator |
| $\delta$ | standard deviation of discharge measurement error |
| $\Theta$ | parameter space |
| $\theta$ | vector of model parameters |
| $\mu$ | vector mean |
| $\sigma, \phi$ | hydrological error model parameters: asymptotic standard deviation and characteristic correlation time, respectively |
| $\Sigma$ | covariance matrix |
| $\psi$ | transformation function |
| $\Omega$ | model transfer function |

## TABLE OF CONTENTS

# 1 INTRODUCTION

The use of hydrological models is fundamental for water resources management (Singh, 1995), including flood forecast (Masseroni et al., 2017). However, these models are affected by multiple sources of uncertainties that must be properly considered (Farzana, 2023; Herrera; Marazuela; Hofmann, 2022; Liu; Gupta, 2007; Moges et al., 2020). These uncertainties are commonly related to input data, parameter estimation, model structure, and output data (Kavetski; Kuczera; Franks, 2006), and their quantification is particularly important in small catchments (Dogulu et al., 2015; Hapuarachchi; Wang; Pagano, 2011), where hydrological responses are rapid and the time available for decision making is limited.

Bayesian inference is a widely used framework for uncertainty analysis, as it allows different sources of uncertainty to be explicitly and separately accounted for, while also enabling the incorporation of prior knowledge, which may be derived from previous information or expert judgment (Sikorska et al., 2013). Moreover, within Bayesian framework, model parameters are treated as random variables described by probability distributions, making the explicit consideration of parametric uncertainty straightforward (Moges et al., 2020).

Many studies addressing uncertainty in hydrological modeling have focused primarily on input data, considering it the dominant source of uncertainty (Huard; Mailhot, 2006; McMillan et al., 2011; Vrugt et al., 2008). In contrast, relatively less attention has been given to uncertainty in output data. McMahon; Peel; and Amirthanathan (2025) analyzed 38 hydrology-related papers published in 2022 that used daily streamflow data and found that only two studies explicitly accounted for uncertainty related to rating curve errors, whereas 13 studies considered uncertainty arising from other sources.

Hydrological model parameter calibration is generally performed using discharge as the output variable. Nevertheless, discharge is typically obtained indirectly through rating curves, which are themselves subject to multiple sources of uncertainties. These include uncertainties in the flow data used for calibration (Westerberg et al., 2022), changes in channel cross-section due to erosion or deposition, vegetation growth, backwater effects, and hysteresis phenomena (McMillan; Westerberg, 2015). Such

uncertainties can significantly affect modelling results and related conclusions (Westerberg et al., 2016, 2022), including water management decisions. The effects tend to be amplified at high flows, for which direct gauging is often unavailable due to operational difficulties and safety risks. This limitation is particularly critical in urban areas and small catchments, where rating curves are frequently unavailable or not regularly updated.

In this context, the present work applied a rainfall-stage model based on the framework proposed by Sikorska and Renard (2017), in which model parameters are calibrated in stage space, considering that stages are much less affected by uncertainties than discharges derived from rating curves. The model employs Bayesian inference to explicitly represent parametric and structural uncertainties associated with both the rating curve and the hydrological model, enabling the assessment of the impact of rating curve uncertainty on stage and discharge predictions.

In this case study, the GR4H hydrological model was adopted due to its simplicity and suitability for hourly simulations, which are compatible with the spatial scales of basins prone to flash floods. Given the scarcity of discharge data in urban environments and small catchments, this work advances by developing a case study based on a rating curve constructed using prior hydraulic and geometric information, without relying on measured discharge data, following the approach proposed by Le Coz et al. (2014).

Two case studies were therefore conducted: one that incorporates available discharge data for rating curve estimation and the other that disregards measurements, aiming to evaluate the potential reduction in uncertainty provided by the inclusion of such data. Subsequently, the so-called true discharge (which is an unknown variable), defined as the hydrological model output combined with an error term, and the discharge estimated from the rating curve were propagated through a hydrodynamic model. This procedure aimed to assess the impact of uncertainty propagation in a nonlinear model and to evaluate the impacts of explicitly accounting for rating curve uncertainty, representing an additional contribution of this study.

This work is associated with the project entitled "*Avanços em ferramentas de nowcasting aplicadas a inundações urbanas*", funded by the Conselho Nacional de Desenvolvimento Científico e Tecnológico (CNPq). This project aims to improve the

understanding of precipitation events and flash floods and to assess their effective integration into decision-making processes related to flood alert systems, with the objective of reducing the impacts of urban flooding.

Floods cause significant social and economic impacts, including loss of human life. Flood alert systems, when properly operated, are crucial for mitigating these impacts and saving lives (Mattos et al., 2022). However, decision-making regarding alert system activation is often challenging. Duarte and Costa (2024) developed a metamodel for sensitivity and uncertainty analysis in loss of life modeling for a dam failure case study and demonstrated that efficient warning and evacuation systems can significantly reduce fatalities. Their results also indicated that alert issuance and hazard identification had the dominant influence on loss of life estimates, highlighting the substantial uncertainty associated with alert system operation.

Decision-making regarding alert system activation is strongly influenced by uncertainties in hydrological and hydrodynamic predictions. Beven (2016a) presented two primary motivations for incorporating uncertainty estimation into hydrological studies. The first is scientific, as the explicit representation of uncertainty enhances process understanding. The second is practical, since accounting for uncertainty in model predictions can significantly influence decision-making in real-world applications. Carr et al. (2021) further argue that probabilistic forecasts provide a substantial amount of additional information that is highly valuable for decision-making, although they may also pose challenges for communication.

This work aimed to improve the understanding of hydrological and hydrodynamic processes by applying a probabilistic framework. The explicit treatment of uncertainty and the analysis of the effects of incorporating discharge data for rating curve calibration provide insights into how model prediction can be improved. This, in turn, may enhance the reliability and accuracy of information used for water resources management and flood alert system activation. The proposed methodology is broadly applicable, with particular relevance to urban and small basins, which frequently lack reliable rating curves and are especially vulnerable to flooding. It is important to note, however, that this work focused on improving the information provided for decision-

making; the use of this information and the optimization of alert system operation itself are beyond the scope of this study and may be the object of future research.

This master's dissertation is organized into seven chapters. Chapter 1 consists of this introduction. Chapter 2 outlines the study objectives, while Chapter 3 provides the literature review. The methodology is described in Chapter 4, and the results and discussion are presented in Chapter 5. Chapter 6 contains the conclusions, and Chapter 7 presents recommendations. Finally, the list of references is provided.

# 2 OBJECTIVES

## 2.1 General objective

Develop a Bayesian-based method to explicitly quantify the uncertainty related to rating curves, rainfall-stage modeling, and flood routing in small catchments.

## 2.2 Specific objectives

The specific objectives of this research are:

- Evaluate the impacts of the explicit consideration of rating curve uncertainty on the prediction capacity of the hydrological model;
- Evaluate the impact of uncertainty decomposition on discharge propagation through a hydrodynamic model; and
- Evaluate the applicability of the developed method in situations where observed discharges are unavailable, by employing a prior rating curve constructed based on hydraulic and geometric knowledge only.

# 3 LITERATURE REVIEW

This chapter is subdivided into two main topics, namely: hydrological and hydrodynamic modelling. The hydrological modeling section includes an introductory overview of definitions and main modelling steps, rainfall-runoff models, uncertainty analysis in hydrological modelling, including Bayesian analysis, and rating curve models. It is important to note that the objective of this chapter is to provide an overview of the main topics that support the development of this research and the discussions of results, rather than an in-depth treatment of each subject.

## 3.1 Hydrological modeling

Hydrological models are mainly used to support water resources management (Singh, 1995), including applications such as flood forecasting (Masseroni et al., 2017). These models represent a simplified approach of the hydrological cycle, and their structure is commonly defined by mathematical equations that relate input variables to outputs through a transformation process (Chow; Maidment; Mays, 1988), as expressed in the Equation (1).

$$Q(t) = \Omega\, I(t) \tag{1}$$

in which $Q(t)$ and $I(t)$ represent, respectively, the output and the input variables, expressed as functions of time, and $\Omega$ denotes the transfer function between input and output.

There are many kinds of hydrological models, depending on the objectives of the study and on the available data. Among them, rainfall-runoff models are widely used, as they transform the rainfall input into the streamflow output.

Chow, Maidment and Mays (1988) classified hydrological models according to the simplifications adopted. Models may differ in their representation of:

- randomness: deterministic or stochastic;
- spatial variation: lumped or distributed for deterministic models; or space-independent or space-correlated for stochastic model; and
- time variation: steady or unsteady flow for deterministic models; or time-independent or time-correlated for stochastic models.

Hydrological models may also be classified as either physical models, which aim to reproduce the system at a reduced scale; or abstract models, which represent hydrological processes through simplified mathematical formulations (Chow; Maidment; Mays, 1988). Abstract models may rely on physical parameters, which correspond to directly measurable properties; or on process parameters, which describe catchment characteristics that cannot be directly observed. In the latter case, calibration is required to estimate parameter values that adequately represent the hydrological behavior of the study area (Singh, 1995).

The calibration process is subject to several challenges, such as equifinality and parameter non-identifiability. Equifinality occurs when different parameter sets result in similar model performance (Beven and Freer, 2001). Identifiability refers to the ability to determine a unique parameter set that optimizes a given likelihood function (Sorooshian; Gupta, 1985). Higher parameter identifiability is generally associated with narrower confidence intervals and, consequently, lower uncertainty (Wriedt; Rode, 2006).

Parameter calibration is inherently uncertain, as it depends on the utilized data (Saadi; Furusho-Percot, 2024), as well as on the chosen calibration procedure, the model structure, and the model spatial-temporal discretization. Clark et al. (2021) demonstrated that commonly used performance criteria, such as Nash-Sutcliffe Efficiency (NSE) and the Kling-Gupta Efficiency (KGE), are affected by substantial sampling uncertainty. Another major issue affecting calibration is parameter time variability, which may arise from land-use changes, climate variability, and other external drivers (Pathiraja et al., 2016).

For a long time, calibration relied primarily on the optimization of objective functions. However, Kavetski, Franks and Kuczera (2003a) emphasized the need to explicitly account for multiple sources of errors during the calibration process. In this context, Bayesian approaches have emerged as a promising framework for calibration, as they treat parameters as random variables. Consequently, calibration results are expressed as posterior probability distributions that combine prior information with information provided by the data (Silva; Naghettini; Fernandes, 2014).

Given the limitations inherent to calibration, a validation step is generally recommended. Model validation consists of evaluating model performance over a time span not used during calibration. A common practice is to divide the available data into two subsets, one used for calibration and the other reserved for model validation (Singh, 1995).

### 3.1.1 Uncertainties in hydrological modelling

Hydrology can be classified as “inexact sciences that are subject to epistemic uncertainties” (Beven, 2016b, p. 2). Consequently, hydrological modeling is inherently affected by uncertainty, which reflects the potential variability in model results (Herrera; Marazuela; Hofmann, 2022). Beven (1989) discussed the frequently misunderstood and misrepresented limitations of physically based models and emphasized the importance of explicitly assessing the uncertainties associated with hydrological models. Since then, a substantial body of research has been developed to address uncertainty in hydrological modelling.

Uncertainty in hydrological models arises from multiple sources. The translation of complex physical phenomena (the water cycle) into mathematical equations, together with parameter calibration and the limitations of measurement techniques, introduces uncertainty that must be quantified (Farzana, 2023; Herrera; Marazuela; Hofmann, 2022; Liu; Gupta, 2007; Moges et al., 2020). Quantifying uncertainty is essential in small catchment contexts (Dogulu et al., 2015; Hapuarachchi; Wang; Pagano, 2011), in which hydrological responses are rapid and decision-making time is limited.

Hydrological modeling uncertainty is commonly classified into four main sources: input uncertainty and output uncertainty (often jointly referred as data uncertainty), parametric uncertainty, and structural uncertainty (Kavetski; Kuczera; Franks, 2006).

Input uncertainty

Input data uncertainty arises from neglected spatial variation when precipitation is measured at only a few locations (Kavetski; Franks; Kuczera, 2003b), temporal variability (Kavetski; Kuczera; Franks, 2006), measurement errors, and data management issues (McMillan; Westerberg; Krueger, 2018). These sources of errors

can introduce bias in the estimated parameters, thereby affecting model output (Huard; Mailhot, 2006; Kavetski; Kuczera; Franks, 2006).

McMillan, Westerberg, and Krueger (2018) estimated that uncertainties in hydrologic data typically range between 10 and 40%. Several authors (Del Giudice et al., 2016; Kavetski; Kuczera; Franks, 2006; Renard et al., 2010) have identified input data uncertainty as one of the dominant sources of uncertainty, highlighting its strong impact on hydrological model predictions when measurement errors are large.

Numerous methods have been proposed to address input data uncertainty. For example, Huard and Mailhot (2006) employed a Bayesian uncertainty framework using the hydrological model “abc”; McMillan et al. (2011) used a multiplicative error formulation to account for rainfall uncertainty; and Vrugt et al. (2008) applied a Markov chain Monte Carlo (MCMC) approach to explicitly consider precipitation error. In contrast, output data uncertainty has received comparatively less attention.

Output uncertainty

Parameter calibration generally relies on discharge data as output variables. Direct discharge measurements typically exhibit relatively low uncertainty. FlowTracker, for example, which is a commonly used equipment, presents measurement uncertainty of approximately 5% (WSC, 2015). However, continuous discharge measurements are often unfeasible from both operational and financial perspectives, particularly in large countries such as Brazil. As a result, discharge is commonly estimated using rating curves, which are subjected to multiple sources of uncertainty and may lead to significant errors, especially when extrapolation beyond the range of observed data is required (Kavetski; Franks; Kuczera, 2003b). Uncertainty in discharge data can strongly influence hydrological model predictions (Westerberg et al., 2022). This topic is further discussed in Subchapter 3.1.1.3.

Parametric uncertainty

Parametric uncertainty arises from limitations in estimating or measuring the model parameters that are used to represent and integrate hydrological processes (Moges et al., 2020). Herrera, Marazuela, and Hofmann (2022) distinguished two main sources

of parametric uncertainties: uncertainty related to parameter distributions and uncertainty associated with parameter estimation. The former, often referred to as prior uncertainty, precedes data analysis and reflects the fact that model parameters may differ in their probability distributions and plausible ranges. The latter is associated with the calibration process, during which issues such as equifinality and non-identifiability may arise as consequences of uncertainty itself. As previously discussed, the calibration process can also be affected by the selected calibration data, the calibration period, and the chosen estimation procedure.

Renard et al. (2010) showed that incorporating additional data during calibration may reduce parameter uncertainty. In this context, parameters are considered well identified when their uncertainty is substantially reduced relative to prior uncertainty, resulting in lower predictive uncertainty (Moges et al., 2020). Nevertheless, within Bayesian inference, misspecification of either the likelihood function or the prior distributions may result in unreliable posterior parameter distributions (Renard et al., 2010).

Structural uncertainty

Hydrological models represent simplified descriptions of the complex processes governing the water cycle. Even when grounded in physical principles, simplifications are unavoidable and introduce structural uncertainty (Kavetski; Franks; Kuczera, 2003b). According to Renard et al. (2010), structural errors in conceptual rainfall-runoff models depend on several factors, including the adopted model formulation, characteristics of the catchment under study, and the spatial and temporal scales of analysis. Moreover, Massmann (2020) argues that models with higher temporal resolutions tend to require more complex structures.

Liu and Gupta (2007) suggested that structural uncertainty may exert a major impact on hydrological model results, as compared to other uncertainties sources, such as parametric and input or output data uncertainties. Despite its importance, the authors considered structural uncertainty as the most challenging to address, being still not fully understood. These findings were supported by Højberg and Refsgaard (2005), who concluded that structural uncertainty tends to dominate overall modeling uncertainty, particularly when predictions involve extrapolation beyond the conditions

used for calibration and validation. Their results indicate that structural uncertainty “cannot be fully compensated for by a parameter uncertainty study” (Højberg; Refsgaard, 2005, p. 9). Although their analysis focused on groundwater systems, the authors argued that these conclusions are likely applicable to environmental models more broadly.

Essery et al. (2013), based on an analysis of 1,701 snow models, concluded that errors in model structure can be partially compensated for during calibration, highlighting the interaction between structural and parametric uncertainty. More generally, structural uncertainty is considered to lie “at the core of hydrological model uncertainty” and to interact with all other uncertainty sources, including input data, output data, and parametric uncertainty (Moges et al., 2020, p. 10).

#### 3.1.1.1 Uncertainty analysis methods

Since hydrological models are widely used to support water resources management, uncertainties associated with their predictions may lead to significant environmental, economic, and social consequences. For this reason, it is essential not only to identify the sources and nature of uncertainties, but also to understand their impacts on hydrological model predictions (Panchanathan et al., 2024).

Moges et al. (2020) argued that uncertainty analysis can help identify model limitations and quantify uncertainties associated with predictions, ultimately contributing to improvements in hydrological modeling. Given the relevance of uncertainty in hydrological applications, numerous methods have been developed to address this issue. The authors classified uncertainty analysis methods into the following categories: “(i) Monte Carlo analysis, (ii) Bayesian statistics, (iii) multi-objective analysis, (iv) least-squares-based inverse modeling, (v) response-surface-based techniques, and (vi) multi-modeling analysis”.

After comparing multiple uncertainty analysis methods, Moges et al. (2020) concluded that no single approach is universally optimal, as each method presents specific strengths and limitations depending on the application. Similarly, Dotto et al. (2012) evaluated several uncertainty assessment techniques in the context of urban stormwater quantity and quality modeling by applying them to the same case study,

using an identical model structure and dataset. Their results indicate that the choice of an uncertainty analysis method should be guided by factors such as model complexity and number of parameters, the modeler's level of expertise, data availability, and the objectives of the study.

Kavetski, Franks and Kuczera (2003b) demonstrated that explicitly separating different sources of errors reduces ambiguity in both parametric and predictive uncertainty, thereby enabling more rigorous testing of the environmental model hypothesis. Similar conclusions were reached by Renard et al. (2010), who showed that predictive uncertainty in runoff simulations is more accurately quantified when rainfall and structural errors are explicitly represented, rather than being lumped into a single additive error term.

In a comprehensive review of methods for reducing uncertainty in hydrological forecasting, Panchanathan et al. (2024) emphasized that the different sources of uncertainties associated with hydrological models (input and output uncertainty, parameter and structural uncertainty) are interrelated and should be jointly considered. Consequently, focusing on only one type of uncertainty may be insufficient for many real-world applications.

Within this context, Bayesian methods stand out as they allow different sources of uncertainties to be described individually, which is essential for improving the predictive performance of hydrological models. Also, Bayesian statistics enables the incorporation of prior knowledge, which can be derived from previous information or expert judgment (Sikorska et al., 2013). Moreover, formal Bayesian approaches allow the explicit quantification of parameter uncertainty (Moges et al., 2020). Samadi, Tufford and Carbone (2018) highlighted that formal Bayesian inference enables the specification of an explicit probabilistic model for residual errors during calibration. The analysis of the statistical properties of these residuals can reveal their underlying nature and can help assess whether the assumed error distribution is appropriate.

Important applications of Bayesian statistics to assess hydrological model uncertainty include the work developed by Beven and Binley (1992), who proposed the Generalized Likelihood Uncertainty Estimation (GLUE), considered an informal Bayesian method, and by Kavetski, Franks and Kuczera (2003b), who introduced the

Bayesian Total Error Analysis (BATEA), a formal method that explicitly accounts for multiple sources of data uncertainty.

The work of Schoups and Vrugt (2010) also represents a significant contribution to Bayesian uncertainty analysis in hydrology. Based on previous work, the authors argued that reliable estimation of parameters and predictive uncertainty requires “an adequate statistical representation of the residual errors”. To this end, they proposed a generalized likelihood function capable of considering the non-normality, heteroscedasticity, and autocorrelation from hydrological model errors. This approach contrasts with more traditional methods, which commonly assume that errors are independent, normally distributed, centered on zero, and characterized by a constant variance. A formal Bayesian framework was adopted due to its strong theoretical foundation and its ability to support diagnostic evaluation of error model assumptions.

The proposed method was applied in two study cases: one humid basin and one drier basin. Results from the humid basin demonstrated that residuals were “better represented by an error model that explicitly accounts for heteroscedasticity, correlation, and nonnormality”, compared to the simplifying assumptions usually assumed in standard least squares approaches. “A Laplacian distribution function characterized by heavier tails than a Gaussian distribution” and a “first-order auto-regressive error model” (AR (1)) were used to this end, and may be considered a special case of the Generalized Likelihood function that supports the residuals model proposed in this study (Schoups; Vrugt, 2010, p. 9). This approach resulted in narrower uncertainty bands and smaller Mean-Square-Errors (MSE) when compared to a standard least-squares approach. For the drier basin, where residual behavior was more complex, the authors also found that the assumptions of normality, constant variance, and independence were violated. In this case, stronger autocorrelation among residuals was observed, and the AR (1) model proved to be insufficient to adequately describe the errors, requiring higher-order autoregressive models. Although Schoups and Vrugt (2010) considered total model residuals (combining input, output, parameter, and structural uncertainty), their findings strongly support the need for an appropriate statistical characterization of model residuals, particularly with respect to heteroscedasticity, non-normality, and autocorrelation, which are detailed below.

Heteroscedasticity

"Heteroscedasticity occurs when the distribution of the residual is dependent on the indicator variable" (Petersen-Øverleir, 2004, p. 2). Sorooshian and Dracup (1980) described heteroscedasticity as time-varying variance, which typically increases with streamflow discharges. Schoups and Vrugt (2010) assumed that the increase in the error standard deviations $\beta_t$ is linear with the mean flow $q_t$, and can be represented by Equation (2):

$$\beta_t = \beta_0 + \beta_1 q_t \quad (2)$$

Where $\beta_0$ and $\beta_1$ are parameters inferred from the data.

In their humid catchment case study, the authors demonstrated that neglecting heteroscedasticity by assuming a "constant (average) error variance results in an overestimation of prediction uncertainty for low flows and an underestimation for high flows" (Schoups; Vrugt, 2010, p. 10). Similar conclusions were reported by Samadi, Tufford, and Carbone (2018), who found that error variance increases with streamflow discharge while analyzing a coastal plain watershed in Atlantic, indicating the presence of heteroscedastic residuals.

Sun, Yuan and Liu (2017) compared three different approaches for addressing heteroscedasticity and demonstrated that the choice of residual variance model affects both calibration and prediction uncertainty. They further noted that heteroscedasticity tends to intensify and become more complex in large, heterogeneous river basins characterized by strong seasonality and climatic variability, posing significant challenges for traditional models that address heteroscedasticity.

Autocorrelation

To the best of the author's knowledge, Aitken (1973) was among the first to detect the correlated errors in discharge simulations while analyzing "Systematic errors in rainfall-runoff models". Ammann, Fenicia, and Reichert (2019) explained that errors in deterministic hydrological models arise from "the memory effect of errors in state variables". According to Sorooshian and Dracup (1980), shorter time steps tend to

produce higher error correlation, making autocorrelation particularly relevant in hourly hydrological models.

To explicitly account for autocorrelation, Autoregressive Moving Average – ARMA (p, q) or Autoregressive - AR(p) models are commonly used. Kuczera (1983) applied an ARMA (p, q) model, which incorporates $p$ autoregressive terms and $q$ terms of the moving average terms associated with random disturbances. From a humid catchment case study, the authors showed that the combined “use of power transformations to stabilize error variance and ARMA models to remove autocorrelation” seemed effective in representing the stochastic behavior of errors.

Schoups and Vrugt (2010, p. 3) argued that “published literature and experience with simulating residual errors of rainfall-runoff models suggests that autoregressive (AR) models typically suffice”. The authors adopted an AR (1) model for both study catchments, obtaining appropriate results for the humid basin but encountering difficulties in the drier basin. Attempts to increase the autoregressive order to AR (2) and AR (4) resulted in unrealistic error bounds, highlighting the complexity of residual error structures in dry environments.

Evin et al. (2013) showed that standardizing raw residuals using a linear model, followed by the application of a First-Order Autoregressive model (AR (1)), can improve the reliability of probabilistic predictions. The authors also identified “strong interactions between the parameters of autoregressive residual error models and the water balance parameters of the hydrological model” (Evin et al., 2013, p. 1).

Non-normality

Schoups and Vrugt (2010) found that residuals from hydrological models are better represented when non-normality is explicitly considered. In their study, residuals were modelled using a “Laplacian distribution function characterized by heavier tails than a Gaussian distribution”.

Non-normality can be addressed by explicitly assuming skewed or heavy-tailed probability distributions for the residuals model. This was done, for example, by Marshall, Sharma and Nott (2006) and Yang, Reichert and Abbaspour (2007), who

assumed that the errors follow a Students t-distribution; Schaefli, Talamba and Musy (2007), who used a mixture model combining two normal distributions, representing low-flow and high-flow errors separately, and by Schoups and Vrugt (2010).

Another approach to address residuals' non-normality is the application of data transformation methods, such as the Box-Cox transformation (Box; Cox, 1982). This approach has been used by several authors (Bates; Campbell, 2001; Kuczera, 1983; Smith et al., 2010; Sun; Yuan; Liu, 2017). Schoups and Vrugt (2010) state that, although Box-Cox transformations may remove heteroscedasticity and skewness, they often fail to account for heavy-tailed residuals, which are common in hydrological applications.

#### 3.1.1.2 Bayesian analysis

Bayesian statistics differ from frequentist approaches in that, when the true value of a parameter cannot be determined, parameters are treated as random variables characterized by probability distributions that represent the current state of knowledge or uncertainty about them. As additional information becomes available, this knowledge is updated, typically leading to a reduction in the variance of the parameter distribution (Naghettini, 2017).

Another distinguishing feature of Bayesian framework is its ability to incorporate sources of information beyond those provided directly by the data. This makes Bayesian analysis particularly valuable in situations where data are scarce. Such information is incorporated through the specification of a prior distribution of the parameter of interest, denoted by $p(\theta)$, which represents the modeler's existing knowledge and state of information about the unknown parameters (Naghettini, 2017).

Considering that the prior distribution reflects the modeler's knowledge and not the complete information, additional evidence must be incorporated through the observed data. During Bayesian inference, the prior distribution is updated using the information contained in the data through the likelihood function, denoted by $f(x|\theta)$, which quantifies "the probability of a particular sample value $\mathrm{x}$ of $\mathrm{X}$ occurring, assuming that $\theta$ is the true value of the parameter" (Naghettini, 2017, p. 499).

Bayes' theorem allows the derivation of the posterior probability density function, which represents the updated knowledge about the parameter $\theta$ after considering the observed data, it is given by Equation (3).

$$p(\theta|x) = \frac{f(x|\theta)\, p(\theta)}{f(x)} \tag{3}$$

Where $p(x)$ defines the prior predictive density function and is given by Equation (4).

$$f(x) = \int_{\Theta} f(x|\theta)\, p(\theta) d\theta \tag{4}$$

Where $\Theta$ denotes the parameter space. Because this integral is evaluated over the entire parameter space, the prior predictive density function acts as a normalizing constant. Consequently, Bayes' theorem is often expressed as Equation (5).

$$p(\theta|x) = f(x|\theta)\, p(\theta) \tag{5}$$

It can also be written as Equation (6).

$$posterior\ density \propto likelihood \times prior\ density \tag{6}$$

A critical step in Bayesian analysis consists of the specification of the prior distribution, which may be classified as non-informative, mildly/vague/weakly informative or informative. Non-informative or vague prior distributions are typically used when prior knowledge about a parameter is limited. Weakly informed priors are generally flat relative to the resulting posterior distribution (Kruschke; Liddell, 2018), and can help prevent unrealistic parameter values.

When more substantial prior knowledge is available, informative prior distributions with smaller variance may be adopted. This can be particularly advantageous in situations of limited observational data for applying Bayes' theorem. However, caution is required when specifying prior distributions (Kruschke; Liddell, 2018), as knowledge about parameters rarely exists in the form of precise probabilistic models. Consequently, prior distributions must be approximated based on available information and expert judgment, which inevitably introduces subjectivity. Since there is no unique procedure

for defining prior distributions, and the choice strongly depends on the modeler's experience, subjectivity in prior elicitation is frequently cited as a major criticism of Bayesian methods (Naghettini, 2017).

Bayesian analysis requires solving Equation (3), which in turn depends on integrating Equation (4). In most practical applications, especially when dealing with high-dimensional parametric spaces, the calculation of Equation (4) cannot be computed analytically (Naghettini, 2017). As a result, several numerical methods have been developed, most notably those based on Markov Chain Monte Carlo (MCMC) techniques. Commonly used MCMC algorithms include Metropolis-Hastings, Gibbs sampling and Hamiltonian Monte Carlo (HMC), which are implemented in widely used software packages such as OpenBUGS, JAGS and Stan.

By representing parameters through probability distributions and allowing the incorporation of prior and informal knowledge, Bayesian analysis provides a powerful framework for handling uncertainty in data-scarce environments, a common characteristic of hydrological systems. Although Bayesian methods originated in the eighteenth century, their widespread application began in the 1980s, driven by increasing problem complexity and advances in computational power. Today, Bayesian inference is widely recognized as a robust and coherent framework for statistical analysis, with demonstrated usefulness in complex applications across many fields, including hydrology and water resources engineering (Naghettini, 2017).

Smith and Marshall (2008) further highlighted the ability of Bayesian methods to continuously update inference as new data become available, an especially valuable feature for hydrological forecasting. Owing to its potential, numerous approaches have incorporated Bayesian methods for uncertainty analysis in hydrological models, particularly through the use of Markov chain Monte Carlo (MCMC) techniques (Smith; Marshall, 2008).

Within the Bayesian paradigm, uncertainty is naturally represented by treating both hydrological model parameters and the parameters governing residual error models as random variables. Their behavior is described by a joint posterior distribution, which provides a comprehensive characterization of uncertainty (Costa; Fernandes, 2017). Parameter uncertainty is directly quantified through credible intervals, such that a

parameter has a specific probability (typically 95%) of lying within a given interval (Naghettini, 2017).

When applying Bayesian methods to uncertainty analysis in hydrological modeling, the likelihood function plays a central role in describing properties of model residuals. While the posterior distribution of hydrological parameters quantifies the uncertainty in simulated streamflow from parameter uncertainty, the parameters of the error model capture uncertainty related to structural deficiencies in the model (Engeland; Gottschalk, 2002). Consequently, the quality of uncertainty assessment and hydrological model performance depend critically on the appropriate specification of both the error model and the prior distribution (Huard; Mailhot, 2008).

#### 3.1.1.3 Rating curve

Streamflow data are essential for water resources management, supporting activities such as flood and drought assessment, hydrological modeling, and long-term monitoring (Coxon et al., 2015). However, the continuous discharge measurement is often unfeasible from both financial and operational perspectives. As a result, streamflow is commonly estimated indirectly using rating curves.

Rating curves are constructed using gauging, that is, paired measurements of stage and discharge (Lucas et al., 2023). A functional relationship between these two variables is then established, allowing continuous monitoring of stages only, which is considerably simpler and cheaper. Periodic discharge measurements are required to verify the persistence and validity of the established relationship over time.

A rating curve is a mathematical equation that links stage (or water level) ($h_t$) to discharge ($q_{rc_t}$) through a set of parameters ($\boldsymbol{\theta_{rc}}$) that must be calibrated, as presented in Equation (7). The stage-discharge relationship is assumed to be monotonic and valid under specific hydraulic control conditions. If changes occur in the river cross-section, such as those induced by major flood events, the rating curve must be revised.

$$q_{rc_t} = f_{rc}(h_t, \boldsymbol{\theta_{rc}}) \tag{7}$$

Rating curves can be represented using different mathematical formulations, the most common being power-law functions and polynomial equations. Power-law functions

are especially attractive because their parameters can be related to physical principles governing hydraulic behavior (Le Coz et al., 2014). Their application, however, requires good hydraulic knowledge of the river cross-section. Numerous studies have highlighted the effectiveness of power-law formulations (Di Baldassarre; Claps, 2011; Petersen-Øverleir, 2004; Reitan; Petersen-Øverleir, 2008). Moreover, power-law models can be extended to multi-segment rating curves, as proposed by Reitan and Petersen-Øverleir (2008) and used by Le Coz et al. (2014).

Despite their widespread use, power-law formulations have received criticism. Fenton (2018) argued that this formulation may oversimplify the actual hydraulic behavior at many gauging stations, as the real stage-discharge relationship may violate the underlying power-law models' assumption, and therefore recommended the use of polynomial formulations. Hrafnkelsson et al. (2012) proposed a Bayesian extension of the standard power-law model using B-splines, showing improved performance compared to the classical formulation. More recently, Hrafnkelsson et al. (2022) introduced a hierarchical Bayesian extension in which the power-law exponent depends on the water elevation. In three of the four datasets analyzed, the proposed method outperformed the traditional power-law function, while results were equivalent on the fourth.

Mailhot et al. (2025) developed a method to account for uncertainty when constructing a rating curve using one or two power law functions across 173 hydrometric stations. Although most of the exponents fell within the expected range, some hydrometric stations presented values outside the expected range. The authors concluded that, despite valid criticisms, extensive empirical evidence indicated that power-law functions usually provide appropriate representations of the stage-discharge relationship in practical applications.

Several sources of uncertainty can affect rating curves. Sikorska et al. (2013) grouped them into four main categories: (1) streamflow data uncertainty; (2) parametric and structural uncertainty; (3) changes in hydrological conditions; and (4) uncertainty related to extrapolation. These sources are discussed below.

a) Uncertainty in streamflow data

River discharge data are affected by uncertainties in both stage and discharge measurements (Di Baldassarre; Montanari, 2009). Lang et al. (2010) showed that, in narrow channels with large water depths, a stage variation of only 1 cm can result in discharge variations of 4-5%. In contrast, in wide rivers, relatively large stage variations may lead to highly uncertain discharge estimates due to the weak sensitivity of discharge to water level at high flows.

Horner et al. (2018) investigated the influence of errors associated with stage observations during discharge gauging on rating curve uncertainty. Systematic and nonsystematic (independent) random errors were considered across six hydrometric stations with contrasting characteristics in France. Their site-specific results showed that, under favorable gauging conditions, random (nonsystematic) errors in stage measurements have a relatively limited effect on rating curve uncertainty. In contrast, systematic errors in stage observations were shown to be non-negligible. Across the six stations analyzed, uncertainty derived from systematic stage errors ranged from 4-12% of the daily mean discharge and 1-3% of the annual mean discharge, assuming that sensors were recalibrated at 30-day intervals.

Discharge uncertainty is also influenced by the method used, such as the area-velocity method (Sikorska et al., 2013). Pelletier (1988), in an extensive review of over 140 studies regarding uncertainty in river discharge, identified three main contributors in the area-velocity method: (1) the determination of the cross-sectional area; (2) velocity measurements, which depend on the exposure time and number of vertical velocity observations; and (3) approximation of the velocity field using discrete points. The author reported that the total uncertainty of a single discharge measurement may exceed 8% at the 95% confidence interval. Although technological advances may reduce these uncertainties, the area-velocity method remains widely used in many countries, including Brazil.

Coxon et al. (2015) developed a framework to quantify discharge uncertainty and applied it to 500 gauging stations in the United Kingdom. Their results showed that discharge uncertainty is influenced not only by local conditions, such as vegetation

changes, but also by management conditions, including the frequency of rating curve updates.

b) Parametric and structural uncertainty

As with hydrological models, rating curves are affected by both parametric and structural uncertainty. Parametric uncertainty is associated with the estimation of model parameters and is influenced by data availability, parameter variability, and the calibration process. Kiang et al. (2018) defined parametric uncertainty as uncertainty associated with identifying rating curve parameters, usually from power-law models, which are affected by limited data for parameter calibration and measurement errors.

Structural uncertainty arises from representing the stage-discharge relationship using simplified mathematical formulations. As previously described, different equations may be adopted, with the power-law function being largely applied. Kiang et al. (2018) described structural uncertainty as the result of model simplifications that fail to capture all relevant hydraulic processes and from potential temporal variability in the stage-discharge relationship. Regarding structural errors, Petersen-Øverleir (2004) proposed a heteroscedastic maximum likelihood model for Norwegian gauging stations and found that accounting for variance heterogeneity improved performance relatively to the non-linear least squares method. Similar results were found by Reitan and Petersen-Øverleir (2008), who applied a Bayesian framework for rating curves estimation and found that ignoring heteroscedasticity can introduce bias to the inference.

c) Changes in hydrological/ hydraulic conditions

Rating curves are generally developed under the assumption of steady flow and stable hydraulic control. Deviations from these assumptions may degrade the stage-discharge relation (Kiang et al., 2018), and, consequently, introduce significant errors (Le Coz et al., 2014).

Such deviations may arise from unsteady flow conditions, backwater effects caused by downstream controls such as tributaries, lakes, or reservoirs; hydraulic hysteresis; or temporal changes in channel properties. These changes include sediment

processes (scour or fill), weed or vegetation growth, variations in channel roughness, ice formation, and other factors (Coxon et al., 2015; Di Baldassarre; Laio; Montanari, 2012; Kiang et al., 2018; Le Coz et al., 2014; Mailhot et al., 2025).

d) Uncertainty from extrapolated data

Another major source of uncertainty arises from the limited range of data used to construct the rating curves. Observations are typically concentrated around medium flows, with sparse data for low and high flows, requiring extrapolation beyond the observed range (Mailhot et al., 2025).

Kiang et al. (2018) compared seven different methods for quantifying rating curve uncertainty and found that uncertainty in extrapolated high flows ranged from 41 to 200% at the 95% uncertainty limits. For low flows, uncertainty ranged from 28% to 101%, while for median flow it ranged between 3 and 17%. These results highlight the substantial impact of extrapolation uncertainty when data are scarce.

Domeneghetti, Castellarin and Brath (2012) showed that extrapolation errors often dominate total rating curve uncertainty, particularly when maximum measured discharges are low. They demonstrated that constraining extrapolated portions of the rating curve using hydraulically consistent information can substantially reduce uncertainty. Lang et al. (2010) similarly found that extrapolation beyond the gauged range can produce large systematic errors, leading to wide uncertainty intervals in flood frequency estimates, and emphasized the importance of incorporating hydraulic expertise in high-flow extrapolation.

Lang et al. (2025), in a case study developed on the Upper Rhine River, found that incorporating historical flood data reduced uncertainty in flood frequency analysis, even though historical data themselves were highly uncertain. This finding highlights the importance of including information from high-flow conditions when constructing rating curves.

Importance of uncertainty consideration

Rating curve uncertainty can be substantial. Coxon et al. (2015) analyzed 500 stations and found that, although most stations exhibited uncertainty intervals below 40% for medium and high flows, uncertainty can be as high as 397% in some cases. This uncertainty propagates into hydrological and hydrodynamic models and can significantly affect water resources management decisions and associated costs (McMillan et al., 2017; Wilby et al., 2017).

Kastali et al. (2022) analyzed the impact of rating curve uncertainty for the calibration of the parameters of the hydrological model HEC-HMS for a historic flood event and showed that highly influential model parameters, such as initial abstraction and curve number, varied between -15.16% and 20% and between -5.18% and 7.8%, respectively, highlighting the importance of accounting for rating curve uncertainty to improve hydrological modeling. Osorio and Reis (2016) compared a semi-Bayesian approach with traditional maximum likelihood estimation to assess the influence of rating curve uncertainties on flood frequency analysis, demonstrating that both measurement and rating curve errors propagate through the analysis and affect the estimated floods. Kastali et al. (2021) investigated the impact of rating curve uncertainty on flood hazard mapping in a flood-prone region of Algeria with existing flood control infrastructure. Their results showed that the estimation of the inundated area varied by approximately 15 – 18% when rating curve uncertainty was considered, leading the authors to conclude that the existing flood control system was inadequate.

These examples illustrate that ignoring rating curve uncertainty may therefore lead to biased model outputs, affecting subsequent analysis and decision-making processes. Consequently, as with hydrological models, rating curve uncertainty should be explicitly acknowledged and represented in the most accurate way possible (Mailhot et al., 2025).

Methods

Numerous approaches have been developed to address rating curve uncertainty. Kiang et al. (2018) identified methods including gauging deviations analysis, fuzzy methods, locally weighted regression (LOWESS), Generalized Likelihood Uncertainty

Estimation, informal and formal Bayesian methods, dynamic rating curve analysis, and perturbation-based hydraulic modeling. As with hydrological models, the authors concluded that there is no universally optimal method for estimating streamflow uncertainty, since each approach relies on different assumptions regarding uncertainty sources and model formulation.

The potential of Bayesian methods was discussed in Subchapter 3.1.1.2. Accordingly, numerous studies have applied Bayesian frameworks to rating curve estimation and uncertainty analysis (Hrafnkelsson et al., 2012, 2022; Le Coz et al., 2014; Mansanarez et al., 2016, 2019a, 2019b; Moyeed; Clarke, 2005; Petersen-Øverleir; Reitan, 2009; Petersen-Øverleir; Soot; Reitan, 2009; Reitan; Petersen-Øverleir, 2008; Sikorska et al., 2013; Steinbakk et al., 2016). Among these, the BaRatin method, proposed by Le Coz et al. (2014), stands out as a promising framework for rating curve estimation. The method incorporates hydraulic knowledge through prior distribution on model parameters by linking power-law formulations to classical hydraulic equations, such as Manning's equation. This requires a detailed understanding of hydraulic behavior at the gauging station. The method also allows for multiple hydraulic controls through a piecewise compound power-law formulation.

BaRatin explicitly accounts for individual uncertainty associated with each gauging and includes a remnant error term. It assumes a stationary rating curve and neglects stage measurement uncertainty. The framework was applied to more than 50 stations, with three cases presented in detail, demonstrating its reliability and versatility when "hydraulic controls are correctly identified and gaugings are validated individually with their uncertainty" (Le Coz et al., 2014, p. 14).

Later, the remnant error term in BaRatin was extended to account for heteroscedasticity, as presented in Sikorska and Renard (2017). This extension aligns with the results reported by Petersen-Øverleir (2004), who found that accounting for heteroscedasticity improved model performance in Norwegian gauging stations.

Due to its potential, the BaRatin framework has been widely applied in subsequent studies, as Das and Das (2026); Garcia, Costa and Silva (2020); Horner et al. (2018); Kastali et al.(2021, 2022); Kiang et al. (2018); Ocio et al. (2017); Osorio and Reis

(2016); Qiu et al. (2021); Sikorska and Renard (2017); Vieira et al. (2022); Zeroual, Meddi and Assani (2016), and others.

### 3.1.2 Rainfall-stage models

As previously noted, rainfall-runoff models are widely used for a variety of hydrological applications. However, their parameters are typically calibrated using discharge observations, which are obtained from rating curves and therefore subject to multiple sources of uncertainties that affect the hydrological model outputs. In this context, a more explicit description and understanding of the uncertainty is needed, especially for decision-making purposes.

To the best of the author's knowledge, Sikorska et al. (2013) were the first to explicitly account for rating curve uncertainty in water-level predictions derived from hydrological models. To achieve this, the authors adopted a Bayesian framework, which enables uncertainty quantification and the incorporation of prior knowledge. They developed a rainfall-water level model that transforms input data from the hydrological model directly into water-level predictions by combining the deterministic component of the hydrological model with the inverse of the water level – runoff model (i.e., the rating curve). In addition to the parametric uncertainty associated with both the hydrological model and the water level-runoff model, an error term was introduced to represent structural uncertainty from both models, measurement uncertainty in discharge observations, and other sources of uncertainty not explicitly considered, such as uncertainties from input data for the hydrological model.

The model proposed by Sikorska et al. (2013) was tested on a case study in the upper part of the Sluzew Creek catchment. The results indicated that the parametric uncertainty associated with the rating curve was slightly larger than that associated with parametric uncertainty from the hydrological model. However, both were much smaller than the one from the structural error. The authors emphasized that the results were case-specific and should not be generalized. Nevertheless, they concluded that the proposed approach represented an innovative model to quantify uncertainty on water-level prediction, yet a better description of the individual uncertainty contribution is still needed.

In this sense, the rainfall-stage model represents a promising approach to explicitly address uncertainty, particularly uncertainty associated with rating curves. However, only a limited number of studies have been published about this topic. Some studies, as Montanari et al. (2009), Sun, Ishidaira and Bastola (2010), Sun, Ishidaira and Bastola (2012a) and Sun, Ishidaira and Bastola (2012b) employed remote sensing-derived water stages or satellite observations of river hydraulic variables to calibrate hydrological models using stage data. These studies concluded that such approaches were a promising way for improving river discharge estimation in large rivers and ungauged basins. Hulsman, Bogaard and Savenije (2018) calibrated the parameters of a hydrological model using water-level observations for a semi-arid area in Kenya, on the Mara River basin, motivated by the large uncertainty associated with the rating curve. They employed the Strickler–Manning formula to convert modelled discharges into water levels and calibrated a slope-roughness parameter, using the Nash–Sutcliffe coefficient as an objective function.

These studies present different methods to deal with the lack of discharge data for calibrating the parameters of hydrological models. Sun, Ishidaira and Bastola (2010) and Sun, Ishidaira and Bastola (2012b) employed the generalized likelihood uncertainty estimation (GLUE) for model calibration and uncertainty analysis, while the others did not present a formal framework for doing so. None of them explicitly considers the uncertainty from multiple sources. In this context, the work by Sikorska and Renard (2017) stands out, as it explicitly considers the uncertainty from the rating curve and the hydrological model and builds a rainfall–stage model in a probabilistic sense. The paper also applies the Bayesian framework for calibrating the rainfall-runoff model, as made by Sikorska et al.(2013).

A major advancement of Sikorska and Renard (2017) lies in their ability to disaggregate structural uncertainty associated with the rating curve from that of the hydrological model, and to estimate discharges together with uncertainty bands. Furthermore, they incorporate the BaRatin method, proposed by Le Coz et al. (2014), as a prior distribution for the rating curve parameters, allowing for the incorporation of multiple controls and a heteroscedastic error model for the rating curve. In the case study developed on the Ardèche river, the authors showed that the resulting uncertainty bands covered most of the observed data, both for stage and discharges. They also

demonstrated that neglecting rating curve uncertainty can significantly affect hydrological model parameter estimates and found a predominance of the hydrological model structural uncertainty.

Although the model proposed by Sikorska and Renard (2017) has some limitations, as it neglects stage error measurement and does not consider uncertainty from the input data, it shows considerable potential, especially in ungauged or poorly gauged basins, a common challenge in Brazil, by enabling hydrological model calibration based on stage observations and providing a description of uncertainty.

## 3.2 Hydrodynamic modeling

Runoff along rivers and channels is one of the main components of the hydrological cycle. It is governed by physical laws and quantitatively represented by variables such as depth, velocity, and flow rate. Flow can be classified as steady or unsteady. Steady flows assume that velocity and water level variations are null, while unsteady flows consider their variability both in time and space (Tucci, 2007). The latter case is present in real-world situations and is discussed below.

To represent runoff along rivers and channels, mathematical models can be used. These models can be described as a set of equations that represent fluid behavior using mathematical equations, typically partial differential or integral equations. To set up a numerical model, the modeler must first represent the physical problem through governing equations and apply simplifications when appropriate. To solve them numerically, the governing equations are then replaced by finite differences or other discrete systems of equations. Subsequently, the spatial and temporal domains must be defined, typically using a grid-based representation. Boundary conditions are then specified at the domain limits, either as prescribed values or as relationships between variables. Finally, initial conditions, representing flow conditions at the initial time ($t = 0$), must be defined to allow numerical calculations to begin (Chadwick; Morfett; Borthwick, 2013).

The application of hydrodynamic modeling is an effective tool for improving the understanding of river conditions (Jahandideh-Tehrani et al., 2020). These models allow water level prediction, which is essential for flood management (Timbadiya; Patel; Porey, 2015), including the assessment of flood alert system activation.

Hydrodynamic models are commonly classified as one-dimensional (1D), two-dimensional (2D), or three-dimensional (3D), according to the number of dimensions in which flow variables are represented. 1D models describe flow variations primarily along the longitudinal direction, assuming uniform velocity and water level across the cross-section. 2D models account for variations in both longitudinal and transversal directions, and 3D models additionally consider vertical flow variability.

1D models can be advantageous in cases of relatively regular channel geometry, such as urban channels, smaller-scale basins, or applications subject to computational constraints. Due to its simplicity, they are computationally efficient and widely used in river hydraulics and flood studies. However, 1D models have limitations in representing complex lateral flow dynamics, particularly under unsteady conditions involving floodplain activation and backflow. In such cases, 2D models provide a more realistic representation of flow patterns and should be preferred when lateral flow processes play a significant role (Merwade et al., 2008).

Despite their advantages, 2D models require a substantially greater quantity and quality of input data, including high-resolution topography and detailed roughness parametrization (Ngo et al., 2023). According to Merwade et al. (2008), the performance of 2D models strongly depends on the accuracy of geometric descriptions of the main channel, floodplain separation, and linear terrain elements such as breaklines that control flood extent. When terrain data quality is insufficient, 2D models may even produce more conservative or less reliable results than simple 1D approaches. In addition, the higher computational cost associated with 2D simulations can limit their applicability, especially in probabilistic frameworks.

3D models are typically reserved for specific applications, such as the detailed analysis of hydraulic structures, due to their very high computational demand, which precludes their use over large spatial domains.

According to Jahandideh-Tehrani et al. (2020), the choice of hydrodynamic model dimensionality depends on several factors, including the characteristics of the study case, spatial scale, and availability of field data. Although 2D and 3D models have become increasingly available, 1D hydrodynamic models remain widely used for simulating river stages and flood flows, particularly in large and complex river systems, where computational efficiency is essential (Chen; Liu, 2017; Rodrigues Do Amaral et al., 2025).

To apply these models, the underlying physical behavior must be understood. The routing of a wave in a channel produces attenuation and translation due to storage effects (both within the main channel and in the floodplain); friction with channel surfaces and diffusion caused by pressure gradient. Flow systems may exhibit different dominant effects depending on the situation. Accordingly, Ponce (2014) distinguished between hydrological models, which consider only storage effects and are based on mass conservation, and the hydraulic models, which consider both storage and momentum effects. Many 1D hydraulic models are based on Saint-Venant equations (Tucci, 2007), which are derived under simplifying assumptions from the mass conservation equations (Equation (8)) and the momentum conservation equation (Equation (9)):

$$\frac{\partial A}{\partial t} + \frac{\partial Q}{\partial x} = q \tag{8}$$

$$\frac{\partial Q}{\partial t} + \frac{\partial}{\partial x}\left(\frac{Q^2}{A}\right) + gA\frac{\partial y}{\partial x} + gAJ - gAS = 0 \tag{9}$$

in which

$q$ represents lateral inflow;

$A$ is the flow cross-sectional area;

$J$ is the friction slope;

$S$ is the bed slope;

$\frac{\partial Q}{\partial t}$ represents local acceleration;

$\frac{\partial}{\partial x}\left(\frac{Q^2}{A}\right)$ represents convective acceleration;

$gA\frac{\partial y}{\partial x}$ represents pressure force;

$gAJ$ represents friction force;

$gAS$ represents gravitational force.

Porto (2006) and Chow, Maidment and Mays (1988) describe the simplifying assumptions required for deriving the Saint-Venant equations: incompressible Newtonian fluid with constant density; one-dimensional flow predominantly in the longitudinal direction, with a cross-section-averaged representative velocity; gradually varied free surface, allowing a hydrostatic pressure distribution and negligible vertical acceleration; gradual variation of cross-sections; small average channel bed slope (thus $\sin S \cong \tan S$ and $\cos S = 1$), with a fixed bed, i. e., negligible scour and deposition effects; roughness effects and losses estimated using equations valid for steady uniform flow, such as Manning's equation; and absence of singularities.

Different types of 1D hydraulic models can be defined depending on the simplifying assumptions adopted concerning the phenomena considered. These include kinematic wave models, diffusive wave models, and hydrodynamic models. Hydrodynamic models use the complete Saint-Venant equations, without neglecting any terms in the momentum equations. As a result, these models require a larger amount of input data for numeric resolution, but offer higher precision and a more realistic physical representation of flow processes (Tucci, 2007).

In most practical situations, analytical solutions to the Saint-Venant equations are not possible. Therefore, numerical methods are employed to compute representative variables such as mean velocity and flow depth at discrete points in time and space. Common numerical approaches used to discretize and solve fluid flow problems include the finite difference method, the finite element method, and the finite volume method (Chadwick; Morfett; Borthwick, 2013).

Finite differences can be defined as approximate solutions of partial differential equations, consisting of replacing each partial derivative with a ratio of differences between adjacent values (Chanson, 2004). Accordingly, the previously continuous system is discretized in time and space based on the adopted spatial ($\Delta x$) and temporal ($\Delta t$) resolutions (Silva, 2006). The finite difference method can be implemented using either an implicit or explicit scheme. In the explicit scheme, information from time $j$ is used to compute variables at the next time step $j+1$. In the implicit scheme, information from time $j+1$ is also required, necessitating more complex numerical procedures such as matrix methods and iterative solutions. While explicit schemes are simpler to implement, they are more susceptible to numerical instability. Based on Taylor series expansion, a finite difference approximation can be derived for central (Equation (10)), backward (Equation (11)), and forward (Equation (12)) difference (Chadwick; Morfett; Borthwick, 2013).

$$\frac{\partial f(x)}{\partial x} = \frac{f(x+\Delta x) - f(x-\Delta x)}{2\Delta x} \tag{10}$$

$$\frac{\partial f(x)}{\partial x} = \frac{f(x) - f(x-\Delta x)}{\Delta x} \tag{11}$$

$$\frac{\partial f(x)}{\partial x} = \frac{f(x+\Delta x) - f(x)}{\Delta x} \tag{12}$$

Three properties must be ensured when solving finite difference equations: convergence, consistency, and stability. Convergence occurs when the numerical solution approaches the analytical solution as $\Delta x$ and $\Delta t$ tend to zero. Consistency implies that the finite difference formulation from the equation tends to the analytical equation as $\Delta x$ and $\Delta t$ tend to zero. Stability is related to the behavior of truncation errors during numerical computation. If these errors grow as calculations progress, the solution becomes unstable. Stability for transient flow problems is commonly assessed using the Courant number, defined as the ratio between physical wave celerity and grid celerity, which can help assess the time step adopted for calculation. A Courant number less than or equal to one is generally considered acceptable (Chadwick; Morfett; Borthwick, 2013; Chaudhry, 2008; Ponce, 2014).

Hydrodynamic river models are subject to multiple sources of uncertainty, which inevitably lead to uncertainty in model outputs. Understanding both the type and magnitude of these uncertainties is essential for a meaningful interpretation of simulation results and for their effective use in decision-making processes (Warmink et al., 2011). Uncertainties in hydrodynamic modeling include sources such as geometric representation (e.g., number and spacing of cross-sections, channel bed slope, mesh quality, among others), model parameters (remarkably Manning's roughness coefficient), representation of hydraulic structures (such as bridges and culverts), model dimensionality, and boundary and initial conditions (Merwade et al., 2008). Camacho et al. (2015) further identified epistemic uncertainty arising from model structure errors, challenging in parameter identification, and errors in input datasets.

Warmink et al. (2011) conducted a Pedigree analysis based on expert judgment to identify the most influential sources of uncertainty in hydrodynamic models used to compute water levels. The results indicate that upstream discharge and channel roughness formulation exert the greatest influence on uncertainty in simulated water levels. Similar conclusions were reported by Merwade et al. (2008), who emphasized the significant impact of Manning's roughness coefficient on hydraulic simulations. This coefficient governs flow resistance within the channel (Chadwick; Morfett; Borthwick, 2013), and exhibits high variability, depending on factors such as vegetation type and density, channel geometry, particle size, channel irregularities, and meandering (Vijay; Sargoankar; Gupta, 2007).

Consequently, the Manning roughness coefficient represents a key parameter in the calibration and validation of hydrodynamic models. Chadwick, Morfett and Borthwick (2013) identified it as the primary parameter to be adjusted in 1D river models. Jahandideh-Tehrani et al. (2020) highlights that accurate estimation of channel roughness is essential for minimizing modeling and simulation errors, noting that due to its high sensitivity, this parameter is commonly selected for calibration. Numerous studies have adopted this approach (Boulomytis et al., 2017; Camacho et al., 2015; Jahandideh-Tehrani et al., 2020; Pappenberger et al., 2005; Pinheiro; Naghettini; Palmier, 2019; Reis et al., 2020).

Pappenberger et al. (2005) analyzed uncertainty in the one-dimensional HEC-RAS model by calibrating the Manning roughness coefficient using the GLUE framework. The authors identified equifinality problems, whereby different parameter values led to similar model performance and emphasized that calibrated parameters often represent effective values rather than physically realistic ones. They also highlighted the strong influence of boundary conditions on model results.

Domeneghetti, Castellarin and Brath (2012) reported that roughness coefficients are sometimes treated as statistical parameters that combine representation of riverbed roughness with compensation for structural model uncertainty, rather than being interpreted strictly as physically based parameters. However, the authors challenge this perspective. In a case study incorporating rating curve uncertainties into hydraulic simulation, they demonstrate that considering uncertainties only in empirical rating curves, while neglecting other sources of uncertainties, can significantly reduce the physical interpretability of the Manning roughness coefficient, transforming it into a calibration parameter. These findings highlight the importance of explicitly accounting for uncertainty in parameter calibration of both hydrological and hydrodynamic models, as well as the need for adequate observation data.

Although some studies have addressed hydrodynamic uncertainty, no studies were identified that explicitly account for rating curve uncertainty in both hydrological and hydrodynamic modeling, highlighting an important research gap.

After hydrodynamic model calibration, the validation process can be conducted, and the model may be applied for predictive purposes (Chadwick; Morfett; Borthwick, 2013).

# 4 METHODOLOGY

This chapter presents the methodology used in this study. The first step was the selection of the study area appropriate for the intended analysis. Subsequently, the rating curve was constructed, with explicit consideration of its uncertainty, for two scenarios: one considering the available discharge measurements for calibration and the second using only hydraulic and geometric data. Next, a rainfall-stage model was developed, allowing the uncertainties from the rating curve and the hydrological model to be explicitly coupled. After, the true (unknown) discharge and rating curve discharges and their associated uncertainty were propagated through the hydrodynamic model. The flowchart that summarizes the main steps of the work is presented in Figure 1. For steps 2 to 4, a Bayesian framework was adopted, as presented in the Subchapter 4.5.

**Figure 1 - Work methodology flowchart**

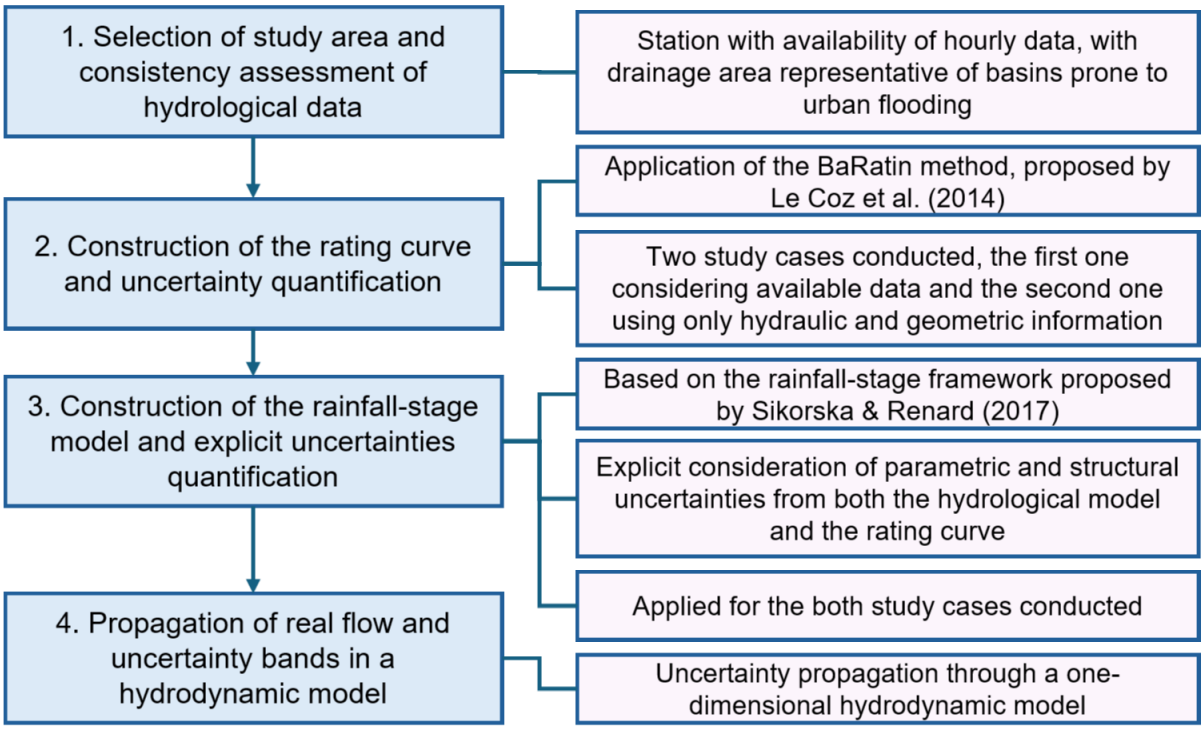

## 4.1 Study area

### 4.1.1 Jardim Streamflow Gauging Station

The study area chosen was the gauging station Jardim (code 40811100), inserted on the Juatuba stream, on the Paraopeba river basin, located in the São Francisco River Basin. The station is installed on one of the tributaries of Serra Azul reservoir, one of the three reservoirs that guarantee the water supply for the Belo Horizonte Metropolitan Region (ANA, 2025a). The station is operated by the Serviço Geológico Brasileiro (SGB), an institution that belongs to the Companhia de Pesquisa em Recursos Mineirais (CPRM).

This station was chosen since it is a telemetric station, with hourly data consistently processed in previous research (Mota et al., 2018), and the length of the time series was adequate for the development of the present study. Moreover, the station has a catchment area of approximately 113 km², which is representative of basins that are susceptible to flash floods and, therefore, can benefit from alert systems, which is one of the objectives of the research.

The hourly data for the station are available for the period of 01/08/1997 until 05/28/2008. For the calibration of the parameters of the hydrological model, nearby rainfall gauging stations with data available for the same period were sought. The stations Alto da Boa Vista (code 2044021), Fazenda Laranjeiras – Jusante (code 2044041), Jardim (code 2044052), and Serra Azul (code 2044054) were chosen. Areal precipitation was estimated using the Thiessen polygon method.

In addition to rainfall data, potential evapotranspiration is also an input variable for the chosen hydrological model (GR4H). Data from the INMET Florestal climate station (code 83581) were used, which was the closest climate station around, located less than 20km from the Jardim streamflow gauging Station. The potential evapotranspiration was calculated based on the methodology FAO Penman-Monteith. All data used were previously consisted by Mota et al. (2018). The stations used are presented on Table 1 and Figure 2.

**Table 1 - Hydrological and weather stations used – Jardim area**

| Information | Station name | Station Code | Latitude | Longitude | Altitude | Responsible Agency |
|---|---|---|---|---|---|---|
| Streamflow | Jardim | 40811100 | -20.0475 | -44.4089 | | SGB-CPRM |
| Rainfall | Alto da Boa Vista | 2044021 | -20.1056 | -44.4011 | 905 | SGB-CPRM |
| | Fazenda Laranjeiras - Jusante | 2044041 | -20.1022 | -44.4847 | 894.7 | SGB-CPRM |
| | Jardim | 2044052 | -20.045 | -44.4078 | 806 | SGB-CPRM |
| | Serra Azul | 2044054 | -20.0867 | -44.4272 | 817 | SGB-CPRM |
| Weather | Florestal | A535 | -19.885278 | -44.416944 | 753.50 | INMET |

Source: Adapted from ANA (2025b) and INMET (2025)

**Figure 2 - Study area - Jardim gauging station**

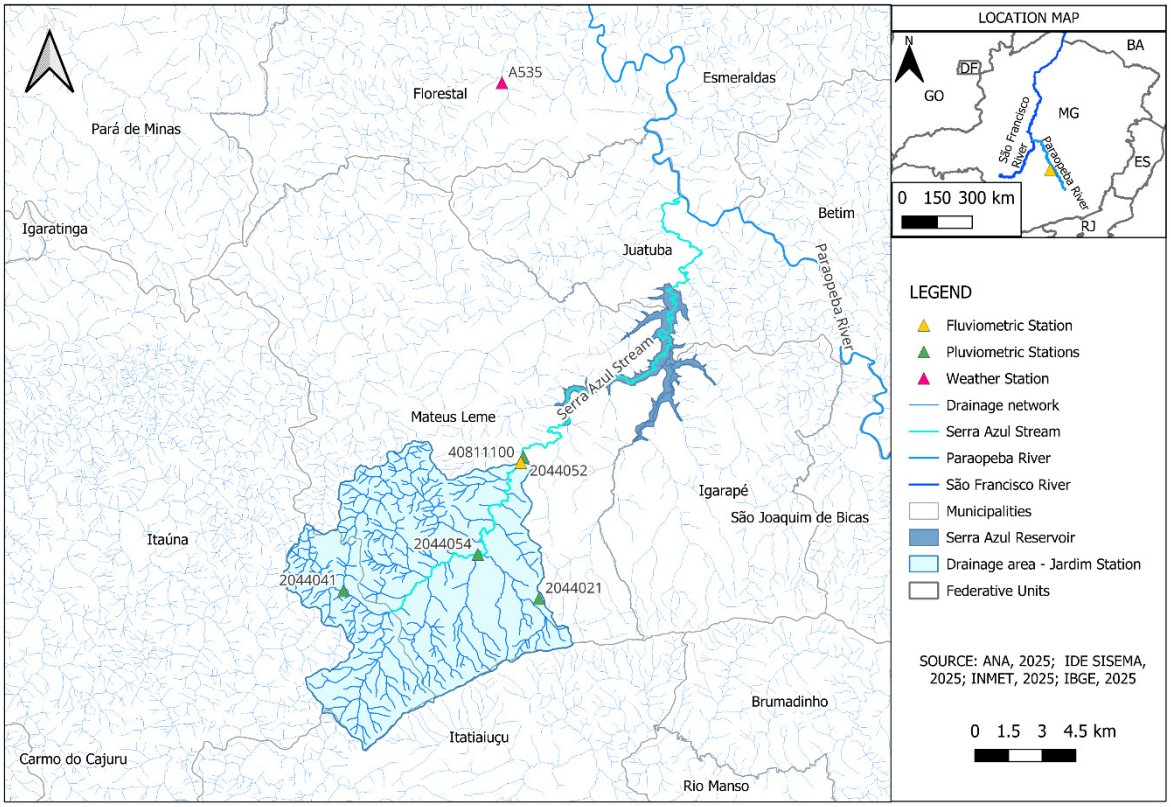


Source: Author's elaboration based on ANA (2025b), SEMAD (2025), INMET (2025) and IBGE (2025)

The measured stages and the calculated precipitation and potential evapotranspiration are shown in Figure 3 and Figure 4. This region, as most of the Brazilian southeast, presents two well-defined periods: the rainy one, from October to March, and the dry one, from April to September. For this data period, the rainy season encompasses nearly 90% of the precipitation, and the potential evapotranspiration (varying from 0.10 to 0.11 mm/h) represents 68% of the precipitation.

Figure 4 shows a change in stage reference that occurred on October 10, 1999. Therefore, only data recorded after this date were used for both the rating curve and the rainfall-stage model. For the rainfall-stage model, the warm-up period extended from July 1, 2000, to September 30, 2000; the calibration period from October 1, 2000, to September 30, 2003, and the validation period from October 1, 2003, to September 30, 2006. This resulted in 2,208 sample points for the warm-up period and 26,292 sample points for each of the calibration and the validation periods.

**Figure 3 - Calculated precipitation - Jardim station drainage area**

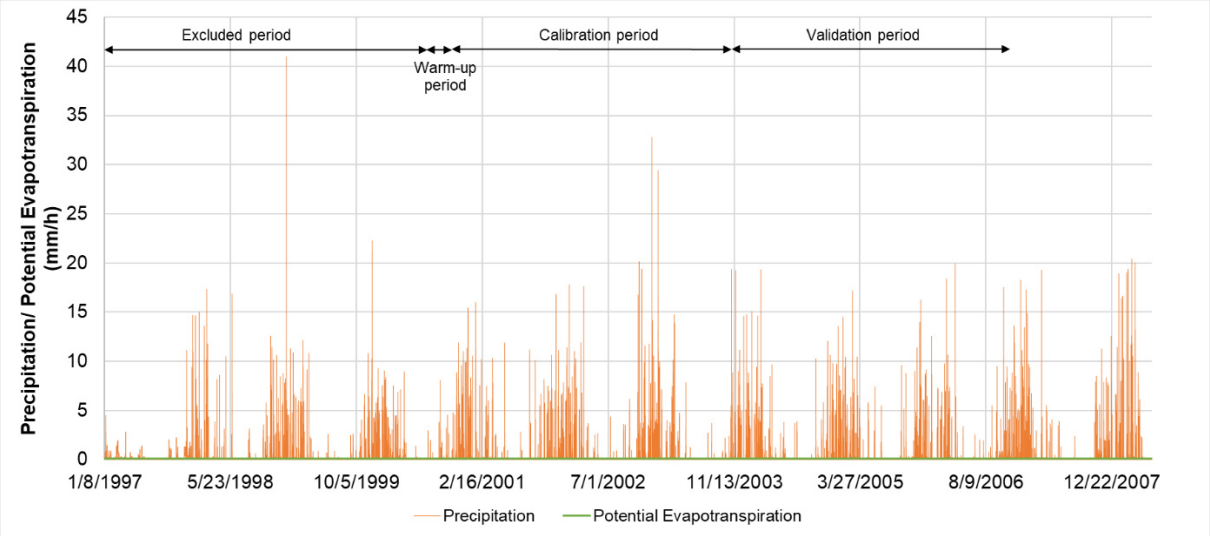


Source: Author's elaboration based on Mota et al. (2018)

**Figure 4 - Measured Stages - Jardim station drainage area**

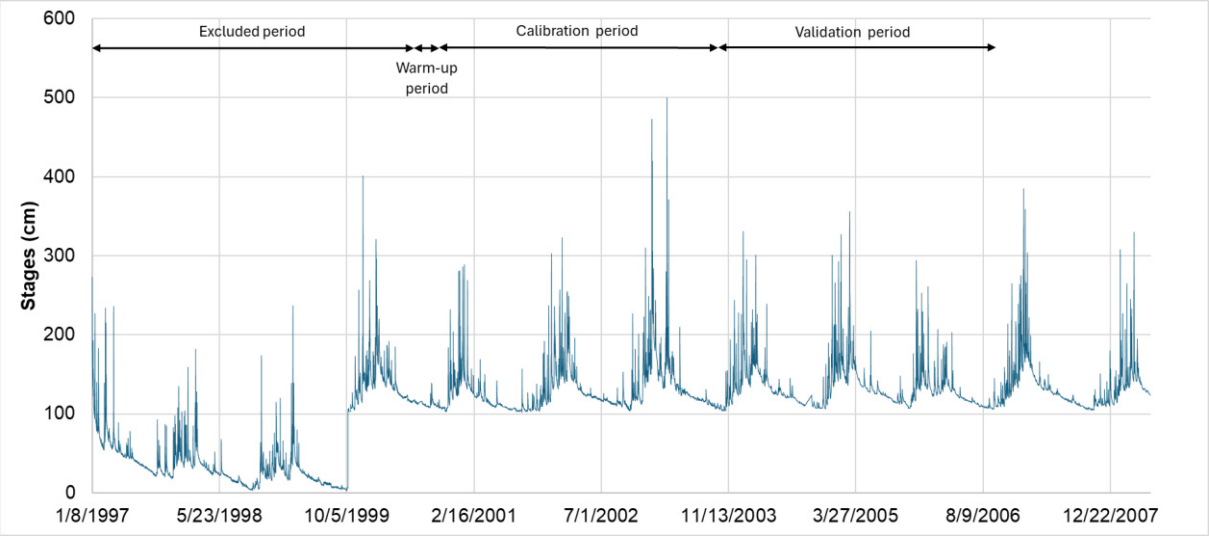


Source: Author's elaboration based on ANA (2025b)

## 4.2 Rating curve model

After selecting the streamflow gauging station, the next step consisted of quantifying the uncertainties associated with the rating curve for the subsequent analysis of the predictive capacity of the hydrological model. The calibration of the rating curve parameters was performed using the BaRatin method, proposed by Le Coz et al. (2014). The method uses Bayesian inference to construct the rating curve and is based on the power-law function, which allows a direct link between mathematical formulation and the physical process governing the stage-discharge relation. Thus, through the specification of prior distributions, the method allows the incorporation of physical knowledge to calibrate the model parameters.

The discharge predicted by the model at time $t$ is defined according to the stage at the section $h_t$ and the model parameters ($\boldsymbol{\theta_{RC}}$), as presented in Equation (13).

$$q_{RC_t} = f_{RC}(h_t, \boldsymbol{\theta_{RC}}) \tag{13}$$

The discharge predicted by the rating curve can also be expressed as the true (unknown) discharge ($q_t$) plus an error term ($E_{RC_t}(\boldsymbol{\beta})$), as shown in Equation (14).

$$q_{RC_t} = q_t + E_{RC_t}(\boldsymbol{\beta}) \tag{14}$$

The errors are considered normally distributed, centered on zero, and heteroscedastic, as defined by Equation (15), in which $\beta_0$ represents the intercept and $\beta_1$ represents the slope for the model errors.

$$E_{RC_t}(\boldsymbol{\beta}) \sim N\,(0, (\beta_0 + q_{RC_t}\beta_1)^2) \tag{15}$$

Errors associated with the stage measurements are assumed to be negligible, as proposed by Le Coz et al. (2014), while discharge measurement errors are considered normally distributed, centered on zero, and with a standard deviation $\delta$ determined based on the utilized measurement equipment. The measured discharge ($q_{m_t}$) is defined as presented in Equation (16).

$$q_{m_t} = q_t + E_{m_t} \quad E_{m_t} \sim N(0, {\delta_t}^2) \tag{16}$$

Combining Equations (14) and (16), the discharge from the rating curve can be defined by Equation (17).

$$q_{m_t} = q_{RC_t} - E_{RC_t}(\boldsymbol{\beta}) + E_{m_t} \quad (17)$$

The likelihood function for the discharges is presented in Equation (18), and it is centered on the rating curve discharge, with variance given by the sum of the rating curve error variance and the measurement error variance. Formally:

$$p(\boldsymbol{q_m}|\boldsymbol{\theta_{RC}}, \boldsymbol{\beta}, \boldsymbol{h_m}) = \prod_{i=1}^{N} N\left(q_{m_{ti}}; q_{RC_{ti}}, (\beta_0 + q_{RC_t} \cdot \beta_1)^2 + \delta_{ti}^2\right) \quad (18)$$

The prior distribution of the rating curve parameters and model errors were defined following the methodology proposed by Le Coz et al. (2014). Discharge was represented using a piecewise power-law formulation, as presented in Equation (19).

$$Q_{RC_t} = \sum_{r=1}^{N_{range}} \left( \mathbf{1}_{[k_{r-1};k_r]}(h_t) \times \sum_{j=1}^{N_{control}} M(r,j) \times a_j \left(h_t - b_j\right)^{c_j} \right) \quad (19)$$

in which $Q_{RC}$ denotes the discharge estimated by the rating curve; $h_t$ is the observed water level; and the parameters $a_j$, $b_j$ and $c_j$ depend on the hydraulic control at the cross section. The function $\mathbf{1}_{[k_{r-1};k_r]}$ assumes 1 if $k_{r-1} \leq h_t \leq k_r$ and 0 otherwise. The parameter $k_r$ define transition stages between successive ranges $r$ and $r + 1$, and require prior specification. This formulation ensures streamflow continuity across stage ranges.

Therefore, defining prior distributions requires a hydraulic analysis to identify the hydraulic controls governing the cross-section across different stage ranges. The authors propose four different control types: channel control and section controls corresponding to rectangular, triangular and orifice shapes. According to the paper, “Most natural channels and artificial canals present cross-sectional shapes that can be fairly approximated by a wide rectangle, or a mixture of wide rectangles”. Based on this proposal and considering the characteristics of the Jardim station, channel control was adopted, assuming the idealized conditions of wide rectangular section and steady, uniform flow for both the channel and the floodplain, which were treated as different stages. This representation and these idealized assumptions constitute a simplification of the actual hydraulic conditions at the sections; therefore, some

deviations may occur. Nevertheless, these simplifications are necessary for approximating the rating curve model to the theoretical reference regime.

Uniform flow can be described by the Manning-Strickler formulation, presented in Equation (20).

$$Q = A\,{}^{1}\!/_{n}\,\mathrm{S}^{1/2}R_h{}^{2/3} \tag{20}$$

in which $A$ is the area cross-section, $n$ is the Manning roughness coefficient, $S$ is the bed slope of the river reach and $R_h$ is the hydraulic radius of the cross-section.

For cross sections governed by channel control, which follows the assumption of rectangular section with uniform flow, as considered for Jardim station, the theoretical mean values for the prior distribution of the coefficients $a$, $b$ and $c$ are presented in Table 2, where $B = \frac{\partial A}{\partial y}$ represents the channel top width. Hence, prior distributions for the rating curve parameters are defined based on the hydraulic characteristics of the cross-section.

**Table 2 - Mean prior values for parameters a, b and c in the case of channel control for wide rectangular sections**

| Control type | Ideal assumptions | a | b | c |
|---|---|---|---|---|
| Channel | Wide rectangle, steady and uniform flow | ${}^{1}\!/_{n}\,BS^{1/2}$ | Average bed level | 5/3 |

Source: Adapted from Le Coz et al. (2014)

The variance of the parameter $a$ is defined by the law of propagation of uncertainty, based on a first-order Taylor series approximation, as defined in JCGM (2008), presented in Equation (21).

$$VAR[a] = \left(\frac{\sqrt{S}}{n}\right)^2 \cdot VAR[B] + \left(-\frac{B\sqrt{S}}{n^2}\right)^2 \cdot VAR\,[n] + \left(\frac{B}{2n\sqrt{S}}\right)^2 \cdot VAR[S] \tag{21}$$

After the definition of the likelihood function and the prior distributions, the parameter's posterior distribution is expressed in Equation (22).

$$\underbrace{p(\boldsymbol{\theta_{RC}}, \boldsymbol{\beta} \mid \boldsymbol{h_m}, \boldsymbol{q_m})}_{\text{posterior}} \propto \underbrace{p(\boldsymbol{q_m} \mid \boldsymbol{\theta_{RC}}, \boldsymbol{\beta}, \boldsymbol{h_m})}_{\text{likelihood}} \times \underbrace{p(\boldsymbol{\theta_{RC}}, \boldsymbol{\beta})}_{\text{prior}} \tag{22}$$

In which $\boldsymbol{h_m}$ and $\boldsymbol{q_m}$ are, respectively, the vectors of measured stages and discharges. Bayesian inference was performed as described in Subsection 4.5. The code used in this study is provided in Appendix A.

After obtaining the posterior distributions for the parameters, they were analyzed through a descriptive analysis, and an evaluation of the distributions using histograms was performed. Also, they were compared with prior distributions in order to evaluate how the knowledge introduced by the data impacted the prior distributions. Finally, they were analyzed using a scatterplot, aiming to understand the correlation among parameters.

Subsequently, the rating curve was constructed according to Equation (13), using the parameters derived from each MCMC iteration. The median and the 95% credible interval were analyzed, resulting in discharge estimates that account for parametric uncertainty. Then, structural uncertainty was incorporated. Hence, total uncertainty bands were calculated for each iteration, considering a normal distribution, centered on the predicted discharge by the rating curve, and with standard deviation given by the error model prescribed in Equation (15).

The median values and the 95% credible interval were analyzed. The gauging data were plotted against the predicted discharges incorporating parametric and total uncertainty to evaluate the coverage probability.

Lastly, the residuals were analyzed to verify whether the underlying assumptions were satisfied. Specifically, heteroscedasticity, serial correlation, and normality of the residuals were investigated. For this analysis, the error was calculated as the difference between observed discharge and the median discharge predicted by the rating curve, accounting for total uncertainty. The standard deviation was determined using Equation (23).

$$sd = \frac{Q_{upper} - Q_{lower}}{4} \tag{23}$$

Where $Q_{upper}$ consists of the 97,5% uncertainty band and $Q_{lower}$ on the 2,5% one, and the denominator provides an approximation for the quantile range associated with the

95% probability. The standardized residuals were calculated by dividing the error by the standard deviation.

### 4.2.1 Jardim Station

Two rating curves were constructed, one using available measured discharge data and another neglecting these data, simulating a scenario without discharge observations.

To determine the rating curve, stage-discharge gaugings and cross-section data from the platform HIDROWEB (ANA, 2025b) were used. Consistently processed gauging from 1978 until 2023 is shown in Figure 5, where it can be observed that the data cluster into two distinct groups. Investigations show that, on October 10$^{th}$, 1999, there was a change in the stage reference of the station. Considering that the consistently processed hourly data (for precipitation, evaporation, and stages) are available from 01/08/1997 until 05/28/2008, a single rating curve covering the period from 1999 to 2023 was constructed, encompassing most of the available data. The decision was to use the data directly as provided by HIDROWEB, rather than attempting to adjust the staff gauge and introduce additional sources of uncertainty, even though some of the discarded sample points could improve the estimation of high flows. This resulted in 84 available discharge gaugings, with stages varying from 91 to 166 cm, as shown in Figure 6.

**Figure 5 - Available gauging for Jardim Station**

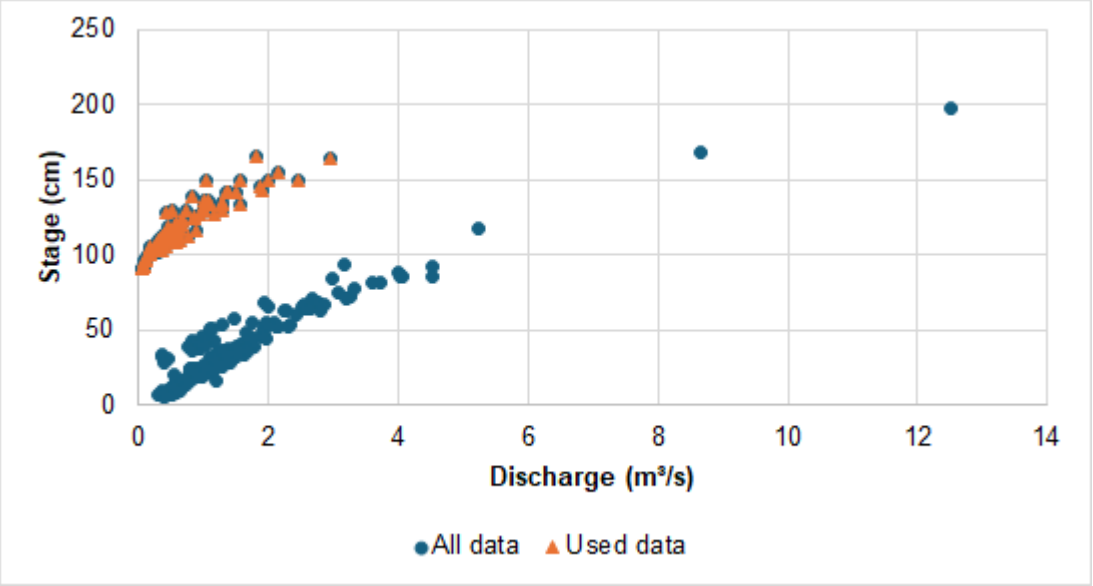


Source: Adapted from ANA (2025b)

**Figure 6 - Used gauging for Jardim Station**

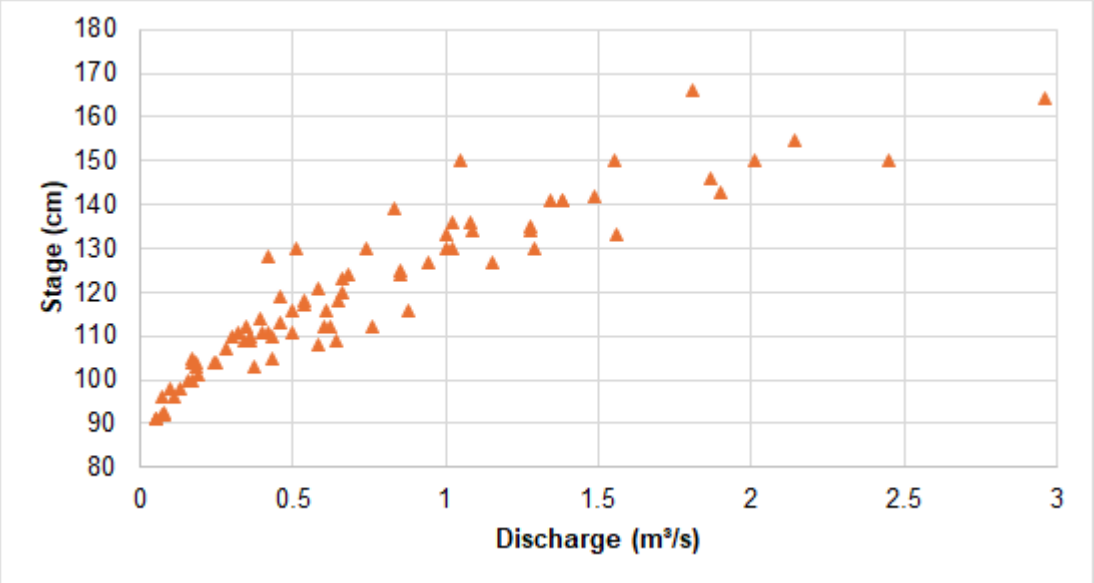


Source: Adapted from ANA (2025b)

Cross-sections are available at two locations: at the sections where there are stage measurements or where there are discharge measurements. Only consistently processed data from the discharge measurement section was used, which resulted in 15 cross-sections, as shown in Figure 7.

**Figure 7 - Cross-section data for Jardim Station**

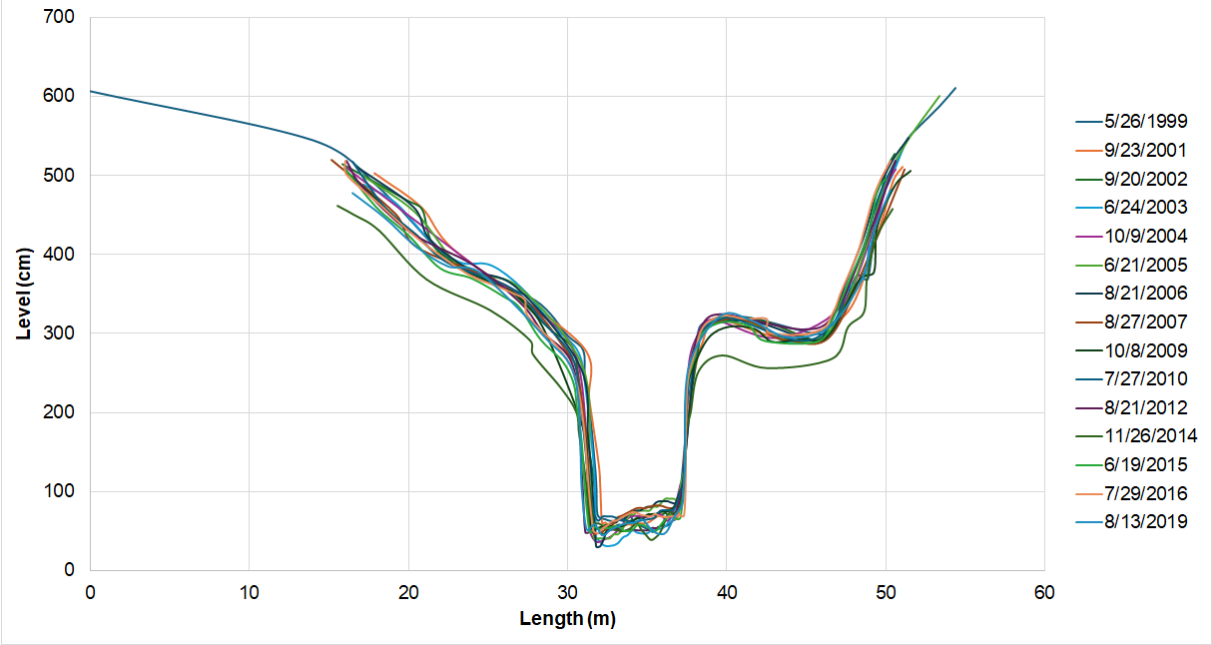


Source: Adapted from ANA (2025b)

Based on the hydraulic behavior of the cross-sections, analyzed considering channel geometry, roughness, expert knowledge, and previous studies, uniform flow conditions were assumed for both low flows (main channel) and high flows (floodplain). Hence, a two-segment power law was defined: $k_1$ represents the average bed level and $k_2$ corresponds to the mean floodplain elevation, presented in Figure 8. Formally, based on the proposal by Le Coz et al. (2014):

$$f_{rc}(h_t, \boldsymbol{\theta_{rc}}) = \begin{cases} a_1(h_t - b_1)^{c_1}, & \text{if } k_1 < h_t < k_2 \\ a_1(h_t - b_1)^{c_1} + a_2(h_t - b_2)^{c_2}, & \text{if } k_2 < h_t \end{cases} \quad (24)$$

Based on the analysis of the cross-sections, parameters $b_1$ and $b_2$, were defined to represent the average bed level and the mean floodplain elevation, respectively, and were assumed equal to the activation stages $k_1$ and $k_2$. These parameters were assumed to follow a normal distribution centered on the mean values, with standard deviations large enough to encompass the temporal variations observed in the cross sections, as indicated in Figure 8.

Parameters $B_1$ and $B_2$, representing the average width of the channel cross-section and the floodplain, respectively, were assumed to follow uniform distributions, with lower and upper bounds defined to encompass the observed variations in the cross

sections over time, as presented in Figure 9. To define these parameters, it was assumed that the cross-section was wide rectangle. However, for the floodplain, the left bank approximates a trapezoidal geometry instead of a rectangular one. To account for this geometry, the effective width ($B_2$) was adjusted, as shown in Figure 9.

**Figure 8 - Cross-sections for Jardim Station - $k_1$ and $k_2$ parameters**

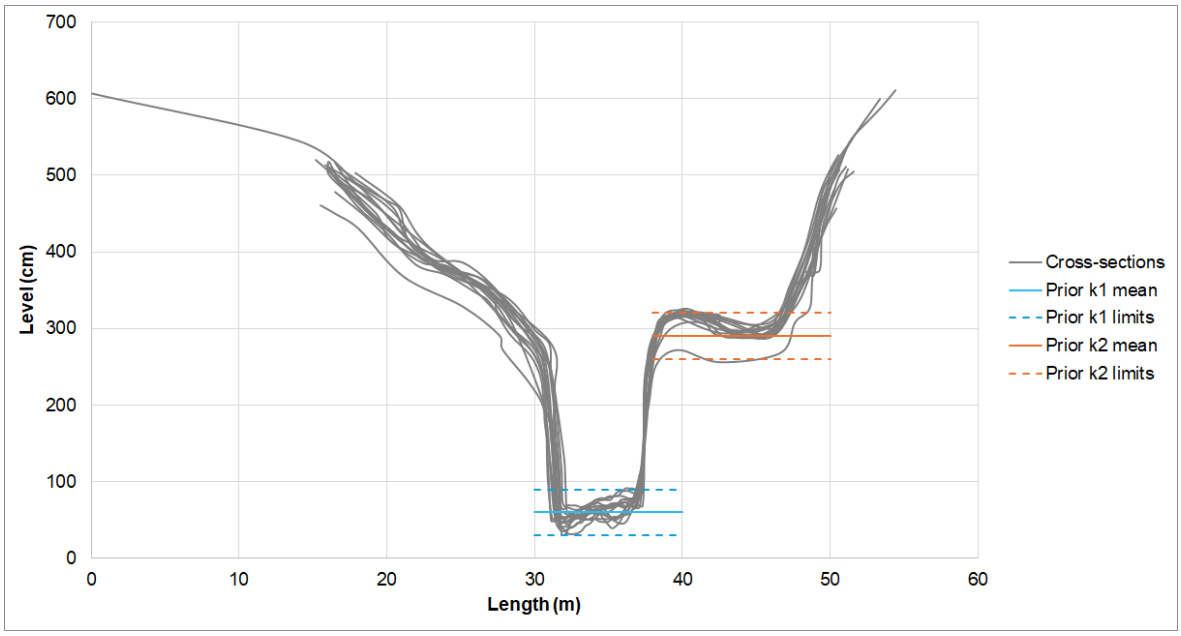


Source: Adapted from ANA (2025b)

**Figure 9 - Cross sections for Jardim Station – $B_1$ and $B_2$ parameters**

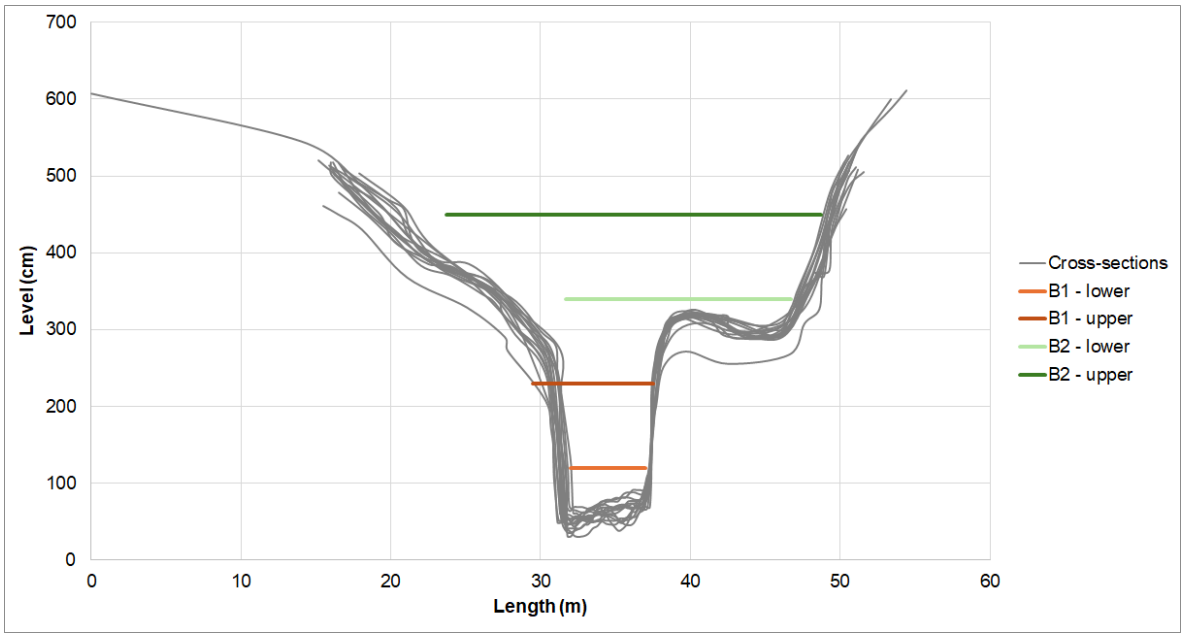


Source: Adapted from ANA (2025b)

The values for the Manning roughness coefficient were determined based on the range presented in the literature (Baptista; Lara, 2016) and on expert knowledge. A Gaussian distribution was assumed for the Manning coefficient, and the midpoint of the reported range was adopted as the mean of the Gaussian distribution. The standard deviation was calculated considering that the range corresponded to the 95% confidence interval, according to Equation (25).

$$n_{sd} = \frac{n_{upper} - n_{mean}}{1.96} \tag{25}$$

in which:

- $n_{sd}$ is the standard deviation for the Manning coefficient;
- $n_{upper}$ is the upper limit of the range for the Manning coefficient; and
- $n_{mean}$ is the mean value of the Manning coefficient considered.

Since two hydraulic controls were identified, two values for the Manning coefficients were defined: for the channel ($n_c$), when $k_1 < h_t < k_2$ and for the floodplain ($n_p$), when $k_2 < h_t$.

Topographic data from the Digital Terrain Model for South America (ANA, 2025c), which has a spatial resolution of 30 meters, were analyzed. However, the available data resolution was incompatible with the intended analysis. Hence, the values for the slope were defined based on expert knowledge.

Lower and upper bounds defined for each variable ($B$, $S$ and $n$) were used to constrain the parameters within specific ranges during sampling for determining the posterior distribution.

Based on the presented information, the prior distributions for the rating curve parameters ($a_1$, $b_1$, $c_1$, $a_2$, $b_2$, $c_2$) were defined – all of them following a Gaussian distribution. For the error model coefficient, $\beta_0$, equivalent to the intercept, it was considered to follow a lognormal distribution - $\beta_0$ ~ lognormal (1, 1); and $\beta_1$, related to the slope, was also considered to follow a lognormal distribution - $\beta_0$ ~ lognormal (0.5, 1), following the approach performed by Mansanarez et al. (2019a). The parameters $a_1$, $c_1$, $a_2$, $c_2$, $\beta_0$, $\beta_1$ were constrained to positive values.

Finally, the discharge measurement uncertainty parameter $\delta$ was defined. For this purpose, the measurement equipment used during discharge gauging campaigns was analyzed: 11 measurements were performed using a FlowTracker, three measurements were conducted with a RiverSurveyor–19, and for the remaining measurements, no information regarding the equipment was available; therefore, the use of a hydrometric propeller was assumed in these cases. Considering that the measurement uncertainty associated with the FlowTracker is approximately 5% (WSC, 2015), a slightly more conservative value was adopted. A discharge measurement uncertainty of 8% was assumed for all measurements.

## 4.3 Rainfall-stage hydrological model

Once parametric and structural uncertainties of the rating curve were defined, the parameters of the rainfall-stage model were calibrated following the methodology proposed by Sikorska and Renard (2017). Two models were developed, one using the estimated rating curve and the other using the prior one.

The objective of the rainfall-stage model is to calibrate the model parameters using stage observations, based on the assumption that the stage measurement errors are negligible. This allows the elimination of the additional uncertainty resulting from the calibration based on the discharges given by the rating curve. For this, the first step consists of defining the hydrological model to be used.

### 4.3.1 Hydrological model GR4H

The hydrological model GR4H (Génie Rural à 4 paramètres Horaires) was chosen due to its simple structure and low computational cost (Chancay; Espitia-Sarmiento, 2021). The models GR4H and GR4J have been widely used and have performed similarly to other conceptual hydrological models (Ayzel; Heistermann, 2021; Bennett et al., 2014; Le Moine; Andréassian; Mathevet, 2008; Li et al., 2017; Van Esse et al., 2013). Moreover, the model enables hourly simulation, compatible with the dimensions of basins that suffer from flash floods.

The GR4H model was proposed by Mathevet (2005), based on the adaptations from the GR4J model (Modèle du Génie Rural à 4 paramètres Journalier), developed by Perrin, Michel and Andréassian (2003). The hourly model follows the same structure as the daily one, with adjustments to specific process factors to better represent hydrological processes at the hourly time scale. It consists of a lumped, deterministic, abstract model with process parameters. Table 3 presents a description of the GR4H model parameters.

**Table 3 - Description of GR4H model parameters**

| Parameter | Description |
|---|---|
| $x_1$ | Maximum capacity of the production store (mm) |
| $x_2$ | Groundwater exchange coefficient (mm/hour) |
| $x_3$ | Maximum capacity of the routing store (mm) |
| $x_4$ | Time base of the unit hydrograph UH1 (hour) |

Source: Adapted from Perrin, Michel and Andréassian (2003)

Figure 10 presents the diagram of the GR4H model for a given time step, corresponding to a discrete model formulation. All water quantities are given in millimeters (mm). The description presented is based on Perrin, Michel and Andréassian (2003), with adjustments on some factors when necessary.

**Figure 10 - Diagram of the GR4H rainfall-runoff model**

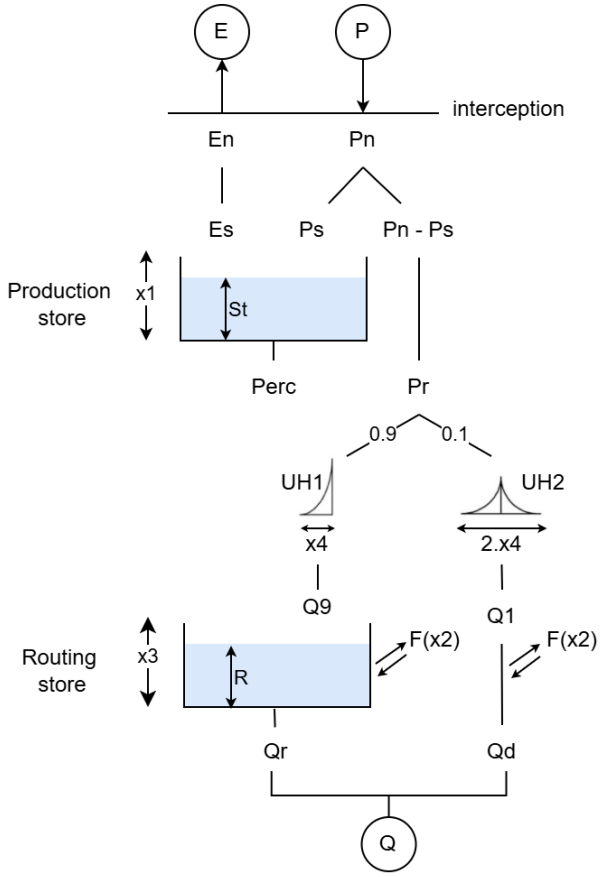


Source: Adapted from Perrin, Michel and Andréassian (2003)

Rainfall ($P$) and potential evapotranspiration ($E$) constitute the model inputs. Rainfall represents an estimation of the mean areal precipitation over the catchment, while potential evapotranspiration is considered to be a long term-average, implying that the same evapotranspiration series is repeated annually.

The first step consists of determining the net rainfall ($P_n$) or net evapotranspiration ($E_n$), given by Equations (26) and (27).

$$\text{If } P \geq E, then\ P_n = P - E\ and\ E_n = 0 \tag{26}$$

$$\text{otherwise } P_n = 0\ and\ E_n = E - P \tag{27}$$

Then, based on the previous step, the production store is updated. If $P \geq E$, a fraction of $P_n$ named $P_s$ goes to the production store, according to Equation (28).

$$P_s = \frac{x_1 \left(1 - \left(\frac{St}{x_1}\right)^2\right) \tanh\left(\frac{P_n}{x_1}\right)}{1 + \frac{S}{x_1} \tanh\left(\frac{P_n}{x_1}\right)} \tag{28}$$

in which $St$ represents the level of the production store and $x_1$ is the Maximum capacity of the production store (mm) (see Table 3).

When $E \geq P$, the level of the production store is reduced based on the evaporation rate $E_s$, determined according to Equation (29).

$$E_s = \frac{St \left(2 - \frac{S}{x_1}\right) \tanh\left(\frac{E_n}{x_1}\right)}{1 + \left(1 - \frac{S}{x_1}\right) \tanh\left(\frac{E_n}{x_1}\right)} \tag{29}$$

Thus, the production store is updated, according to Equation (30). It's important to note that the level of $St$ is limited by parameter $x_1$ and can never exceed it.

$$St = St - E_s + P_s \tag{30}$$

The production store is reduced due to the percolation leakage, calculated by Equation (31). On the GR4J, the fraction is 4/9, however this value is adjusted to 4/21 on the hourly model, due to the change on time scale, to prevent the soil moisture from draining too quickly (Bennett et al., 2014).

$$Perc = St \left\{1 - \left[1 + \left(\frac{4}{21} \frac{St}{x_1}\right)^4\right]^{-1/4}\right\} \tag{31}$$

Hence, the level of the reservoir is updated again, according to Equation (32):

$$St = St - Perc \tag{32}$$

Then, the quantity of water propagated in the channel phase is given by $P_r$ and can be calculated by Equation (33).

$$P_r = Perc + (P_n - P_s) \tag{33}$$

Subsequently, the value of $P_r$ is partitioned into two components, $UH_1$ and $UH_2$, which together represent the time lag between rainfall occurrence and the corresponding streamflow peak. The use of unit hydrograph ordinates enables the redistribution of effective rainfall over multiple consecutive time steps. 90% of $P_r$ is directed to the unit hydrograph $UH_1$, which has a time base of $x_4$ hours, and then is directed to the routing store ($R$), when the propagation is non-linear. The rest of $P_r$, 10%, is directed to the unit hydrograph $UH_2$, with time base of $2\,x_4$ hours. The split 90% - 10% was kept as proposed in the original paper; however, in an adaptation of the GR4H model for a urbanized catchment, Saadi, Oudin and Ribstein (2021) proposed that this fraction must be calibrated, represented by a new parameter.

The $UH_1$ and $UH_2$ ordinates are derived from $SH_1$ and $SH_2$, respectively, which represent S-curves describing cumulative proportion of the input as a function of time.

$$SH_1(t) = \begin{cases} 0 & \text{for } t \leq 0 \\ \left(\frac{t}{x_4}\right)^{5/4} & \text{for } 0 < t < x_4 \\ 1 & \text{for } t \geq x_4 \end{cases} \tag{34}$$

$$SH_2(t) = \begin{cases} 0 & \text{for } t \leq 0 \\ \frac{1}{2}\left(\frac{t}{x_4}\right)^{5/4} & \text{for } 0 < t \leq x_4 \\ 1 - \frac{1}{2}\left(2 - \frac{t}{x_4}\right)^{5/4} & \text{for } x_4 < t < 2x_4 \\ 1 & \text{for } t \geq 2x_4 \end{cases} \tag{35}$$

Another difference between the GR4J and G4RH model is observed here: the exponent 5/4 instead of 5/2 for the term $\left(\frac{t}{x_4}\right)$. The reduction on the exponent allows the attenuation of the unit hydrograph, necessary due to the change from daily to hourly scale (Bennett et al., 2014).

Then, the ordinates from $UH_1$ and $UH_2$ can be calculated as presented on Equations (36) and (37).

$$UH_1(j) = SH_1(j) - SH_1(j-1) \quad (36)$$

$$UH_2(j) = SH_2(j) - SH_2(j-1) \quad (37)$$

in which $j$ is an integer. If $x_4$ is set as 3.8 hours, for example, $UH_1$ has 4 ordinates and $UH_2$ has 8. Therefore, the flows from each parcel can be calculated as presented on Equations (38) and (39).

$$Q9(i) = 0{,}9. \sum_{k=1}^{l} UH\ 1(k). Pr(i-k+1) \quad (38)$$

$$Q1(i) = 0{,}1. \sum_{k=1}^{m} UH\ 2(k). Pr(i-k+1) \quad (39)$$

With $l = int\,(x_4) + 1$ and $m = int\,(2\,x_4) + 1$, with int(.) being the integer part.

A groundwater exchange term, representing gains or losses, is then applied to the routing store and $Q_1$ can be calculated by Equation (40).

$$F = x_2 \left(\frac{R}{x_3}\right)^{7/2} \quad (40)$$

in which:

- $R$ is the level in the routing store (mm);
- $x_3$ is the maximum capacity for the routing store (mm); and
- $x_2$ is the water exchange coefficient (mm/hour). It can represent water gain (when positive), losses (when negative), or the absence of exchange between groundwater (when zero).

The water exchange term $F$ is bounded by $x_2$, since the parameter defines the maximum amount of water that can be added or removed from each flow component regarding the routing store.

After accounting for the catchment water exchange, the level of the routing store is updated by Equation (41).

$$R = max(0; R + Q_9 + F) \tag{41}$$

The outflow $Q_r$ from the routing store can be calculated by Equation (42).

$$Q_r = R\left\{1 - \left[1 + \left(\frac{R}{x_3}\right)^4\right]^{\frac{-1}{4}}\right\} \tag{42}$$

The level on the reservoir is updated one more time according to Equation (43). This component enables the representation of prolonged streamflow recessions when such behavior is required.

$$R = R - Q_r \tag{43}$$

The parcel of $P_r$ that went to $UH_2$ is also affected by groundwater exchange, and the flow is calculated according to Equation (44).

$$Q_d = max(0; Q_1 + F) \tag{44}$$

Finally, the total streamflow can be calculated by Equation (45).

$$Q = Q_r + Q_d \tag{45}$$

This model was implemented in STAN, according to the equations presented above. The results for a deterministic run were compared with the results from the "RunModel_GR4H" function from R package AirGR, and the difference was observed beyond the eighth decimal place.

The GR4H model has two state variables: the level of the reservoir $St$, representing the production store, and the level of the reservoir $R$, representing the routing store. The default values for the first step are presented in Equations (46) and (47).

$$St[1] = 0.3 \cdot x_1 \quad (46)$$

$$R[1] = 0.5 \cdot x_3 \quad (47)$$

An attempt to calibrate the state variables was made. However, parametric uncertainty increased significantly, while predictive performance did not improve. Therefore, the approach chosen was adding a burn-in period of three months at the beginning of the simulation, at the end of the dry period, allowing sufficient time for the model to empty the reservoirs. This burn-in period was excluded from the likelihood calculation. This approach is consistent with the findings of Huard and Mailhot (2008), who founded that uncertainty associated with the initial state of the model persists only during the first few months of simulation. After this, the internal states converge toward a stable state. The authors used the GR2M model, which belongs to the same family as GR4H but operated at a monthly time step. Based on this behavior, they concluded that, for sufficiently long time series, explicitly accounting for initial state uncertainty has only a marginal influence on model results.

To define the prior distributions for the model parameters, literature values were analyzed. The median values and the 80% confidence interval reported by Perrin, Michel and Andréassian (2003) for the GR4J model is presented in Table 4.

**Table 4 - Values of median model parameters and 80% confidence interval for the GR4J model**

| GR4J Parameter | Median value | 80% Confidence interval |
|---|---|---|
| $x_1$ (mm) | 350 | 100 - 1200 |
| $x_2$ (mm) | 0 | -5 to 3 |
| $x_3$ (mm) | 90 | 20 - 300 |
| $x_4$ (days) | 1.7 | 1.1 – 2.9 |

Source: Perrin, Michel and Andréassian (2003)

Since the median value was not positioned on the range mean, an asymmetric distribution was chosen: in this case, the lognormal distribution.

Ranges used for the GR4H model parameters were searched in the literature, and the results found are presented in Table 5. The work by Matos and Silva (2024) was performed in Jardim Station.

**Table 5 - Ranges for the GR4H model parameters**

| GR4H Parameter | Ranges | | | |
|---|---|---|---|---|
| | **Ayzel and Heistermann (2021)** | **Hann Coulibaly and Biondi (2019)** | **Haruna et al. (2022)** | **Matos and Silva (2024)** |
| $x_1$ (mm) | 0.1 - 1500 | 1 - 2000 | 1 - 1500 | 500 - 5000 |
| $x_2$ (mm) | -10 - 10 | -10 - 5 | -10 - 10 | -10 - 10 |
| $x_3$ (mm) | 0.1 - 500 | 1 - 500 | 0 - 500 | 1 - 500 |
| $x_4$ (hours) | 0.5 - 24 | 0.5 - 96 | 0 - 10 | 0.5 - 20 |

Based on various simulations, parameters intervals were narrowed to improve model performance. Retaining excessively wide ranges proved to be counterproductive, as it hindered the convergence of the rainfall-stage model. Also, the $x_2$ parameter proved to be highly sensitive, the most sensible among all parameters: while keeping the remaining parameters centered around the mean value of their respective ranges, changing it from -10 mm to 10mm resulted in the biggest difference in the generated discharges. Given that this research focuses on flash floods and high-flow events, groundwater exchange should have a minor impact. The $x_2$ parameter was therefore restricted to values close to zero, representing minimal groundwater exchange.

After the establishment of the ranges, in order to use the lognormal distribution, the mean and the standard deviation were calculated based on Equations (48) and (49).

$$mean_{\ln} = \frac{\ln(x_{upper}) + \ln(x_{lower})}{2} \tag{48}$$

$$sd_{\ln} = \frac{\ln(x_{upper}) - mean_{\ln}}{1.96} \tag{49}$$

The ranges and the parameters for the lognormal distribution for the GR4H parameters are presented in Table 6. The $x_2$ parameter was assumed to follow a uniform distribution, due to the restricted range considered.

**Table 6 - Adopted ranges for the GR4H model parameters**

| GR4H Parameter | Range | $\bar{x}_{ln}$ | $sd_{ln}$ |
|---|---|---|---|
| $x_1$ (mm) | 1 - 2000 | 3.800451 | 1.939006 |
| $x_2$ (mm) | -1 to 0.3 | - | - |
| $x_3$ (mm) | 0.01 - 500 | 0.804719 | 2.760148 |
| $x_4$ (hours) | 0.01 - 10 | -1.151293 | 1.762182 |

### 4.3.2 Rainfall-stage model

After defining the hydrological model, the remaining components of the rainfall-stage model can be formulated. As for the rating curve calibration step, Bayesian inference was performed using the STAN software to calibrate the parameters of the hydrological model, also using the MCMC method. A more detailed description of the methodology applied for Bayesian analysis is provided in Subchapter 4.5.

The model was constructed based on the method proposed by Sikorska and Renard (2017). For the calibration of the model parameters, the first step is the computation of discharges, using the chosen hydrological model, according to Equation (50).

$$q_{HM_t} = f_{HM}((p,e)_{\mathbf{1:}\boldsymbol{t}}, \boldsymbol{\theta_{HM}}) \tag{50}$$

in which $(p,e)_{\mathbf{1:}\boldsymbol{t}}$ is the vector of input data and $\boldsymbol{\theta_{HM}}$ is the vector of hydrological model parameters (in this case, $x_1$, $x_2$. $x_3$ and $x_4$). As presented for the predictive discharges from the rating curve (Equation (14)), it is possible to consider a structural error $B_t$ which accounts for the difference between the discharge predicted by the hydrological model $q_{HM}$ and the true (unknown) discharge $q$, as presented in the Equation (51). In a complementary way, a transformation $\psi$ is performed. In this case, a Box-Cox transformation was chosen, which aims to transform the residual distribution closer to a Gaussian distribution.

$$\psi\left(q_{HM_t}\right) = \psi(q_t) + B_t(\sigma, \phi) \tag{51}$$

The Box-Cox transformation (Box; Cox, 1982) can be described by Equation (52).

$$\psi(y) = \begin{cases} \left(y^{\lambda} - 1\right)/\lambda & (\lambda \neq 0) \\ \ln(y) & (\lambda = 0) \end{cases} \tag{52}$$

Here, $\lambda = 0$ was utilized, which corresponds to a logarithmic transformation of discharge.

The residuals are considered autocorrelated, with a correlation structure similar to a first-order autoregressive process, i.e., an AR (1) model. An Ornstein-Uhlenbeck (OU) process (Uhlenbeck; Ornstein, 1930) was used, with a covariance function given by Equation (53).

$$Var\big(B_t(\sigma,\phi)\big) = \sigma^2 \cdot \exp\left(\frac{-\left|t_i - t_j\right|}{\phi}\right) \tag{53}$$

in which $\sigma$ represents the asymptotic standard deviation for infinitely spaced time points and $\phi$ is a characteristic correlation time (Sikorska; Renard, 2017).

By combining Equations (13), (14) and (51), the true stage at time $t$, $h_t$, can be defined via Equation (54).

$$h_t = {f_{RC}}^{-1}\Big(\psi^{-1}\big[\psi\big(q_{HM_t}\big) - B_t(\sigma,\phi)\big] + E_{RC_t}(\boldsymbol{\beta})\Big) \tag{54}$$

A first-order approximation of the backward transformation $\psi^{-1}$ based on a first-order Taylor expansion is applied, according to Equation (55).

$$\begin{aligned}\psi^{-1}\big[\psi\big(q_{HM_t}\big) - B_t(\sigma,\phi)\big] \\ \approx\ \psi^{-1}\big[\psi\big(q_{HM_t}\big)\big] - \ (\psi^{-1})'\big[\psi\big(q_{HM_t}\big)\big]\ x\ B_t(\sigma,\phi)\end{aligned} \tag{55}$$

The inverse-derivative rule is used, according to Equation (56).

$$(\psi^{-1})'(z) = \frac{1}{(\psi)'(\psi^{-1}(z))} \tag{56}$$

Therefore, applying this rule to Equation (55) results in Equation (57).

$$\begin{aligned}\psi^{-1}\big[\psi\big(q_{HM_t}\big) - B_t(\sigma,\phi)\big] \ &\approx\ q_{HM_t} - \frac{B_t(\sigma,\phi)}{\psi'\big(\psi^{-1}\big[\psi\big(q_{HM_t}\big)\big]\big)} \\ &=\ q_{HM_t} - \frac{B_t(\sigma,\phi)}{\psi'\big(q_{HM_t}\big)}\end{aligned} \tag{57}$$

Finally, equation (58) is derived:

$$h_t \approx {f_{RC}}^{-1}\left(q_{HM_t}(\boldsymbol{\theta_{HM}}) - \frac{B_t(\sigma,\phi)}{d_t^{(\psi)}(\boldsymbol{\theta_{HM}})} + E_{RC_t}(\boldsymbol{\beta}), \boldsymbol{\theta_{RC}}\right) \tag{58}$$

The term $q_{HM_t}(\boldsymbol{\theta_{HM}}) - \frac{B_t(\sigma,\phi)}{d_t^{(\psi)}(\boldsymbol{\theta_{HM}})} + E_{RC}(\boldsymbol{\beta})$ is assumed to follow a multivariate Gaussian distribution, with mean vector $\boldsymbol{\mu}$ with size N (where N is the number of data), given by Equation (59) and covariance matrix $\boldsymbol{\Sigma}$ (size N x N), defined by Equation (60).

$$\mu(\boldsymbol{\theta_{HM}}) = \Big(q_{HM_{t_1}}(\boldsymbol{\theta_{HM}}), \ldots, q_{HM_{t_N}}(\boldsymbol{\theta_{HM}})\Big) \tag{59}$$

$$\Sigma(\boldsymbol{\theta_{HM}}, \sigma, \phi, \boldsymbol{\beta}) = D^{(\psi)}\Sigma^{(HM)}D^{(\psi)} + \Sigma^{(RC)} \tag{60}$$

The matrix $\Sigma(\boldsymbol{\theta_{HM}}, \sigma, \phi, \boldsymbol{\beta})$ incorporates the structural errors from the hydrological model (presented on Equations (61) e (62)), and from the rating curve, as presented in the Equation (63).

$$D^{(\psi)}(i,i) = \frac{1}{d_{t_i}^{(\psi)}(\theta_{HM})}; D^{(\psi)}(i,j) = 0 \; if \; i \neq j \tag{61}$$

$$\Sigma^{(HM)}(i,j) = \sigma^2 \cdot \exp\left(\frac{-|t_i - t_j|}{\phi}\right) \tag{62}$$

$$\Sigma^{(RC)}(i,i) = \left(\beta_0 + \beta_1 \cdot q_{HM_{t_i}}\right)^2; \Sigma^{(RC)}(i,j) = 0 \; \; if \; i \neq j \tag{63}$$

Based on these considerations, the likelihood function is presented in Equation (64), and considers that the stage distribution follows a multivariate Gaussian distribution, assessed at the discharge given by the rating curve, with mean vector based on the hydrological model and covariance matrix $\boldsymbol{\Sigma}$, which accounts for the structural errors both from the hydrological model and the rating curve.

$$\begin{aligned} p(\boldsymbol{h}|\boldsymbol{\theta_{HM}}, \boldsymbol{\theta_{RC}}, \sigma, \phi, \boldsymbol{\beta}, \boldsymbol{p}, \boldsymbol{e}) \\ = f_{MG}\left(f_{RC}(h, \theta_{RC}); \mu(\boldsymbol{\theta_{HM}}), \Sigma(\boldsymbol{\theta_{HM}}, \sigma, \phi, \boldsymbol{\beta})\right) \\ \times \prod_{k=1}^{N} \left|\left(f'_{RC}\left(h_{t_k}, \boldsymbol{\theta_{RC}}\right)\right)\right| \end{aligned} \tag{64}$$

Due to the change of variables from discharge to stage, the Jacobian term arises (given by $\prod_{k=1}^{N} \left|\left(f'_{RC}\left(h_{t_k}, \boldsymbol{\theta_{RC}}\right)\right)\right|$) to adjust the probability distribution.

The prior distribution for the GR4H hydrological model parameters were presented in the Subchapter 4.3.1. For the model error of the hydrological model, a sensitivity analysis was performed for better understanding the impact of the parameters. The parameter $\sigma$ was then defined following a uniform distribution, limited to 0.20, to match the order of magnitude from the discharges calculated by the model on the unit mm.

Ammann, Fenicia, and Reichert (2019) discuss the non-stationarity of residuals auto-correlation: while on dry season a higher autocorrelation is expected, this is reduced on the wet season. The Jardim catchment, as previously presented, has two well-established seasons, and a three-month period with no rainfall could lead to $\phi$ values higher than 2000. However, this value is largely reduced on the rainy season. Drumond (2004) used tracers to define the time of concentration on some basins, including the

drainage area for Jardim Station basin, and found that the time of concentration tends to approximately 15.5 hours. Considering the focus of the study on flood events, lower values of $\phi$ were therefore adopted, and the parameter was limited to a maximum of 200 hours. Moreover, high values of $\phi$ lead to computational trouble in calculating the likelihood function. As for the parameters for the hydrological model, a non-symmetric distribution was chosen, and the lognormal distribution was used, with mean equal to 50 hours. Therefore, $\phi$ parameter was considered as: $\phi$ ~ lognormal (3.912023, 1).

The prior distributions for the rating curve parameters are obtained from the posterior distributions given by the BaRatin method, as presented in the Subchapter 5.1. While Sikorska and Renard (2017) considered that the prior distribution for the rating curve parameters followed a multivariate Gaussian distribution, the choice here was to consider an individual distribution for each parameter. This was made for two main reasons: (1) the correlation between parameters was low, as presented in Subchapter 5.1.1; and (2) to allow the parameters to be restricted to positive values. Also, this could be used in case any of the parameters did not follow a Gaussian distribution. Additionally, as done by Sikorska and Renard (2017), the parameters from the rating curve were restricted to the 95% credibility interval (from 2.5% to 97.5% quantile); after considering that, without the restriction, parameters tended to assume values that were not physically expected according to the hydraulic analysis made during the construction of the rating curve for applying the BaRatin method. Also, the maximum value for $b_1$ was constrained to the minimum value of stage measured, to ensure only positive discharges, and the minimum value for $b_2$ was constrained to $b_1$ value on each iteration to ensure physical consistency.

After defining prior distributions for all parameters and the likelihood function, posterior distributions were computed using the STAN software. The code used in this study is provided in Appendix B. Instead of relying on STAN's native "multi_normal_lpdf" function, a computationally optimized implementation of the likelihood was developed using artificial intelligence tools, resulting in a substantial reduction in computation time. Differences between the likelihood values obtained with the two implementations were observed only beyond the eighth decimal place, which was considered acceptable for the purposes of this study.

Simulations were performed using a computer with the following specifications: Intel(R) Xeon(R) E5-2620 2.10 GHz (with 16 physical cores and 32 logical processors) with 64 GB of RAM.

Posterior distributions allow for obtaining the so-called true discharges at Jardim Station. This was done following the method proposed by Sikorska and Renard (2017), presented in Figure 11.

**Figure 11 - Diagram for the full calibration strategy for the rainfall-stage model**

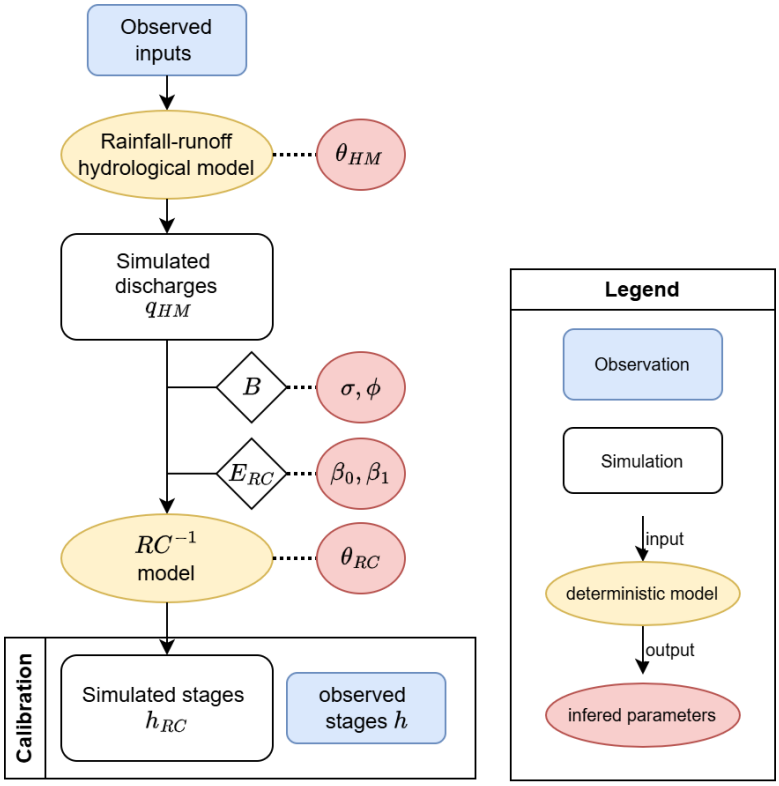


Source: Adapted from Sikorska and Renard (2017)

First, the discharges from the hydrological model (GR4H) were computed for each iteration run, using the observed inputs. Then, the structural error from the hydrological model $B_t(\sigma, \phi)$ was computed, again for each iteration. The so-called true discharge was calculated by Equation (65).

$$\mathrm{q}_t = q_{HM_t}(\boldsymbol{\theta_{HM}}) - \frac{B_t(\sigma, \phi)}{d_t^{(\psi)}(\boldsymbol{\theta_{HM}})} \tag{65}$$

Then, the structural error from the rating curve was computed for each iteration, and the discharge from the rating curve was defined. Finally, the stages were computed for

each iteration using the parameters estimated for the rating curve, as presented by Equation (66).

$$h_t \approx f_{rc}^{-1}\left(q_{HM_t}(\boldsymbol{\theta_{HM}}) - \frac{B_t(\sigma,\phi)}{d_t^{(\psi)}(\boldsymbol{\theta_{HM}})} + E_{RC}(\boldsymbol{\beta}), \boldsymbol{\theta_{rc}}\right) \quad (66)$$

After generating the calculated stages, the model performance was evaluated by the coverage probability for the 95% credibility interval (from 2.5% to 97.5% quantile). As presented by Sikorska et al. (2013), the coverage probability for $\alpha$ should be larger or equal to $1 - \alpha$, i.e., 95% in this study. Since this study focuses on flood events, the coverage probability for stages above-average was also analyzed. Also, Nash-Sutcliffe efficiency (NSE), root mean squared error (RMSE), and Pearson correlation coefficient (r) were used to evaluate the performance of median stages.

## 4.4 Hydrodynamic model

Considering the upstream discharge as one of the most influential sources of uncertainty in hydrodynamic models (Warmink et al., 2011), the so-called true discharge and the rating curve discharge were then routed through a hydrodynamic model in order to evaluate the impact of rating curve uncertainties on discharge and stage predictions.

A one-dimensional (1D) model was chosen due to its lower computational cost and to reduce the incorporation of additional uncertainty due to the large data requirements of 2D models. Although 1D models have limitations, particularly when flow extends into the floodplain, they can be advantageous in cases of relatively regular cross-sections, such as urban systems and smaller basins, and under computational constraints, as in Bayesian analysis, which require a large number of model iterations.

Calibration is recommended because hydrodynamic models are affected by multiple sources of uncertainties. Therefore, stage data downstream Jardim station were sought. A gauge station operated by COPASA (Companhia de Saneamento de Minas Gerais), the company responsible for operating the Serra Azul Reservoir and supplying water for the region, was identified. However, the available stage data did not have

sufficient temporal resolution for model calibration. Therefore, uncertainty propagation was performed considering only uncertainty in the upstream hydrographs. This was achieved by propagating the so-called true discharges and rating curve discharges on a fictitious reach with a length of 100km, to evaluate how the explicit consideration of rating curve uncertainty could influence information used for water management decisions, including for alert systems activation. The length of 100 km was adopted to allow the observation of peak propagation and attenuation. Nevertheless, this reach is fictitious, since the cross-section and the slope were kept constant along its entire length, and such an extent exceeds the Serra Azul Reservoir located downstream of Jardim station.

An attempt to solve the Saint-Venant equations using the finite differences method, adopting a diffuse explicit scheme due to its simplicity was made. The code was implemented directly on STAN software. However, the routing of hydrographs resulted in flattened peaks, which were much more pronounced than expected from numerical diffusion alone. When compared to the results obtained using the HEC-RAS software, the results from the model based on explicit resolution of Saint-Venant equations also exhibit peak anticipation, in addition to peak flattening. No clear explanation was identified for this behavior. The hydraulic characteristics were verified, and results for cross-sectional inundated area, hydraulic radius, and top width were similar to those obtained when using HEC-RAS. Furthermore, different spatial and temporal discretizations were tested, for example, 20 km and 1 hour, 5 km and 15 minutes, 2 km and 5 minutes, all of which satisfied the Courant condition below 1 throughout the entire simulation period.

Hydrographs to be routed in the hydrodynamic model were obtained through the rainfall-stage models, considering the model errors described in Subchapter 4.3.2. To obtain the so-called true discharges, the AR (1) error model associated with the hydrological model was applied. Rating curve discharges were obtained by applying the rating curve model error, which assumed time-independent errors. This leads to random errors and, consequently, discontinuous hydrographs, which lack physical meaning and pose challenges for propagation through the hydrodynamic model.

To overcome both these limitations, ensembles of both rating curve and true discharges were sorted by magnitude, and the median discharges as well as the limits of the 95% credibility interval were propagated using the HEC-RAS software. This procedure aimed to circumvent the issues associated with the explicit numerical scheme and to reduce the impact of the model errors considered.

HEC-RAS (Hydrologic Engineering Center - River Analysis System) is a software developed by the Hydrologic Engineering Center from the United States Army Corps of Engineers. It allows the simulation of one-dimensional steady or unsteady flow, two-dimensional unsteady flow, sediment transport, and water quality modeling (USACE, 2026). For the one-dimensional unsteady flow simulations, Saint-Venant equations are employed. HEC-RAS is widely used in both academic and professional applications due to its broad applicability, free availability, and reliability. In the 1D unsteady flow module, the modeler defines the cross-section geometry, including spacing between sections, as well as boundary and initial conditions. The time step can be specified by the user or automatically adjusted based on the Courant number.

## 4.5 Bayesian analysis

Bayesian inference was performed using STAN, a “probabilistic programming language for specifying statistical models” (Carpenter et al., 2017, p. 2). It uses the Hamiltonian Monte Carlo (HMC) method (STAN, 2025a), which is generally more efficient and robust than Metropolis or Gibbs sampling, as it avoids performing random-walk behavior. Also, it uses the No-U-Turn Sampler (NUTS), which eliminates the need to define the step size and a desired number of steps, which was a drawback of HMC (Hoffman; Gelman, 2014).

To accept and use the posterior distribution obtained by Bayesian inference, it is necessary to analyze whether there was proper exploration of the sample space and assess convergence, i.e., ensure that the samples generated by MCMC are precise representations of the target distributions. While convergence is theoretically guaranteed only for an infinite number of samples, practical diagnostics are used to assess convergence for finite sample iterations (STAN, 2025e).

To facilitate convergence, an adequate number of iterations and chains should be used. Also, the number of iterations for warm-up and thinning can be used. All these parameters are defined by the user on STAN. Four chains were utilized in this study according to STAN team recommendations (STAN, 2025b). The definition of the number of iterations varied according to the model, with more iterations being used for the rainfall-stage model in comparison to the rating curve model. Also, the used warm-up iterations also varied, with half of the total number of iterations allocated to warm-up, which were excluded from the final calculation of the marginal posterior distributions.

Particularly for complex models, draws are mostly positively correlated, and autocorrelation tends to decrease as lag increases. In those cases, thin can be used, which involves retaining only one for each x samples made, depending on the defined thin value. This increases proportionally the number of the effective sample size (ESS), and it is indicated mostly in cases of memory issues and when posterior draws are reused for inference (STAN, 2025c). Thinning was used for the rainfall-runoff model and was not used for the rating curve model.

Also, initial values for the parameters can be provided by the user. No initial values were given, and the ones defined by STAN were used. For unconstrained parameters, a value is drawn from a uniform distribution, where ranges can vary, but are always symmetric around 0. For parameters subject to lower and upper bounds, “the initial value of 0 on the unconstrained scale corresponds to a value at the midpoint of the constraint interval” (STAN, 2025d).

To assess convergence, diagnosis metrics were analyzed. First, the Brooks-Gelman-Rubin $\hat{R}$ criteria is analyzed, which compares the convergence between- and within-chain, and was considered adequate when < 1.01 (STAN, 2025b; Vehtari et al., 2021). Another important criterion is the effective sample size (ESS). Since the draws made are correlated, the estimation of the posterior distribution can be less precise when compared to independent draws. Hence, the ESS corresponds to an estimation of the number of independent samples required to achieve the same level of precision (Carpenter et al., 2017). In this context, bulk-ESS and tail-ESS should be analyzed. Bulk-ESS is useful for diagnosing problems in the center, while tail-ESS is

recommended for diagnosing problems on the distribution's tails (Vehtari et al., 2021). Bulk-ESS greater than 100 times the number of chains is recommended (STAN, 2025b).

The number of divergences was also analyzed. Divergences represent discontinuities in the log posterior density and can result in biased estimates (STAN, 2025b). Models were only accepted when they had 0 divergences in all chains.

In addition to $\hat{R}$ and ESS diagnostics, the Monte Carlo Standard Error (MCSE) was evaluated for the quantities of interest and assessed in light of the accuracy required for the application (STAN, 2025b). The MCSE provides an estimation of the uncertainty associated with the Monte Carlo sampling, typically in relation to posterior expectations (RDocumentation, 2025). No specific threshold recommendation was found.

The following functions from the package CmdStanR were used, which present useful diagnostic information and summaries:

- mod.fit$cmdstan_diagnose(): evaluates divergences, effective sample size and $\hat{R}$ for all parameters, and a complete analysis of the process; and
- mod.fit$cmdstan_summary(): presents the mean, quantiles of 5%, 50% and 95%, MCSE, ESS_bulk, ESS_tail, ESS_bulk/s, $\hat{R}$ and other metrics for the logposterior, model parameters, and others.

Package Bayesplot was also used to plot additional information to assess the convergence of the model. The following functions were used:

- bayesplot::mcmc_hist(mod.fit$draws()): histograms of the marginal distributions;
- bayesplot::mcmc_hist_by_chain(mod.fit$draws()): histograms for the marginal distributions for each chain;
- bayesplot::mcmc_dens(mod.fit$draws()): density for the marginal distributions;
- bayesplot::mcmc_acf(mod.fit$draws()): autocorrelation from the draws for each parameter for each chain; and
- bayesplot::mcmc_trace(mod.fit$draws()): traces for each parameter for each chain.

# 5 RESULTS AND DISCUSSION

The results will be subdivided into the main topics, namely: rating curve, rainfall-stage model, and hydrodynamic model.

## 5.1 Rating curve

### 5.1.1 Estimated rating curve

Following the analysis of the cross-section of Jardim station, the hyperparameters of the prior distributions were defined. First, lower and upper bounds for $B$, $n$ and $S$ were defined, as presented in Table 7. These values were used to calculate the mean and standard deviation for the parameters $a_1$ and $a_2$.

**Table 7 - Rating curve prior hyperparameters for Jardim Station**

| Parameter | Lower | Upper |
|---|---|---|
| $B_1$ (m) | 5 | 8 |
| $n_c$ | 0.025 | 0.045 |
| S (m/m) | 0.0001 | 0.0005 |
| $B_2$ (m) | 15 | 25 |
| $n_p$ | 0.020 | 0.08 |

The presented hyperparameters ($B_1$, $n_c$, $S$, $B_2$ and $n_p$) were constrained to the ranges shown in Table 7 during inference.

The parameters $n_c$, $a_1$, $b_1$, $c_1$, $n_p$, $a_2$, $b_2$ and $c_2$ were assumed to follow Gaussian distributions with means and standard deviations presented in Table 8. These parameters were constrained to positive values.

**Table 8 - Rating curve prior parameters for Jardim Station**

| Parameter | Mean | Standard deviation (Sd) |
|---|---|---|
| $a_1$ | 3.22 | 0.89 |
| $b_1$ | 0.60 | 0.15 |
| $c_1$ | 5/3 | 0.025 |
| $a_2$ | 6.92 | 2.70 |
| $b_2$ | 2.9 | 0.15 |
| $c_2$ | 5/3 | 0.025 |

Posterior distributions were obtained through Bayesian inference by combining the prior distributions with the likelihood function. Four Markov chains with 4,000 iterations each were run, with the first 2,000 iterations used for warm-up and the remaining 2,000 used for sampling. No thinning was applied. The simulation required only a few seconds to complete.

The hyperparameters $B_1$, $B_2$, $n_c$, $n_p$ and $S$ were used to define the parameters $a_1$ and $a_2$. However, since these hyperparameters were not directly included in the specification of the likelihood function, they were not updated during the Bayesian inference process.

To assess the convergence of the model, some metrics were analyzed. Rank-normalized split effective sample size and Rank-normalized split $\hat{R}$ values complied with the recommended threshold; no divergent transitions were found, and no problems were found. Furthermore, MCSE values were at least two orders of magnitude smaller than the corresponding posterior means, which was considered acceptable, and all the $\hat{R}$ values were equal to 1, indicating probable convergence. The results are presented on Table 9, which suggests that the model has likely converged.

**Table 9 - Descriptive Statistics from the Rating-curve Parameters**

| Parameter | Mean | MCSE | ESS_bulk | ESS_tail | $\hat{R}$ |
|---|---|---|---|---|---|
| lp__ | 8.40E+01 | 5.60E-02 | 2663 | 4040 | 1 |
| $a_1$ | 3.50E+00 | 2.40E-03 | 8666 | 5798 | 1 |
| $b_1$ | 8.30E-01 | 1.40E-04 | 7544 | 5306 | 1 |
| $c_1$ | 1.70E+00 | 2.20E-04 | 12537 | 5749 | 1 |
| $a_2$ | 6.90E+00 | 4.00E-02 | 3929 | 1482 | 1 |
| $b_2$ | 2.90E+00 | 1.30E-03 | 13120 | 4535 | 1 |
| $c_2$ | 1.70E+00 | 2.30E-04 | 12138 | 6138 | 1 |
| $\beta_0$ | 2.80E-02 | 1.20E-04 | 9281 | 6205 | 1 |
| $\beta_1$ | 2.00E-01 | 2.90E-04 | 9895 | 5897 | 1 |

Table 10 summarizes the posterior distribution for the rating curve parameters.

**Table 10 - Descriptive Statistics from the Rating-curve Parameters**

| Parameter | 2.50% | 50.00% | 97.50% |
|---|---|---|---|
| $a_1$ | 3.04E+00 | 3.46E+00 | 3.90E+00 |
| $b_1$ | 8.04E-01 | 8.31E-01 | 8.53E-01 |

| Parameter | 2.50% | 50.00% | 97.50% |
|---|---|---|---|
| $c_1$ | 1.62E+00 | 1.67E+00 | 1.71E+00 |
| $a_2$ | 1.57E+00 | 6.84E+00 | 1.22E+01 |
| $b_2$ | 2.60E+00 | 2.90E+00 | 3.20E+00 |
| $c_2$ | 1.62E+00 | 1.67E+00 | 1.72E+00 |
| $\beta_0$ | 1.07E-02 | 2.66E-02 | 5.54E-02 |
| $\beta_1$ | 1.47E-01 | 2.02E-01 | 2.62E-01 |

Based on the descriptive statistics of the parameters and on the defined prior distributions, a comparison between prior and posterior distributions for the rating curve parameters for the Jardim station is shown in Figure 12.

**Figure 12 - Comparison between prior and posterior distribution for rating curve parameters**

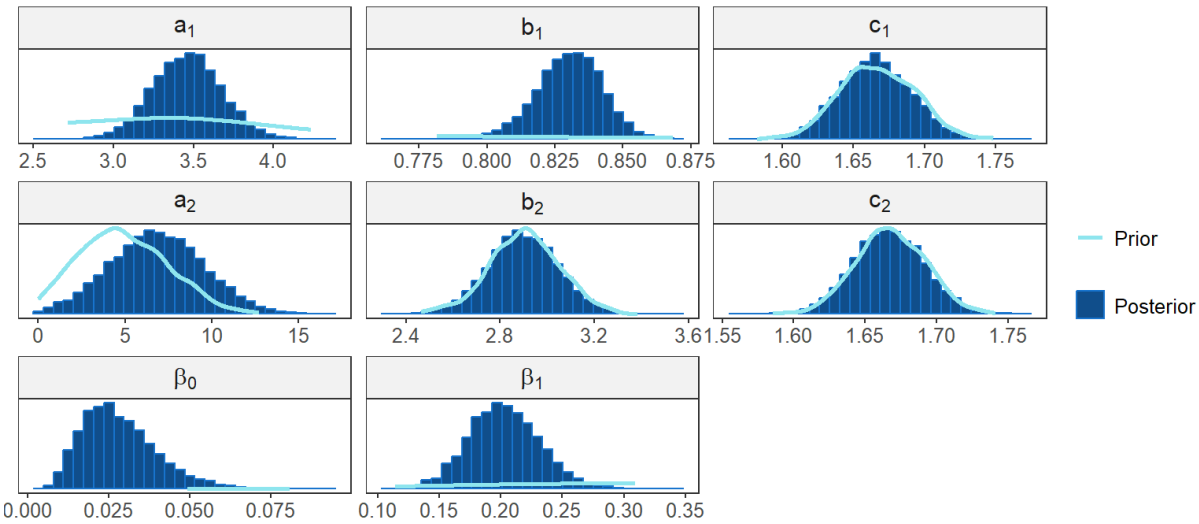


The posterior distributions of parameters $a_1$ and $b_1$ became substantially narrower, indicating that the contribution of the data to reduce the posterior distribution range is large. This was not observed for the parameters $a_2$ and $b_2$, probably due to the absence of discharge measurements associated with floodplain stages. For parameters $c_1$ and $c_2$ the uncertainty band was already tight, so no significant change was observed. For the model error parameters ($\beta_0$ and $\beta_1$) prior distributions were weakly informative. After sampling, they got much narrower, indicating the significant contribution of the data to reduce the posterior distribution range.

For parameters $a_1$, $b_1$, $c_1$, $a_2$, $b_2$ and $c_2$, and model error parameter $\beta_1$, the distributions were considered symmetric and unimodal. For parameter $\beta_0$, the distribution was

slightly right-skewed. However, for simplifications, it was also considered normally distributed when used as a prior distribution for the rainfall-stage model.

Figure 13 shows the scatterplot matrix of the MCMC samples for the posterior distribution of the rating curve parameters. Overall, weak correlations between most parameters were observed, except for the parameters $a_1$ and $b_1$, which have a correlation coefficient of 0.800, and between the parameters of the error model, $\beta_0$ and $\beta_1$, which have a correlation of - 0.585.

**Figure 13 - Scatterplot matrix for posterior distribution for rating curve parameters**

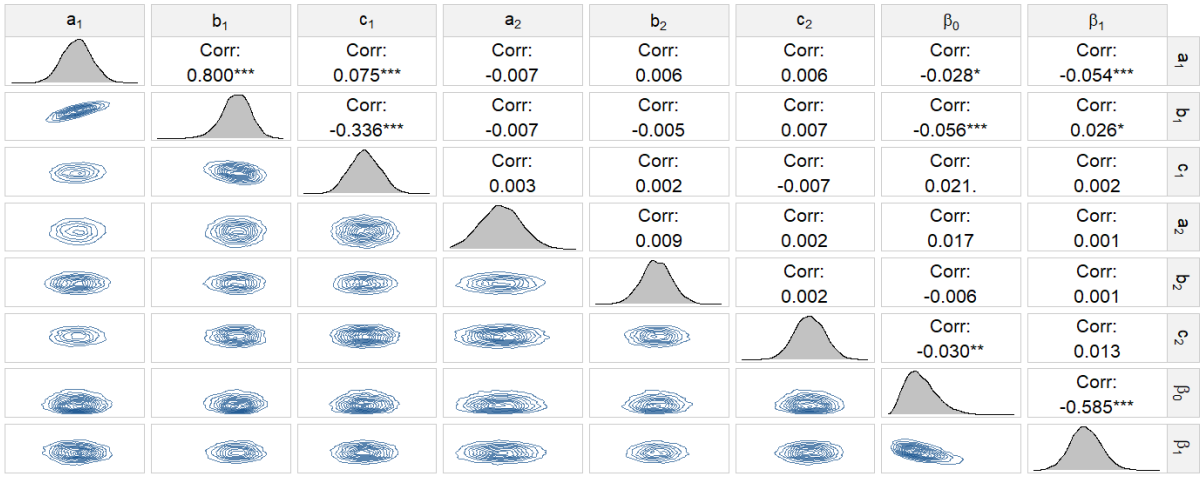


Based on the joint posterior distributions of the parameters, the rating curve was estimated, presented in Figure 14 and Figure 15. For low flows, the error could be greater than the predicted discharge itself, resulting in negative values. To ensure physical consistency, negative discharge values were truncated at zero. The coverage probability of gaugings was approximately 93% for the theoretical credible intervals of 95%.

**Figure 14 - Predicted estimated rating curve**

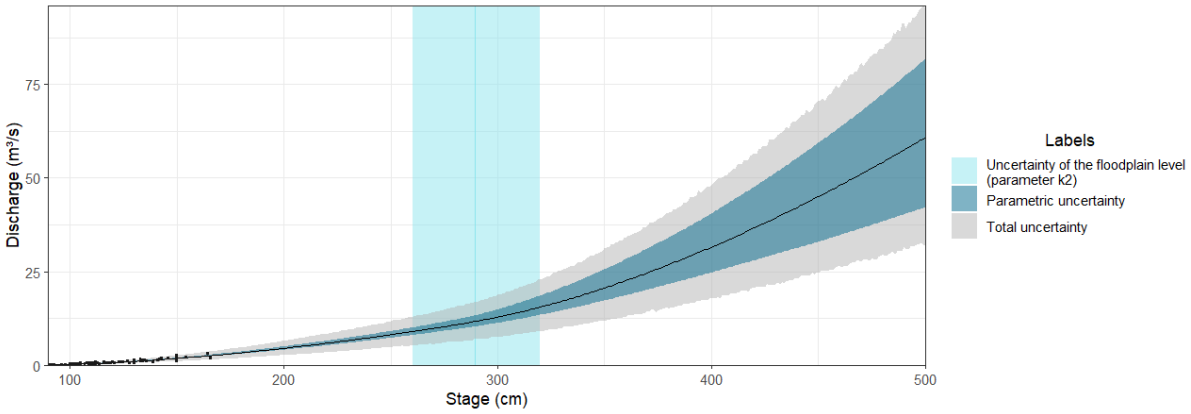


**Figure 15 - Predicted estimated rating curve - zoom on gaugings**

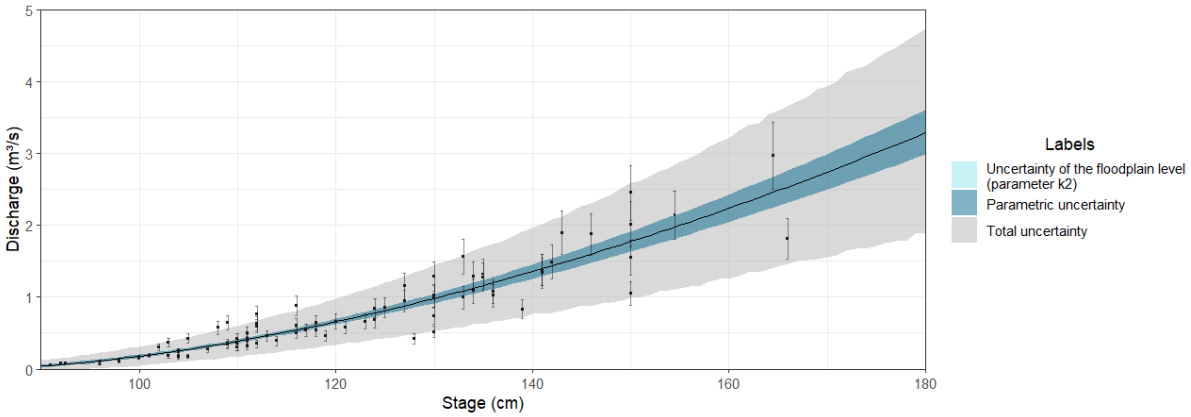


Figure 14 and Figure 15 show wide uncertainty bands across all stages. For a stage of 500 cm, for example, which corresponds to the maximum stage measured, the predicted discharges range approximately from 30 to 100 m³/s. As discussed in the literature review, discharge uncertainty can affect several applications, such as flood frequency analysis, hydrological, and hydrodynamic models. Consequently, it may also influence water resources management decisions, including the criteria used for flood alert system activation.

For lower flows (Figure 15), where most of the gauging is located, structural uncertainty prevails, while for high flows, where there is a lack of gauging, especially on the floodplain, the parametric uncertainty prevails. This behavior is likely due to the large uncertainty associated with the parameter $k_2$, that represents the level of the floodplain, which is equal to $b_2$, indicated in light blue in Figure 14.

Finally, the residuals' behavior, presented in Figure 16, was analyzed to evaluate the error model used.

**Figure 16 - Diagnostic residual plots for the proposed error model**

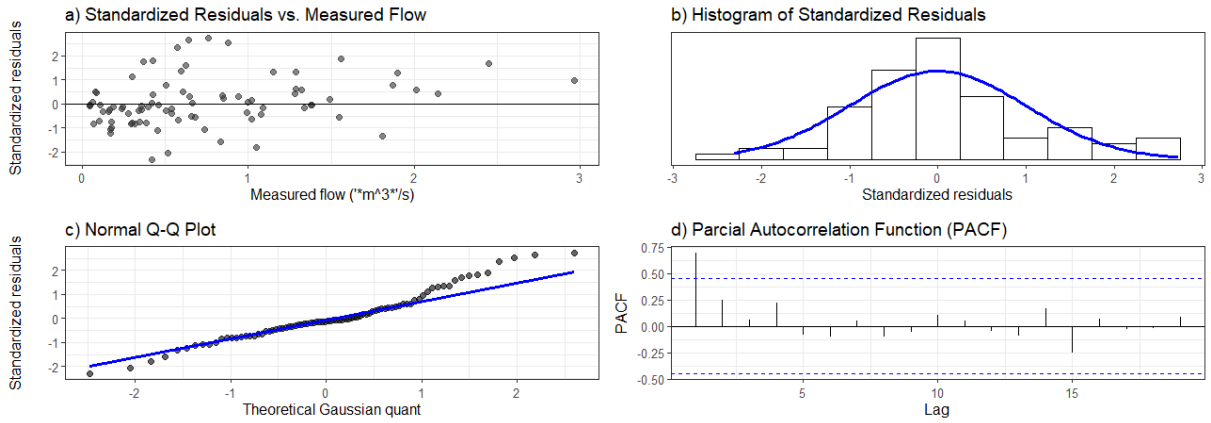


Plot (a) shows that heteroscedasticity was successfully removed by the proposed model error. However, residuals show a slight deviation from the assumed normal distribution, as presented in plots (b) and (c). Finally, the partial autocorrelation function (PACF), shown in plot (d), indicated first-order autocorrelation, suggesting that the assumption of independent errors is violated. The high value at the first lag may result from multiple gaugings with identical or very similar stage values measured sequentially in time. This issue could be addressed by adopting an error model that explicitly accounts for autocorrelation.

### 5.1.2 Prior rating curve scenario

A scenario without discharge data was also developed, simulating conditions in which no discharge observations are available. In this scenario, only the prior distributions presented on Table 8 were used. For the rating curve error model, the prior distributions were defined as $\beta_0$ ~ lognormal (0, 1) and $\beta_1$ ~ lognormal (-0.693147, 1).

Based on these assumptions, the resulting prior rating curve is shown in Figure 17 and Figure 18. As previously observed, at low flows, the estimated error may exceed the predicted discharge, leading to negative values. To ensure physical consistency, negative discharge values were truncated at zero. The results indicate wide uncertainty

bands, both parametric and structural, across the entire range of stages. Owing to this large uncertainty, all gauging observations fall within the 95% credibility interval.

**Figure 17 - Predicted prior rating curve**

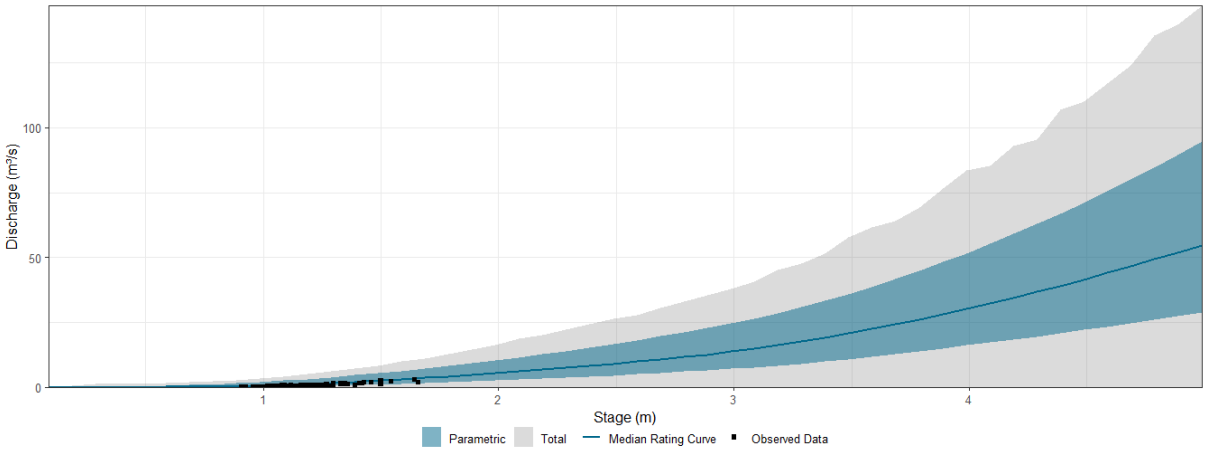


**Figure 18 - Predicted prior rating curve - zoom on gaugings**

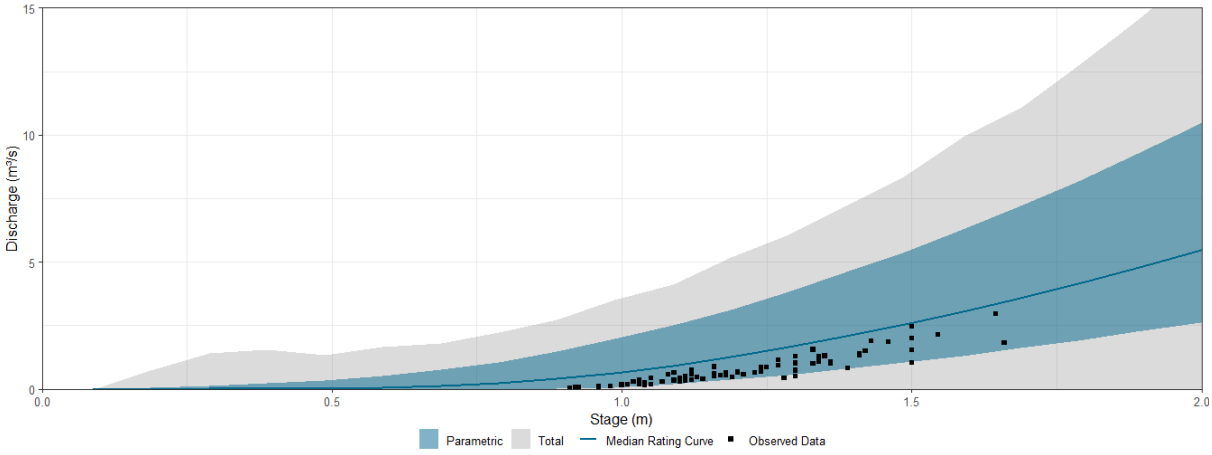


### 5.1.3 Limitations of the rating curve model

The BaRatin method has great potential as it facilitates the construction of a prior rating curve based on hydraulic and geometric information from the cross-section and, through Bayesian inference, updates the parameter probability distributions when data are available. However, some limitations should be pointed out, based on the results found and on the literature review:

- the method assumes that the stage measurements errors are negligible, which may not always be valid;
- in this case study, due to data limitations and practical constraints, discharge measurement uncertainty (8%) was assumed to be constant across all gaugings;
- the model assumes a single, time-invariant rating curve for the entire period of analysis. However, temporal changes in cross-section geometry, vegetation, and channel conditions may occur, particularly affecting low-flow conditions. This was not considered, since the objective of this work is focused on high flows. In the case of lower flows analysis, another model of errors, such as the one proposed by Garcia, Costa and Silva (2020) could be used;
- the application of the method requires selecting a control type and adopting idealized hydraulic assumptions. In this case, channel control was considered, with the assumption of wide rectangle, steady, and uniform flow. However, the analysis of the cross-section showed that, in the floodplain, the cross-section deviates slightly from the rectangular section on the left side, approaching a trapezoidal-like format. Also, particularly for high flows, the assumption of steady and uniform flow may not be fully satisfied;
- in this case, there was a lack of data to precisely define some information, as the channel slope and the Manning roughness coefficient. In-situ visits were not conducted in the study area, so the analysis was based on a literature review and previous expert information. The available topographic information data did not have sufficient spatial resolution to accurately represent the cross-section geometry.
- no discharge gauging was available for the floodplain, resulting in substantial uncertainty after Bayesian inference of parameters $a_2$, $b_2$ and $c_2$. Therefore, the performance of the rating curve based on data coverage could not be assessed for high flows, which is the main interest of this research;
- the gauging data available was concentrated on similar stages, sometimes sequentially over time, which introduced significant autocorrelation in the residuals.

Despite these limitations, the method enables the construction of a rating curve that explicitly accounts for both structural and parametric uncertainty, even in the absence of observed discharges, while providing good data coverage (although slightly above the reference threshold when data were used). Moreover, it allowed the definition of more informative prior distributions for use in the rainfall-stage model.

## 5.2 Rainfall-stage hydrological model

### 5.2.1 Estimated rating curve scenario

The prior distributions for the rainfall-stage parameters are presented in Table 11 and Table 12.

**Table 11 - Prior Distribution for Hydrological model and error model parameters for rainfall-stage model**

| Parameter | $\bar{x}_{ln}$ | $sd_{ln}$ | Lower limit | Upper limit |
|---|---|---|---|---|
| $x_1$ | 3.800451 | 1.939006 | 1 | 2000 |
| $x_2$ | - | - | -1 | 0.30 |
| $x_3$ | 0.804719 | 2.760148 | 0.01 | 500 |
| $x_4$ | -1.151293 | 1.762182 | 0.01 | 10.00 |
| $\sigma$ | - | - | 0 | 0.150 |
| $\phi$ | 3.912023 | 1 | 0 | 200 |

**Table 12 - Prior Distribution for Rating-Curve parameters for rainfall-stage model**

| Parameter | Mean | Standard deviation | Lower limit | Upper limit |
|---|---|---|---|---|
| $a_1$ | 3.46161 | 0.21873 | 3.02415 | 3.89907 |
| $b_1$ | 0.83016 | 0.01235 | 0.80547 | 0.85485 |
| $c_1$ | 1.66568 | 0.02502 | 1.61563 | 1.71573 |
| $a_2$ | 6.87431 | 2.69079 | 1.49273 | 12.25590 |
| $b_2$ | 2.89810 | 0.15075 | 2.59659 | 3.19961 |
| $c_2$ | 1.66665 | 0.02481 | 1.61702 | 1.71627 |
| $\beta_0$ | 0.02829 | 0.01159 | 0.00511 | 0.05147 |
| $\beta_1$ | 0.20283 | 0.02907 | 0.14469 | 0.26096 |

By combining the prior distribution with the likelihood function, posterior distributions were obtained through Bayesian inference. For this, four chains with 8,000 iterations

each were used, 4,000 used for warm-up and 4,000 used for sampling. A thinning of 10 was used. The total simulation time was 9 hours and 54 minutes.

To assess the convergence of the model, some metrics were analyzed. Rank-normalized split effective sample size and Rank-normalized split $\hat{R}$ values complied with the recommended threshold; no divergent transitions were detected, and no sampling problems were identified. Furthermore, MCSE values were at least three orders of magnitude smaller than the corresponding posterior means, so they were considered acceptable, and all the $\hat{R}$ were equal to 1, indicating convergence. The results are presented in Table 13, which indicates probable convergence.

**Table 13 - Descriptive Statistics from the Rainfall-stage Parameters**

| Parameter | Mean | MCSE | ESS_bulk | ESS_tail | $\widehat{R}$ |
|---|---|---|---|---|---|
| lp__ | 5.50E+04 | 7.80E-02 | 1440 | 1614 | 1 |
| $x_1$ | 1.90E+03 | 5.10E-01 | 1641 | 1642 | 1 |
| $x_2$ | -9.10E-01 | 3.10E-04 | 1532 | 1518 | 1 |
| $x_3$ | 4.60E+01 | 1.40E-02 | 1598 | 1420 | 1 |
| $x_4$ | 1.00E+01 | 5.00E-05 | 1591 | 1571 | 1 |
| $\sigma$ | 1.50E-01 | 4.90E-07 | 1457 | 1408 | 1 |
| $\phi$ | 8.10E+01 | 4.10E-02 | 1673 | 1514 | 1 |
| $a_1$ | 3.90E+00 | 1.80E-05 | 1535 | 1376 | 1 |
| $b_1$ | 8.50E-01 | 6.40E-07 | 1664 | 1305 | 1 |
| $c_1$ | 1.70E+00 | 5.50E-06 | 1660 | 1500 | 1 |
| $a_2$ | 1.50E+00 | 8.40E-04 | 1462 | 1559 | 1 |
| $b_2$ | 3.20E+00 | 2.50E-04 | 1640 | 1497 | 1 |
| $c_2$ | 1.70E+00 | 5.60E-04 | 1486 | 1457 | 1 |
| $\beta_0$ | 5.10E-03 | 1.40E-07 | 1506 | 1398 | 1 |
| $\beta_1$ | 1.40E-01 | 2.50E-07 | 1413 | 1431 | 1 |

Table 14 presents the summary of the posterior distribution for the parameters of the rainfall-stage model and the rating curve. The comparison between prior and posterior distributions for all parameters is presented in Figure 19. In general, the data were highly informative for most parameters, except for $c_2$, for which the variance was already small. Moreover, all distributions were unimodal. The rating curve parameters, except $c_2$, and the hydrological model parameters $x_4$ and $\sigma$ were strongly influenced by the imposed parameter bounds. This fact suggests that the prior bounds might be too narrow. However, the convergence for the equilibrium distribution was not achieved when these ranges were increased, probably because of the very complex structure of

the rainfall-stage model. As a result, the prior bounds were fixed at the initial values for subsequent analysis.

**Table 14 - Descriptive Statistics - Posterior distribution for Rainfall-stage parameters**

| Parameter | 2.50 % | 50.00% | 97.50 % |
|---|---|---|---|
| $x_1$ | 1839.41 | 1879.41 | 1921.03 |
| $x_2$ | -0.93559 | -0.91213 | -0.88914 |
| $x_3$ | 44.6576 | 45.7268 | 46.8339 |
| $x_4$ | 9.99283 | 9.99856 | 9.99996 |
| $\sigma$ | 0.14993 | 0.14999 | 0.15000 |
| $\phi$ | 78.0562 | 81.1503 | 84.4011 |
| $a_1$ | 3.89648 | 3.89855 | 3.89905 |
| $b_1$ | 0.85475 | 0.85483 | 0.85485 |
| $c_1$ | 1.71494 | 1.71558 | 1.71573 |
| $a_2$ | 1.49333 | 1.51389 | 1.61053 |
| $b_2$ | 3.16374 | 3.19213 | 3.19936 |
| $c_2$ | 1.62562 | 1.67032 | 1.71011 |
| $\beta_0$ | 0.00511 | 0.00511 | 0.00513 |
| $\beta_1$ | 0.14469 | 0.14470 | 0.14473 |

**Figure 19 - Comparison between prior and posterior distribution for rainfall-stage parameters**

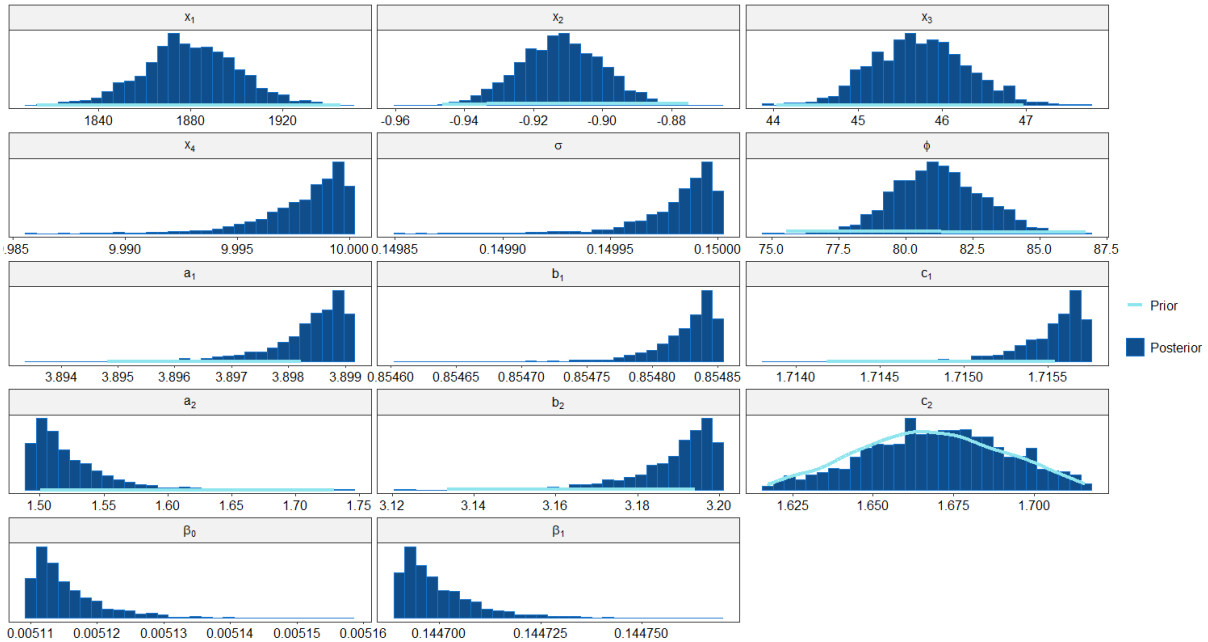


Figure 20 shows the scatterplot matrix of the MCMC samples for the posterior distribution of the rainfall-stage model parameters. Based on the conceptual structure

of the GR4H model, some correlation among the parameters could be expected *a priori*. However, in general, low correlation between parameters was observed. This behavior is likely related to the parameter constraints imposed on the prior distributions. The correlation factor was higher than 0.5 only between parameters $x_2$ and $x_3$, with a value of -0.593.

Based on the joint posterior distribution for the rainfall-stage parameters, the stages and their 95% credible intervals are estimated and presented in Figure 21.

**Figure 20 - Scatter-plot matrix for posterior distribution for rating-stage model parameters**

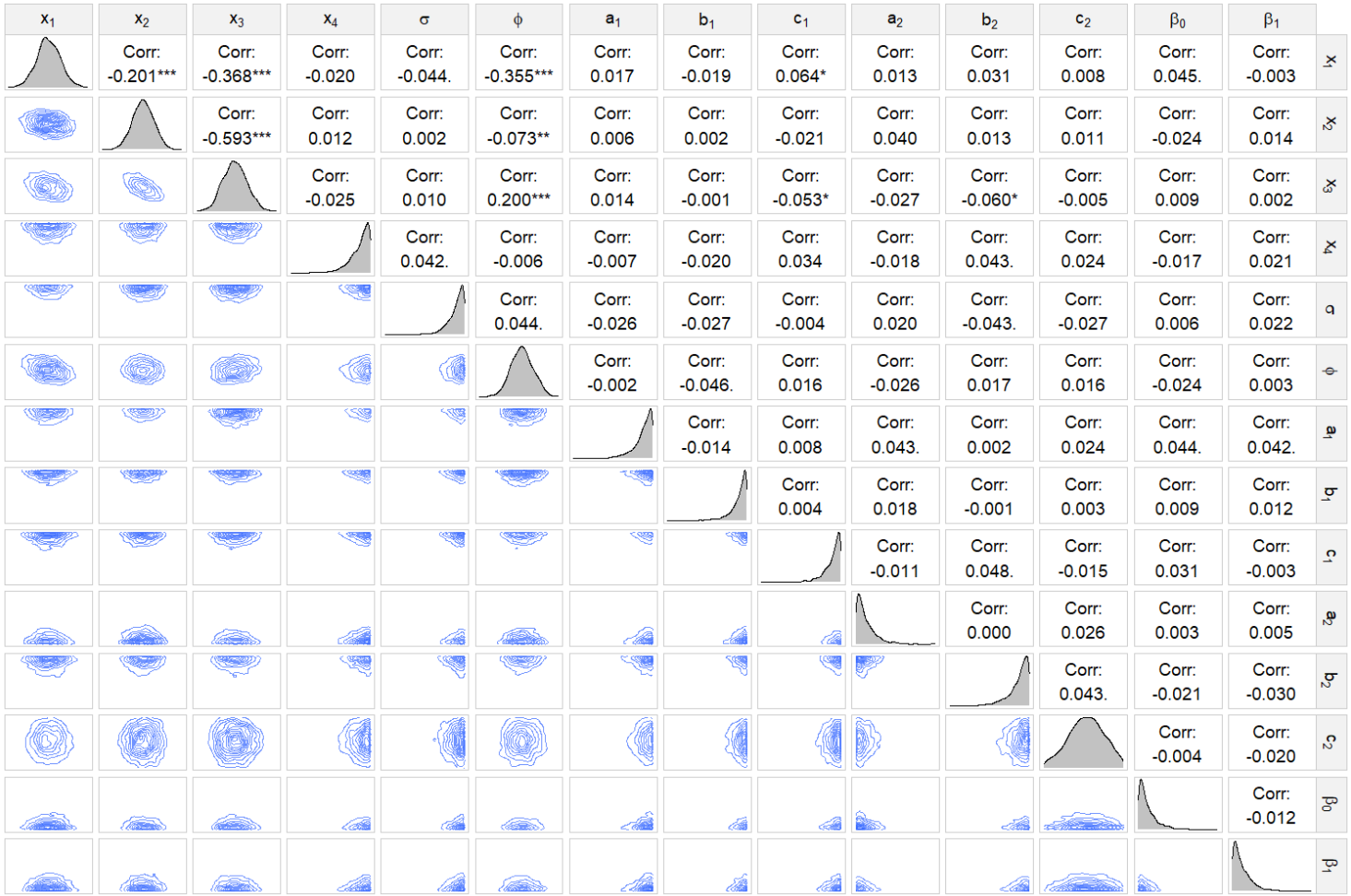

**Figure 21 - Prediction stages and uncertainty bands**

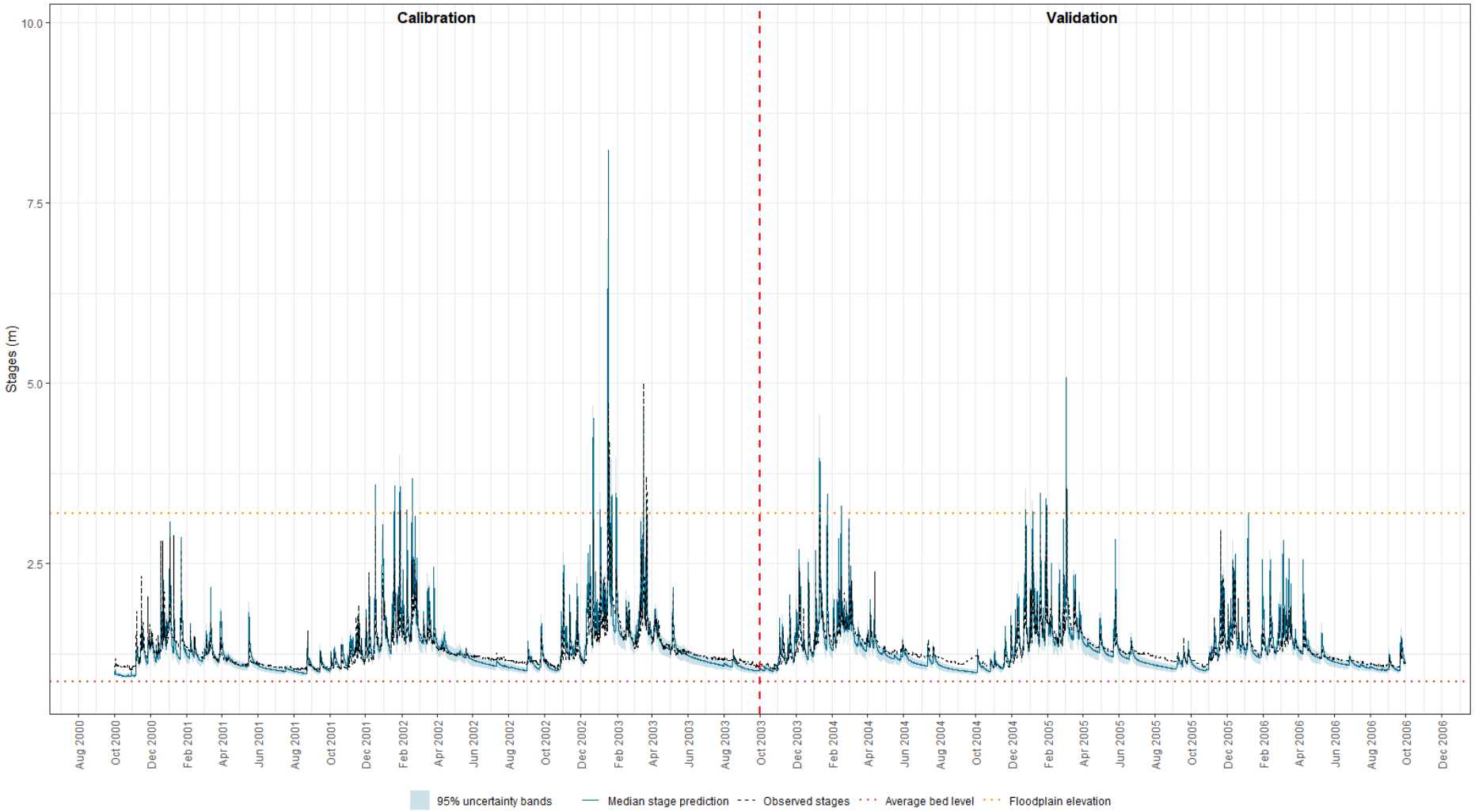

The model performed better for high flows. During recession periods, the model tends to underestimate discharges. Since the objective of the research is focused on high flows, the results were considered acceptable. However, this behavior should be considered in broader applications. According to Perrin, Michel, and Andréassian (2003), the percolation function, which depends on $x_1$, does not contribute much to the streamflow but can have an impact on low-flow situations. Moreover, the routing reservoir $R$, for which the size is related to the parameter $x_3$, allows the representation of streamflow recessions where necessary. Therefore, parameters $x_1$ and $x_3$ should be inspected more deeply when analyzing low flows. Furthermore, model performance could be impacted by the model errors employed.

For a deeper understanding of the model, Table 14 presents the performance metrics for the rainfall-stage model for Jardim Station, which shows that the coverage probability for above-average stages is higher than the coverage probability in general, aligned with the research's objective. The Nash–Sutcliffe efficiency (NSE) was above 0.5, the Root Mean Square Error (RMSE) values were between 0.1 – 0.2, and the Pearson correlation coefficient (rPearson) was above 0.9, which was considered appropriate model performance.

**Table 15 - Metrics performance for the rainfall-stage model**

| Period | NSE | RMSE | rPearson | Coverage probability for 95% CI | Coverage probability – above-average stage for 95% CI |
|---|---|---|---|---|---|
| Full period | 0.638 | 0.166 | 0.913 | 60.85 % | 75.13 % |
| Calibration | 0.667 | 0.174 | 0.911 | 61.00 % | 72.31 % |
| Validation | 0.592 | 0.157 | 0.918 | 60.69 % | 77.46 % |

For assessing model performance focusing only on high flows, a threshold of 2.5 m was chosen to define the peaks, given that the maximum measured stage was 5 m. Figure 22 shows the peak coverage in stage prediction. Of the 29 identified peaks, 22 were covered, approximately 76%. During the validation period, coverage increased to 92% (11 out of 12 peaks).

**Figure 22 - Peak coverage analysis in stage prediction**

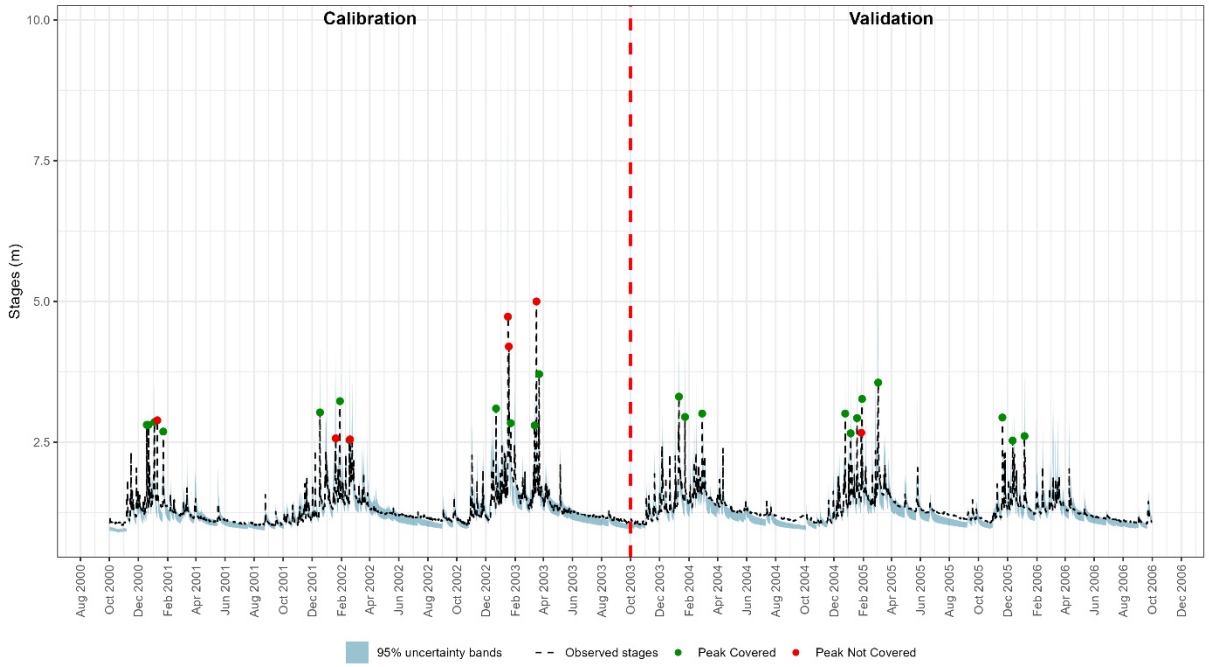


The relative contribution of each source of uncertainty is presented in Figure 23 for discharge and in Figure 24 for stages. It is possible to see the prevalence of structural uncertainty from the hydrological model.

**Figure 23 - Sources of uncertainties in discharge prediction**

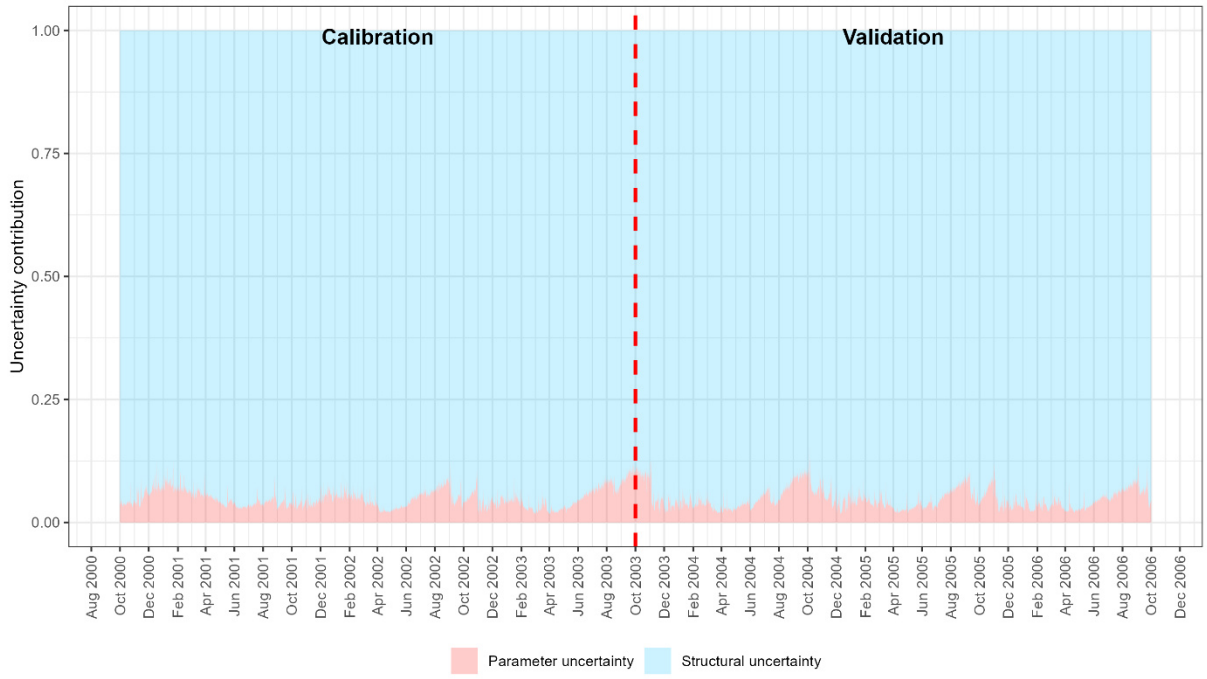

**Figure 24 - Sources of uncertainties in stage prediction**

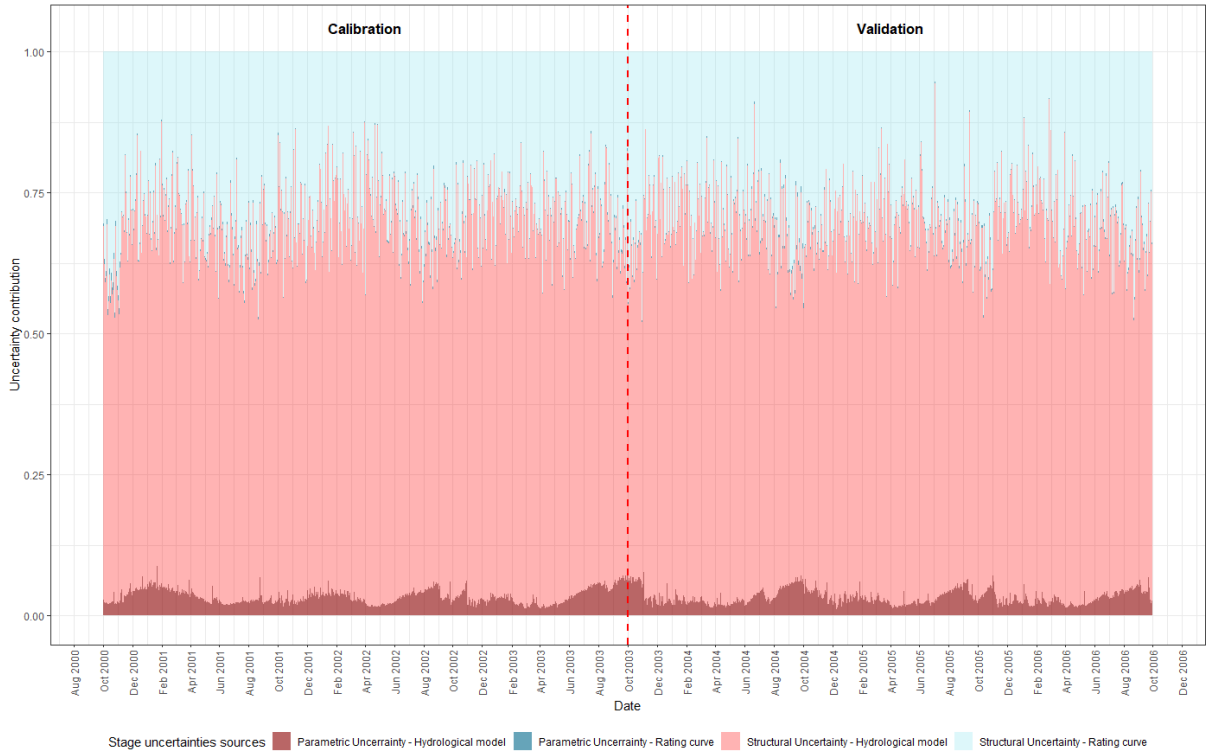


For a deeper analysis, Table 16 presents the mean, minimum, and maximum contribution from each uncertainty source for stage prediction. Even though hydrological model structural uncertainty prevails, rating curve structural uncertainty is on average 30% and reaches 54%, indicating the importance of its consideration. Parametric uncertainty is low both for the hydrological model and the rating curve, which may be attributed to the large amount of data used for calibration – over 26,292 values, excluding the warm-up period.

**Table 16 - Contribution source for stage uncertainty**

| Source | Mean | Minimum | Maximum |
|---|---|---|---|
| Parametric Uncertainty – Hydrological model | 3% | 1% | 11% |
| Structural Uncertainty – Hydrological model | 66% | 43% | 99% |
| Parametric Uncertainty – Rating curve | ~0% | ~0% | 2% |
| Structural Uncertainty – Rating curve | 30% | ~0% | 54% |

Figure 25 shows the comparison between stage predictions and sources of uncertainties. During the first two years, wet periods were associated with higher parametric uncertainty from the hydrological model. In the following years, higher parametric uncertainty from the hydrological model is then related to the dry periods,

and it is possible to observe a detachment between the observed and simulated stages during these periods. This behavior could be related to parameters $x_1$ and $x_3$, which can have an impact on low flow situations and have a relatively large standard deviation, especially $x_1$. For the rating curve uncertainty, no pattern was identified due to the high variability.

**Figure 25 - Comparison between sources of uncertainties and stage prediction**

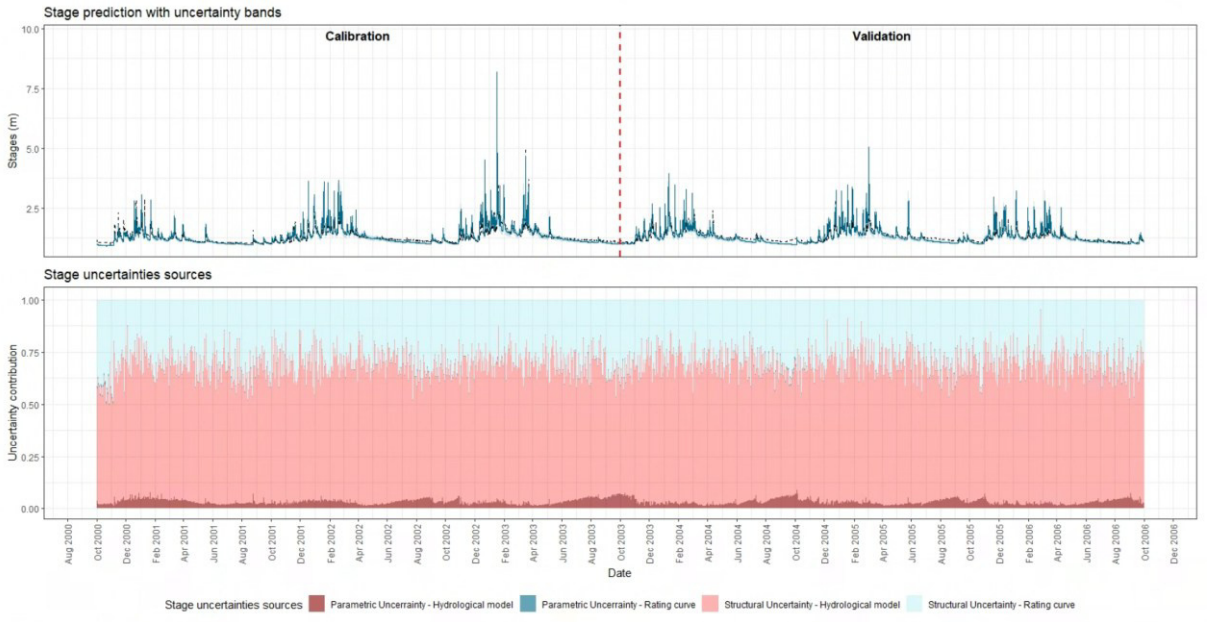


Finally, considering the joint posterior distribution for the rating curve parameters, the estimated rating curve is updated. The comparison between the rating curve before and after the calibration of the parameters of the rainfall-stage model is presented in Figure 26. The uncertainty bands became narrower, centered on lower values. However, there is no gauging for higher flows to assess its improvement.

**Figure 26 - Comparison between prior and posterior rating curve**

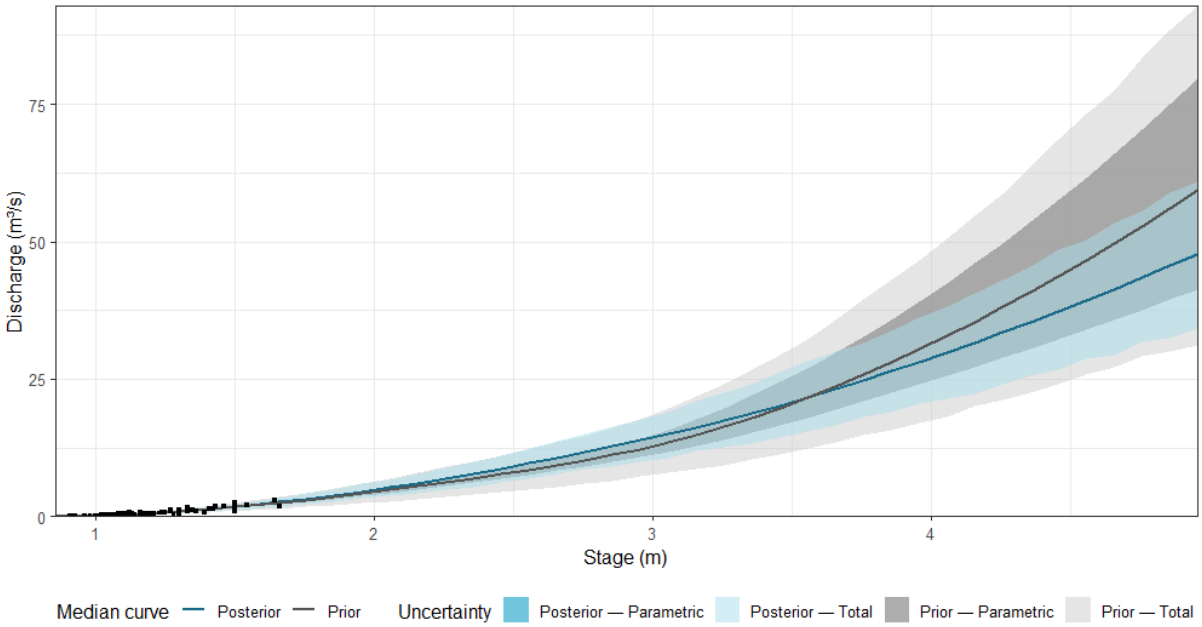


### 5.2.2 Prior rating curve scenario

Prior distributions for the rainfall-stage parameters for the hydrological model were the same as those used for the calibrated rating curve and are presented in Table 11. The prior distributions for the rating curve parameters are presented in Table 8. In some preliminary tests, the posterior distributions for the parameter $\beta_1$ assumed values close to zero, with a mean value as low as 0.00013. This behavior resulted in systematic overestimation of stages throughout the entire period, with almost no data coverage. Considering that heteroscedasticity was expected and was observed during the rating curve calibration, the parameter $\beta_1$ was constrained to the interval (0.2, 1). Parameter $\beta_0$ was constrained to the interval (0, 1).

The Bayesian calibration procedure was the same as that described in Subchapter 5.1.1. Total simulation time was approximately 13 hours. Rank-normalized split effective sample size and Rank-normalized split $\hat{R}$ values complied with the recommended threshold; no divergent transitions were detected, and no sampling problems were identified. Furthermore, MCSE values were at least three orders of magnitude smaller than the corresponding posterior means, so it was considered

acceptable, and all the $\hat{R}$ were equal to 1, indicating probable convergence. The results are presented in Table 17.

**Table 17 - Descriptive Statistics from the Rainfall-stage Parameters**

| Parameter | Mean | MCSE | ESS_bulk | ESS_tail | $\hat{R}$ |
|---|---|---|---|---|---|
| lp__ | 6.30E+04 | 7.70E-02 | 1451 | 1493 | 1 |
| $x_1$ | 6.00E+02 | 2.70E-01 | 1589 | 1574 | 1 |
| $x_2$ | 3.00E-01 | 7.70E-07 | 1680 | 1499 | 1 |
| $x_3$ | 3.00E+00 | 3.20E-04 | 1424 | 1496 | 1 |
| $x_4$ | 1.00E+01 | 5.90E-05 | 1422 | 1434 | 1 |
| $\sigma$ | 1.50E-01 | 1.10E-06 | 1484 | 1460 | 1 |
| $\phi$ | 5.90E+01 | 2.70E-02 | 1504 | 1495 | 1 |
| $a_1$ | 5.00E+00 | 2.40E-05 | 1738 | 1607 | 1 |
| $b_1$ | 6.30E-01 | 1.20E-04 | 1522 | 1611 | 1 |
| $c_1$ | 1.60E+00 | 6.10E-06 | 1526 | 1409 | 1 |
| $a_2$ | 1.50E+00 | 2.70E-04 | 1562 | 1565 | 1 |
| $b_2$ | 3.20E+00 | 1.10E-04 | 1693 | 1509 | 1 |
| $c_2$ | 1.70E+00 | 5.30E-04 | 1707 | 1706 | 1 |
| $\beta_0$ | 3.50E-05 | 2.50E-07 | 1797 | 1570 | 1 |
| $\beta_1$ | 2.00E-01 | 1.20E-06 | 1638 | 1615 | 1 |

Table 18 presents the summary of the posterior distribution for the rainfall-stage parameters.

**Table 18 - Descriptive Statistics - Posterior distribution for Rainfall-stage parameters**

| Parameter | 2.50 % | 50.00% | 97.50 % |
|---|---|---|---|
| $x_1$ | 576.245 | 597.361 | 619.794 |
| $x_2$ | 0.29989 | 0.29998 | 0.30000 |
| $x_3$ | 2.93315 | 2.95524 | 2.97847 |
| $x_4$ | 9.99159 | 9.99845 | 9.99994 |
| $\sigma$ | 0.14984 | 0.14997 | 0.15000 |
| $\phi$ | 57.1620 | 59.1700 | 61.3209 |
| $a_1$ | 4.98700 | 4.98991 | 4.99064 |
| $b_1$ | 0.61836 | 0.62779 | 0.63648 |
| $c_1$ | 1.61667 | 1.61683 | 1.61755 |
| $a_2$ | 1.50040 | 1.50784 | 1.53961 |
| $b_2$ | 3.18277 | 3.19652 | 3.19988 |
| $c_2$ | 1.62320 | 1.66188 | 1.70545 |
| $\beta_0$ | 0.00002 | 0.00003 | 0.00006 |
| $\beta_1$ | 0.20000 | 0.20003 | 0.20018 |

Figure 27 presents a comparison between the prior and posterior distributions for all parameters. In general, the data significantly contributed to reducing the posterior distribution range for most parameters, except for $c_2$, for which the prior variance was already small. These results were consistent with those obtained using the estimated rating curve. However, some parameters exhibited different posterior distributions, highlighting the influence of broader prior specifications.

All distributions were unimodal. As observed in the model using the calibrated rating curve, parameters were strongly influenced by the imposed bounds. In this case, the effect was noticeable for the rating curve parameters except for $c_2$ and $\beta_0$, and hydrological model parameters $x_2$, $x_4$ and $\sigma$.

**Figure 27 - Comparison between prior and posterior distribution for rainfall-stage parameters**

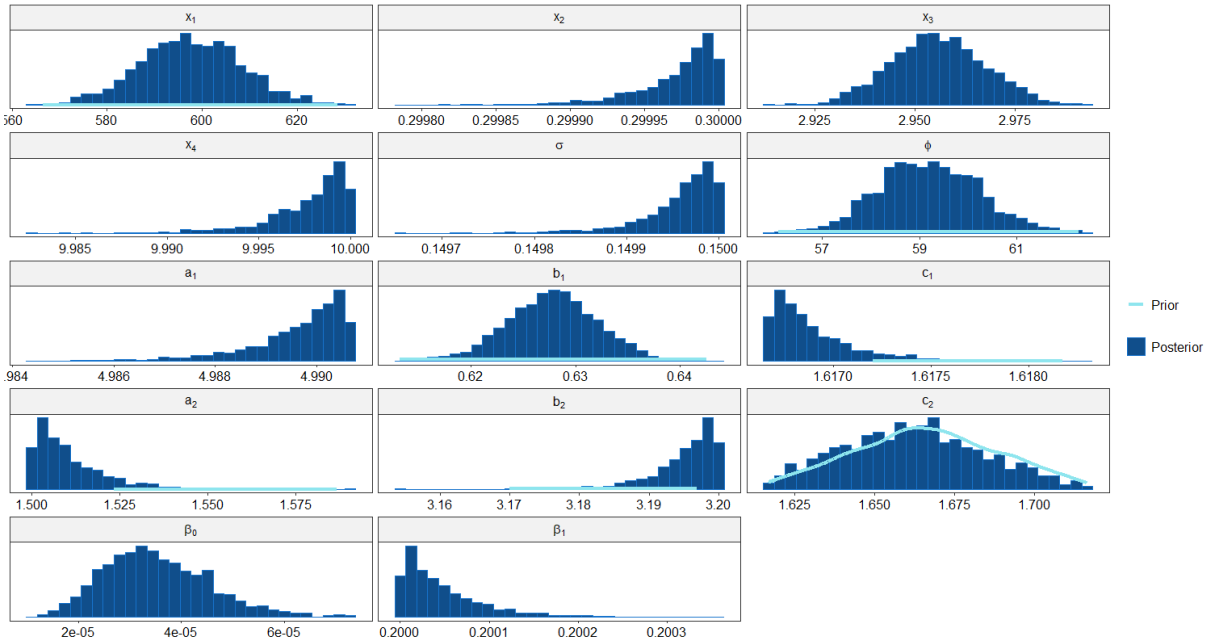


Figure 28 presents the scatterplot matrix of the MCMC samples for the rainfall-stage model parameters. Although high correlation among parameters was expected, overall correlation was low, similar to the model using the calibrated rating curve. This behavior is likely related to the parameter constraints imposed during inference. For the calibrated rating curve, the correlation coefficient exceeded 0.5 only for parameters $x_2$ and $x_3$, with a value of -0.593, whereas in this case, this correlation was 0.478. In

contrast, a correlation coefficient greater than 0.5 was observed between parameters $b_1$ and $\phi$, with a value of 0.796, for which no clear explanation was identified.

Based on the joint posterior distributions of the rainfall-stage parameters, predicted stages and their associated 95% credible interval were estimated and are presented in Figure 29.

**Figure 28 - Scatter-plot matrix for posterior distribution for rating curve parameters**

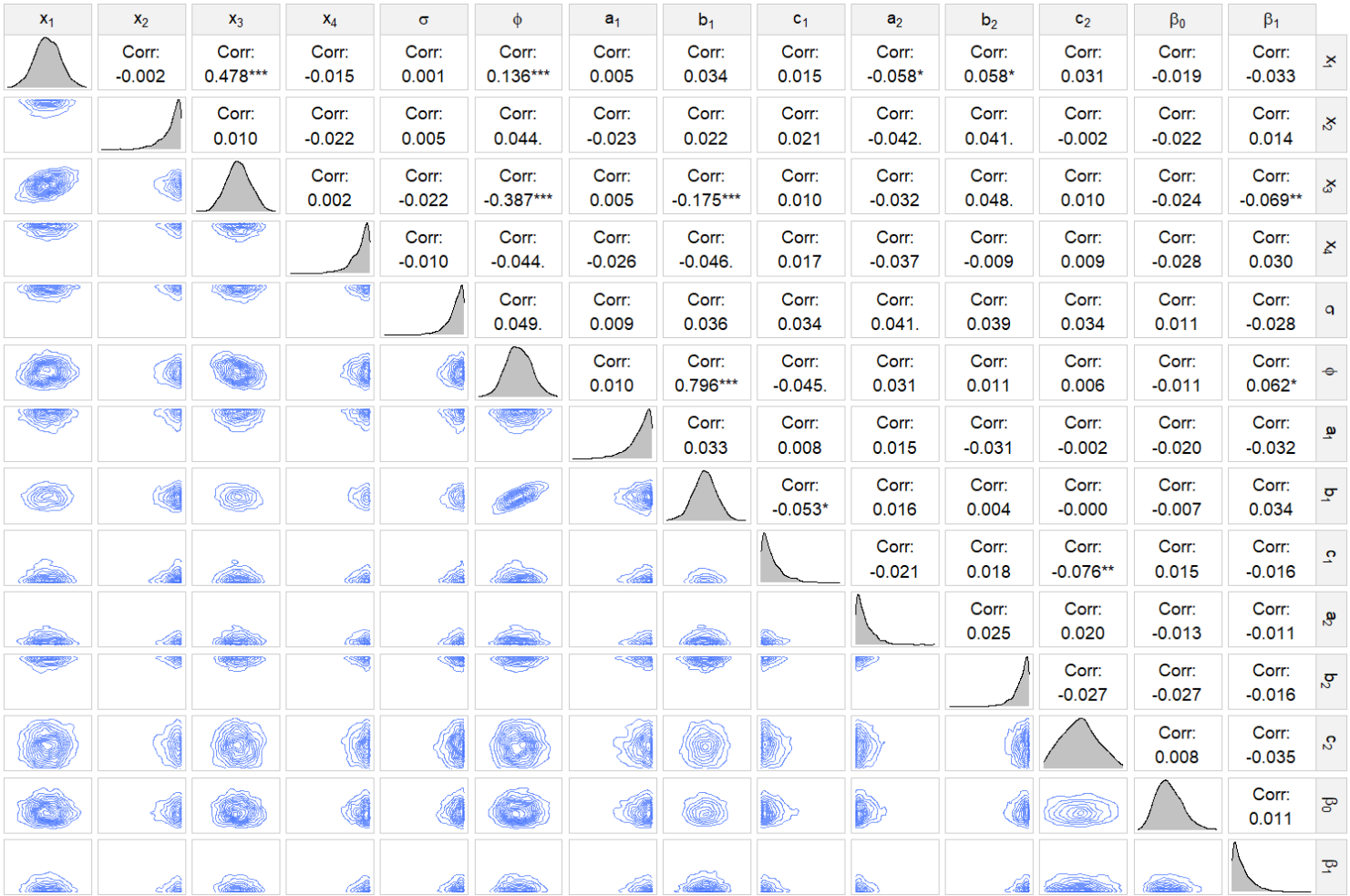

**Figure 29 - Prediction stages and uncertainty bands**

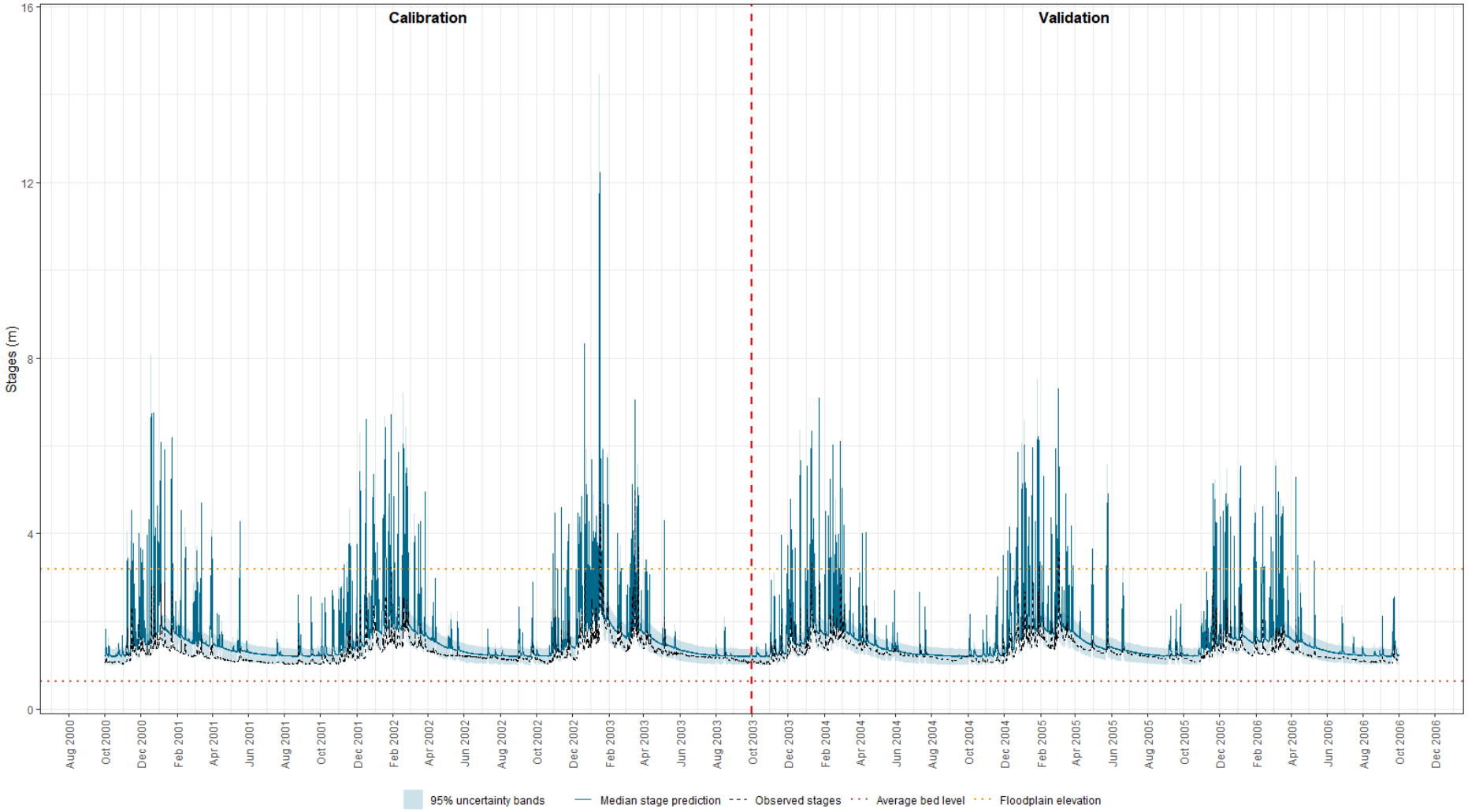

The results indicate a tendency for the model to systematically overestimate simulated discharges throughout the entire period, particularly during high-flow events. This behavior may be related, for example, to the posterior mean of the hydrological model parameter $x_3$, which represents the maximum capacity of the routing store (mm), and assumed a substantially lower value than the obtained using the calibrated rating curve. These results highlight the limited performance of the model when wider prior distributions are adopted for rating curve parameters. Moreover, model performance could be impacted by the model errors employed.

For further evaluation, Table 19 presents the performance metrics of the rainfall-stage model. Although the coverage probability for the 95% credibility interval increased, as compared to the model using the estimated rating curve, it decreased when considering above-average stages, which are the primary focus of this study. Additionally, substantial deterioration was observed in the NSE, RMSE, and Pearson correlation performances.

**Table 19 - Metrics performance for the Rainfall-stage model**

| Period | NSE | RMSE | rPearson | Coverage probability for 95% CI | Coverage probability – above-average stage for 95% CI |
|---|---|---|---|---|---|
| Full period | -4.473 | 0.643 | 0.737 | 79.00 | 66.02 |
| Calibration | -4.008 | 0.675 | 0.743 | 75.01 | 59.11 |
| Validation | -5.189 | 0.611 | 0.733 | 82.98 | 71.74 |

For assessing model performance focusing only on high flows, Figure 30 shows the peak coverage in stage prediction. The results reinforce the decline in model performance when using the prior rating curve. Of the 29 identified peak events, only 14 were covered by the 95% credibility interval, corresponding to approximately 48%.

**Figure 30 - Peak coverage Analysis in stage prediction**

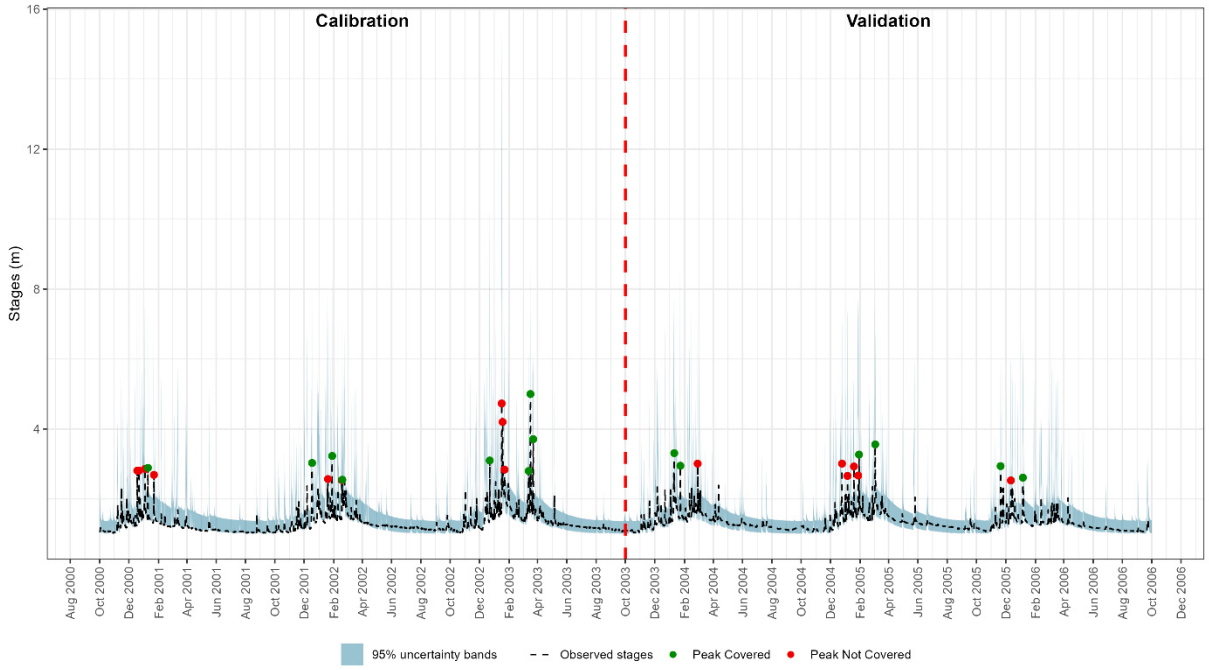


The relative contribution of each source of uncertainty is presented in Figure 31 for discharge predictions and in Figure 32 for stage predictions. Results were generally consistent with those obtained using the estimated rating curve, including the dominance of structural uncertainty associated with the hydrological model. However, as expected, structural uncertainty related to the rating curve represented a larger proportion of total uncertainty in this case.

**Figure 31 - Sources of uncertainties in discharge prediction**

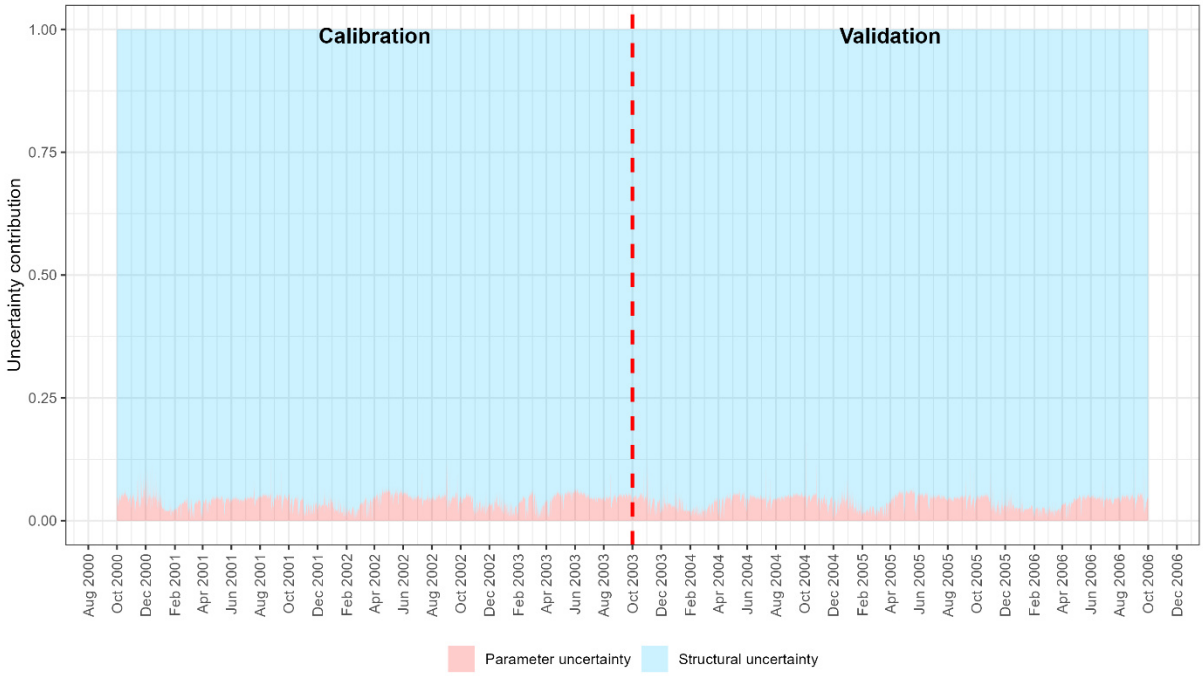


**Figure 32 - Sources of uncertainties in stage prediction**

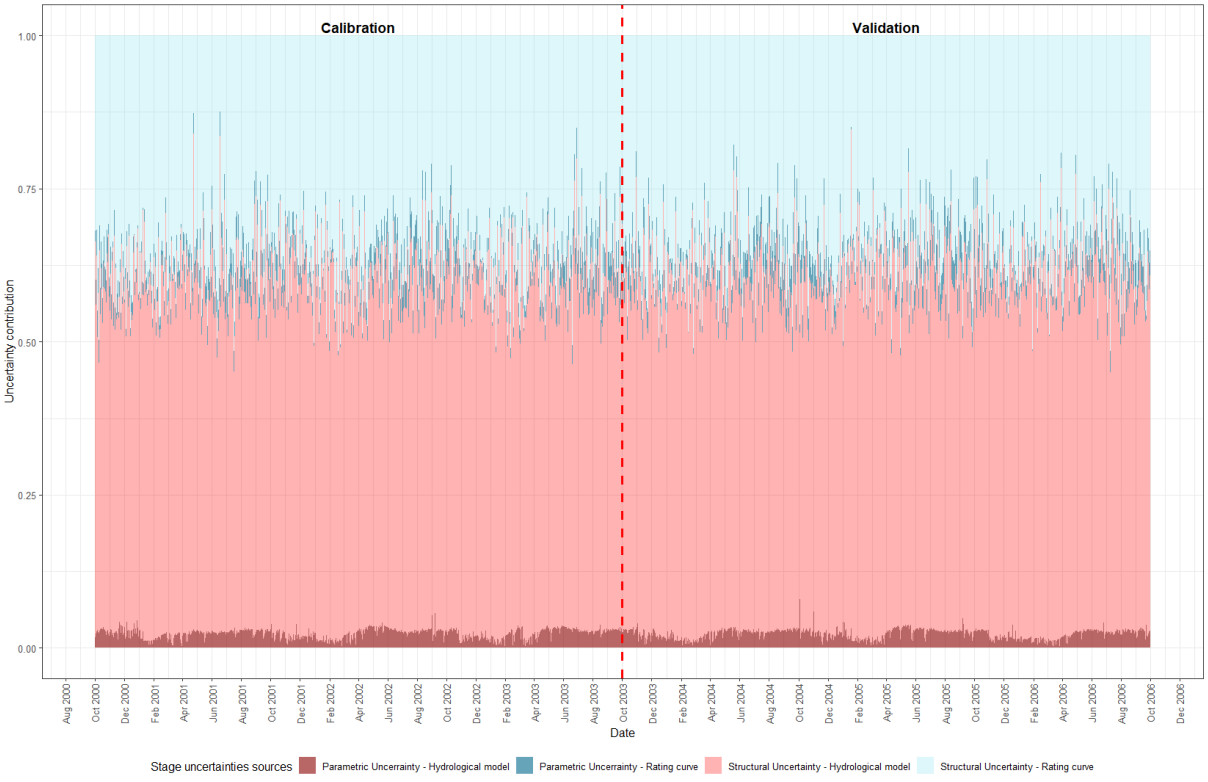


For a more detailed assessment, Table 20 presents the mean, minimum, and maximum contribution from each uncertainty source to stage prediction. Compared to the model using the estimated rating curve, structural uncertainty from the hydrological

model remained dominant, but decreased from an average of 66% to 58%. Conversely, structural uncertainty associated with the rating curve increased from an average of 30% to 37%, reaching a maximum of 57%. Parametric uncertainty remained the least significant component, decreasing on average from 3% to 2% for the hydrological model and increasing on average from 0% to 3% for the rating curve.

**Table 20 - Contribution source for stage uncertainty**

| Source | Mean | Minimum | Maximum |
|---|---|---|---|
| Parametric Uncertainty – Hydrological model | 2% | ~0% | 10% |
| Structural Uncertainty – Hydrological model | 58% | 39% | 89% |
| Parametric Uncertainty – Rating curve | 3% | ~0% | 6% |
| Structural Uncertainty – Rating curve | 37% | 7% | 57% |

Figure 33 compares stage predictions with the relative contribution of uncertainty sources. Wet periods were associated with lower parametric uncertainty from the hydrological model; however, the difference was not pronounced. Some peaks in structural uncertainty associated with the hydrological model occurred during wet periods. Overall, no clear temporal pattern was identified due to the high variability of uncertainty contributions.

**Figure 33 - Comparison between sources of uncertainties and stage prediction**

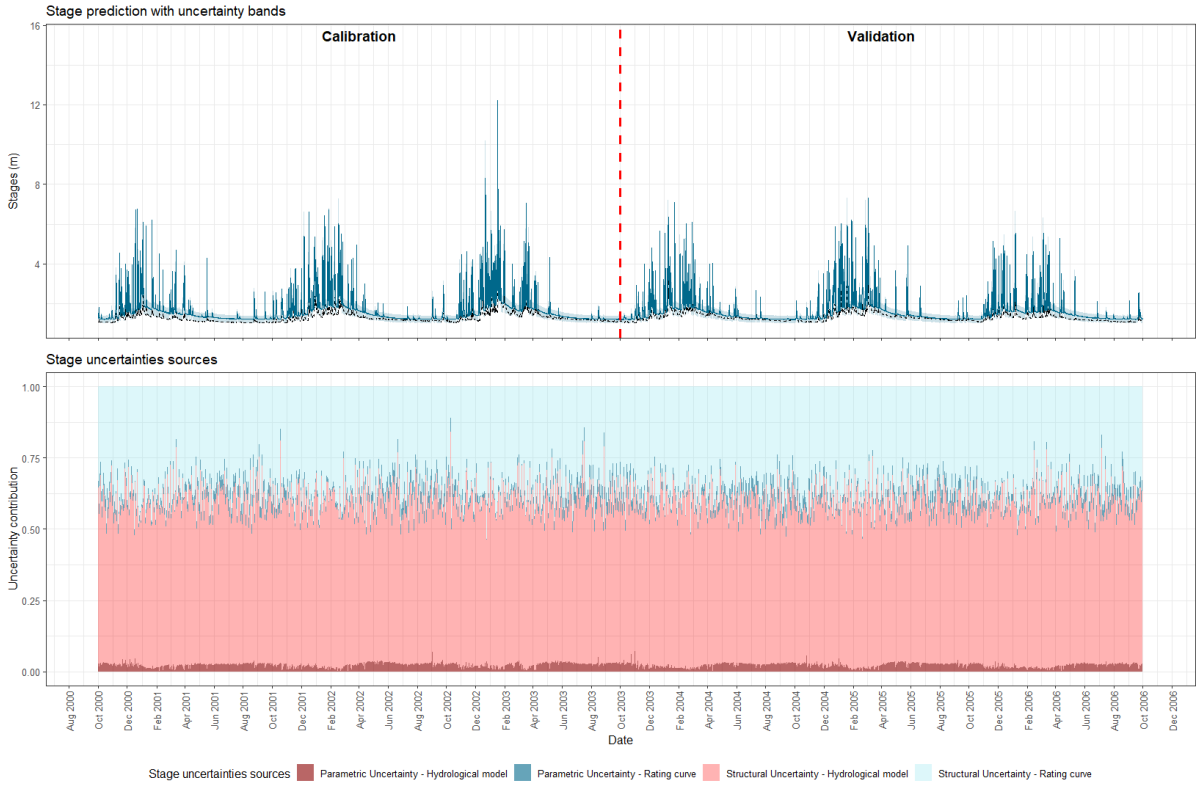


Finally, considering the joint posterior distribution of the rating curve parameters, the rating curve was updated. Figure 34 compares the rating curve before and after rainfall-stage model calibration. The uncertainty bands became narrower and more centered around the median curve. Nevertheless, uncertainty remained high, particularly for high flows, which could be explained by the reduced number of stage measurements at high stages.

**Figure 34 - Comparison between prior and posterior rating curve**

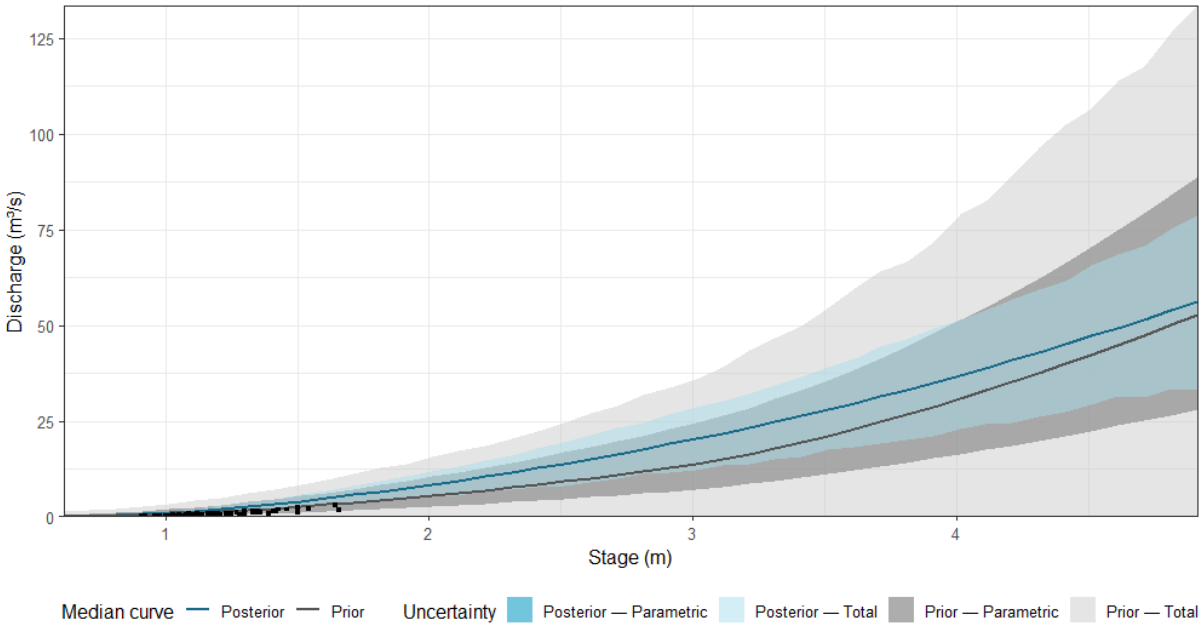


### 5.2.3 Limitations of the rainfall-runoff model

The rainfall-stage model developed in this study comprises 14 parameters: four from the hydrological model, six from the rating curve, and four from the error models (two associated with the hydrological model and two with the rating curve). As a result, the model is complex and prone to parameter compensation effects, as well as difficulties in convergence.

Wide prior ranges for the hydrological model parameters led to significant identifiability issues and hindered convergence. Parameter $x_2$ was particularly problematic, as it was highly sensitive and had a strong influence on simulated discharges. Additionally, equifinality issues were observed during some tests performed. To address this problem, parameter ranges were restricted based on values reported in the literature.

The hydrological error model is characterized by two parameters: $\sigma$ and $\phi$. A wide prior distribution was assigned to the $\phi$ parameter, and the available data were sufficient to allow its identification. However, the $\phi$ parameter was assumed to be time-independent, despite expected differences between dry and wet periods. The $\sigma$ parameter was constrained to ensure that the magnitude of the errors remained consistent with the magnitude of simulated discharges. Moreover, sensitivity analysis

showed that higher values of $\sigma$ resulted in wider uncertainty bands, while data coverage probability did not increase proportionally.

For the rating curve parameters, wide prior ranges resulted in posterior distributions that were far from physically expected values; therefore, these ranges were also restricted, as was done for the model error parameters. For the rainfall-stage model using the prior rating curve, that is, considering only geometric and hydraulic characteristics, the variance of the prior distributions was much larger, which led to convergence difficulties. Consequently, prior distributions were further restricted based on the 95% credibility interval, using the proposed mean values and standard deviation. Furthermore, to assess data coverage and model convergence, the $\beta_1$ parameter was restricted, as it represents the expected heteroscedasticity.

The model enables the representations of both parametric and structural uncertainties associated with the rating curve and the hydrological model. However, uncertainty in input data (precipitation, evapotranspiration, and stages) is not explicitly represented, although it may be significant in some cases. As a result, structural uncertainty related to the hydrological model prevails and may implicitly incorporate other sources of uncertainties. In addition, compensation effects may occur between parameters and uncertainty components. Moreover, the GR4H has a relatively simple structure. The use of more parametrized models could improve the representation of hydrological processes; however, this would likely increase parametric uncertainty, complicate convergence, and raise computational costs. The assessment of uncertainty sources also indicated that structural uncertainty associated with the rating curve is significant, particularly when using the prior rating curve.

For the model using the estimated rating curve, diagnostic metrics suggest that the convergence was likely achieved. Coverage probability remained below the theoretical threshold. For above-average values, which are the focus of this study, performance improved, although it remained below the theoretical threshold. Other commonly used metrics in hydrology (NSE, RMSE, and rPearson) showed good model performance. In contrast, for the model using the prior rating curve, although convergence was likely achieved, performance metrics were considerably worse, especially for high flows. These findings are consistent with the results reported by Sikorska and Renard (2017),

as in their case study, discharge observations were available across the full range of flows, leading to better model performance. Moreover, model performance might be impacted by the model errors prescribed.

Despite these limitations, the proposed method shows potential when discharge measurements are available, as it enables hydrological simulations based on stage observations, particularly for high-flow conditions, which are the primary focus of this study. However, when using only the prior rating curve, that is, simulating cases in which rating curves are unavailable, results showed poor model performance, highlighting the need for discharge observations. Furthermore, the model should be applied to a case study with regular cross-section and available topographic and Manning roughness data, to assess whether a prior rating curve with tighter prior distributions, even in the absence of discharge data, could lead to improved performance.

## 5.3 Uncertainty propagation through hydrodynamic model

Using the rainfall-stage model presented in Subchapter 5.2.1, ensembles of true discharges and rating curve discharges were subsequently routed through the one-dimensional hydrodynamic model. This procedure aimed to evaluate the impact of explicitly accounting for rating curve uncertainty on hydrodynamic model outputs.

For the hydrodynamic model, a bed slope of 0.0004 m/m was adopted. Manning's roughness coefficients of 0.035 for the main channel and 0.060 for the floodplain were considered. These values fall within the ranges inferred from the rating curve analysis (Subchapter 5.1.1), although the model was not highly informative with respect to these quantities. A total reach length of 100 km was considered, with a spatial discretization of 5 km and a temporal discretization of 15 minutes. These discretization choices were considered consistent with typical monitoring conditions, including those observed in urban basins prone to flash floods.

Regarding geometric definition, the cross-section measured in 2007 was assumed to represent average conditions among all available measurements, and levees were

used to define the floodplain. Vertical discretization was defined using 500 points with an increment of 1 cm. Concerning computational options and tolerances, the maximum number of iterations was set to 40. All other parameters were kept as their default values.

The upstream boundary condition was defined using hydrographs obtained from the rainfall-stage model, whereas the downstream boundary condition was specified as normal depth, based on the adopted riverbed slope. The initial condition was defined by the first value of the hydrographs.

### 5.3.1 Estimated rating curve

Based on the stage predictions and associated uncertainty bands (Figure 21, Subchapter 5.2.1), peak events potentially associated with floodplain activation were sought. Additional selection criteria included smooth hydrograph shape, coverage probability, and post-peak recession behavior. Figure 35 shows the selected event, which lasted 150 hours, from 2003-12-05 20:00:00 to 2003-12-12 01:00:00.

**Figure 35 - Prediction stages and uncertainty bands – selected event for hydrodynamic propagation**

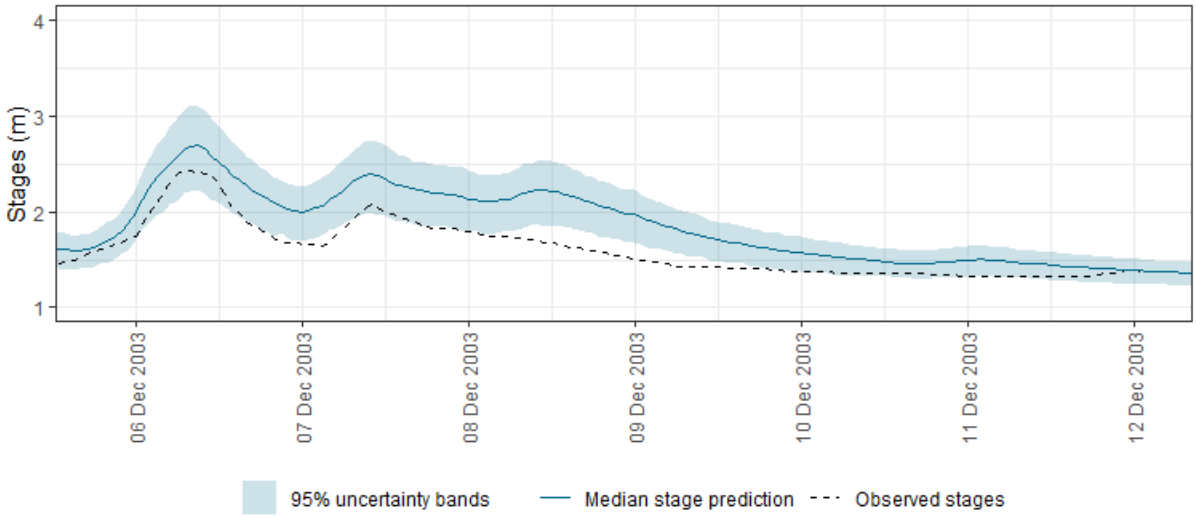


Results from the hydrodynamic propagation performed using HEC-RAS are presented below. For all simulations, the overall volume accounting error percentage was evaluated, with a maximum of 0.5844%.

Figure 36 presents the routing of true discharges and rating curve discharges, both derived from the rainfall-stage model, through the hydrodynamic model. Across all sections, median values of true and rating curve discharges were very similar. At the first section, corresponding to the outflow hydrograph from the rainfall-stage model, the maximum 95% credible interval was 47% wider for the rating curve discharge (9.30 $m^3/s$) than for the true discharge (6.31 $m^3/s$). The largest difference occurs before the hydrograph peak, likely due to floodplain activation, where rating curve uncertainty is higher because of the absence of discharge measurements for rating curve construction. In downstream sections, spaced at 5 km intervals, hydrograph attenuation and propagation effects were observed. Across all sections, the difference between the maximum value of the credible intervals for the rating curve discharges and true discharges ranged from 30% to 43%, with the largest difference occurring in the last section, indicating the persistent impact of rating curve uncertainty. Over the entire period, the 95% credible interval was, on average, 40% wider for rating curve discharges, as compared to the true counterparts.

**Figure 36 - Propagation of true discharges and rating curve discharges through the hydrodynamic model – Discharge variable**

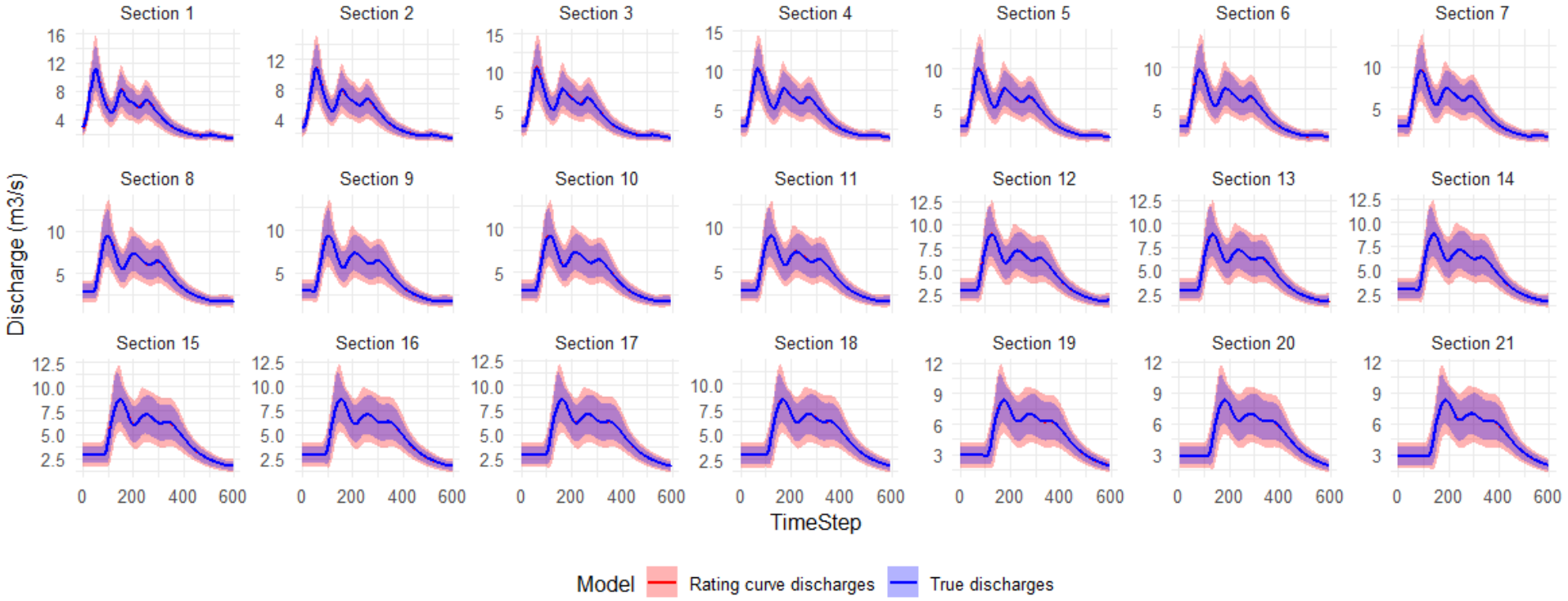

Figure 37 presents the results of velocity behavior during the routing of true discharges and rating curve discharges. At the first model section, the maximum 95% credibility interval is 52% wider for velocities computed using rating curve discharge (0.185 m/s) than for those based on the true discharges (0.122 m/s). As observed for discharge, the largest difference occurred near the hydrograph peak. The difference between the maximum credible interval values ranged from 37% to 41% across sections, with the lowest difference observed in the last section. Overall, throughout the entire period, the 95% credible interval was, on average, 44% wider for velocities derived from rating curve discharges, which was considered significant. Reduced uncertainty in velocity prediction may improve the assessment of property damage and potential loss of life in flood analyses. Median velocity values were very similar for both discharge representations.

**Figure 37 - Propagation of true discharges and rating curve discharges through the hydrodynamic model – Velocity variable**

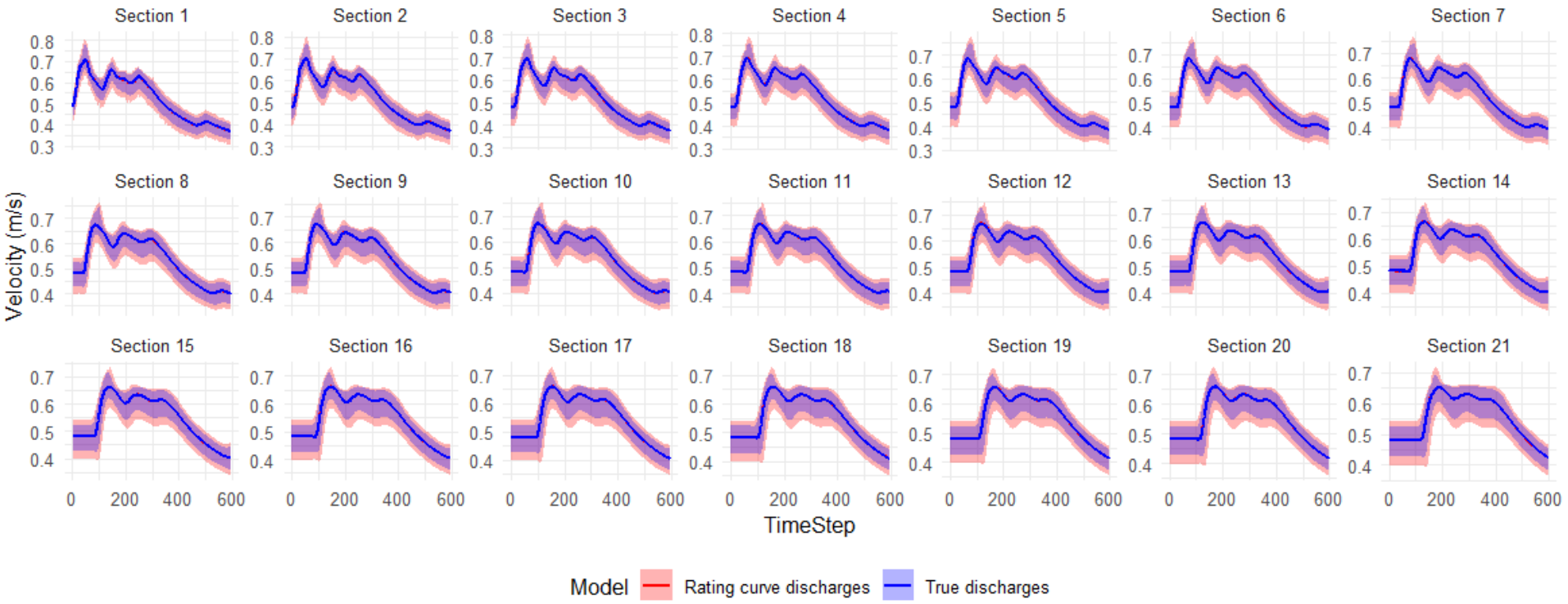

Figure 38 presents the results of flow depth behavior during the routing of true discharges and rating curve discharges. Over the entire period, the 95% credible intervals for depth were, on average, 40% wider when using rating curve discharges, as compared to true discharges. At the first section, the 95% credible intervals for depths obtained using rating curves was 36% larger (1.014 m) than those obtained using true discharges (0.748 m). This difference increased downstream, reaching 49% in the last section (1.2622 m for rating curve discharges and 0.8488 m for true discharges). Median depth values remained very similar between the two models.

The depth variable is particularly relevant for defining flood alert system activation criteria. In addition, uncertainty in depth can influence floodplain activation. Analysis of HEC-RAS results showed that for the 97.5% quantile of true discharges, floodplain inundation occurred from sections 1 to 7. In contrast, for the 97.5% quantile of rating curve discharges, floodplain inundation extended from sections 1 to 11. Median and 2.5% quantile values for both discharge representations did not result in floodplain inundation. These results highlight the importance of explicitly accounting for rating curve uncertainty in flood management applications.

**Figure 38 - Propagation of true discharges and rating curve discharges through the hydrodynamic model – Depth variable**

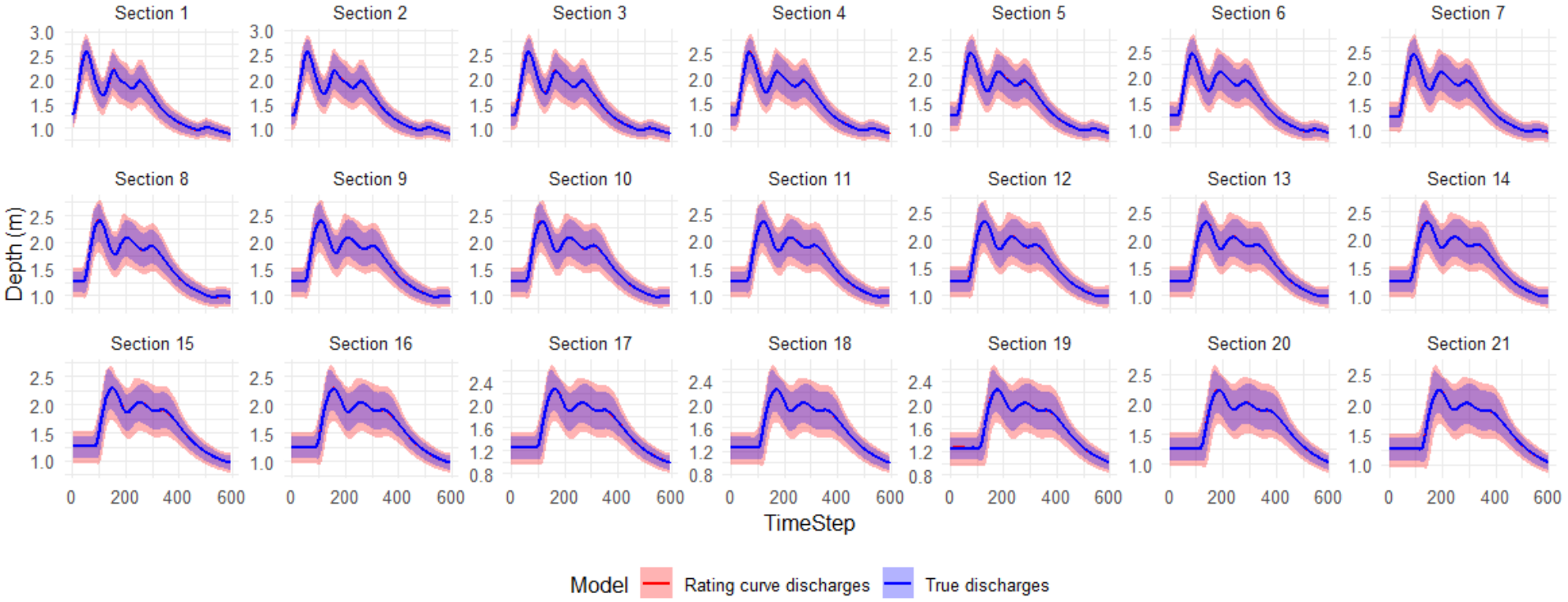

### 5.3.2 Prior rating curve

The same procedure used to identify peak events for hydrodynamic propagation with the estimated rating curve model was applied to the prior rating curve model. However, as discussed in Subchapter 5.2.2, this model systematically overestimated stages and exhibited wide uncertainty bands, as presented in Figure 39. Consequently, it was considered unreliable for prediction. Moreover, the pronounced overestimation would require extrapolation of stages beyond the available cross-sections, and no additional topographic information was available to support such simulation. Therefore, flood waves derived from the prior rating curve model were not routed through the hydrodynamic model.

**Figure 39 - Prediction stages and uncertainty bands – zoom**

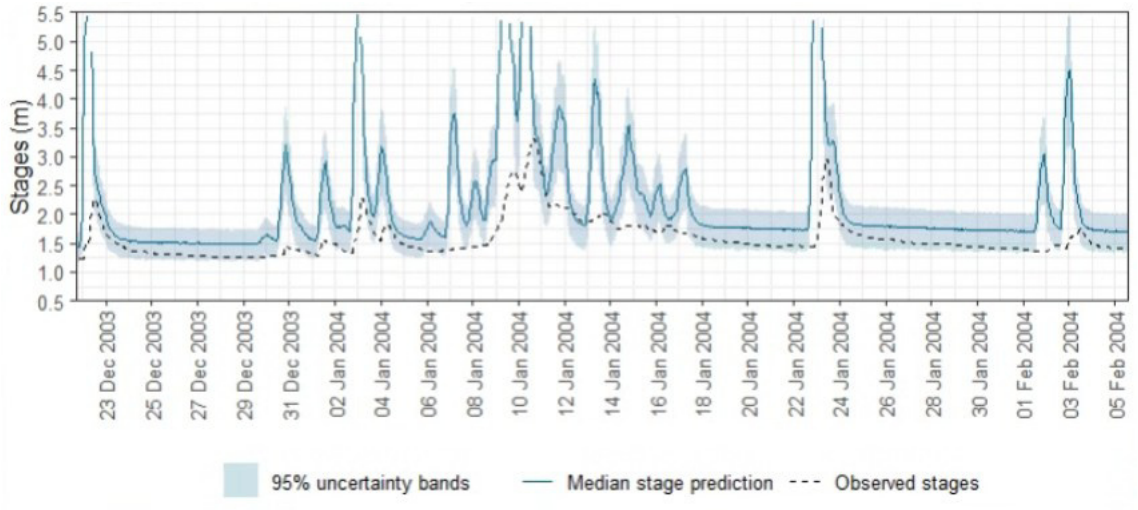


### 5.3.3 Limitations of the hydrodynamic model

The HEC-RAS one-dimensional unsteady flow module was used to route discharges obtained from the rainfall-stage model through numerical solution of the Saint-Venant equations. Although this 1D approach is computationally efficient, it relies on simplifying assumptions that may not hold under floodplain flow conditions. Nevertheless, it can be considered appropriate for urban channels with relatively regular cross-sections.

Discharges were obtained from the rainfall-stage model, accounting for uncertainties from both the hydrological model and the rating curve. In particular, the rating curve error model assumes time-independent errors, which results in discontinuities in the discharge time series. Although this formulation is mathematically consistent, it lacks physical realism and complicates hydrodynamic propagation. To address this issue, discharge ensembles were sorted by magnitude, and the limits corresponding to the 95% credibility interval were selected for hydrodynamic propagation. These propagated hydrographs do not necessarily correspond to individual realizations from the rainfall-stage model.

Furthermore, uncertainty propagation was assessed using only one flood event, which limits the generalization of the results. For the median estimates, stages derived from the true discharges and from the rating curve discharges did not inundate the floodplain. However, inundation occurred for the 97.5% quantile, indicating that upper-bound discharge uncertainty may critically affect floodplain activation and, consequently, water resources management decisions. Due to the high variability of uncertainty sources, the selection of different events could lead to different uncertainty estimates. Nevertheless, in the example performed, the contribution of rating curve uncertainty did not exhibit significant variability during routing along the river sections.

Finally, a major limitation of this part of the study was the lack of downstream stage data required for hydrodynamic model calibration, particularly for Manning's roughness coefficient. This parameter aggregates several sources of uncertainty in hydrodynamic modeling and can substantially influence simulation results. In the analysis performed, only uncertainty related to the upstream discharge boundary condition was propagated using a fictitious model with fixed roughness coefficients, slope, and cross-section geometry; lateral inflow was not considered. Consequently, total predictive uncertainty was likely underestimated, since uncertainty in Manning's roughness coefficient was not included. This limitation hinders model validation and its use for prediction.

# 6 CONCLUSIONS

The objective of this work was to develop a hydrological modeling framework that explicitly accounts for parametric and structural uncertainties associated with both the rating curve and the hydrological model using the Bayesian approach proposed by Sikorska and Renard (2017), and to propagate these uncertainties through a hydrodynamic model in order to assess their impact. The proposed rainfall-stage model enabled discharge prediction even in situations where discharge observations are unavailable, which is particularly advantageous in urban or small catchment environments, where rating curves are often poorly defined or absent. This is achieved through the construction of a prior rating curve that relates rating-curve parameters to hydraulic knowledge, as proposed in the BaRatin method (Le Coz et al., 2014). Overall, the proposed method aims to improve the reliability of information used for decision-making processes in flood alert systems.

For the estimated rating curve, results indicated satisfactory coverage probability, with 93% of the observations lying within the 95% credibility interval. Nevertheless, uncertainty bands were relatively wide at high stages, likely due to the scarcity of discharge measurements in this range, highlighting the importance of collecting high-flow observations. This finding is consistent with previous studies reporting large uncertainty associated with rating curve extrapolation beyond the range of available data. In the case of the prior rating curve, uncertainty bands were even wider, as expected, and encompassed all observed data.

The rainfall-stage model using the estimated rating curve yielded adequate model performance, although coverage probabilities remained below the theoretical coverage. During the validation period, the 95% credible intervals covered 60% of the observations, increasing to 72% for above-average stages, which are the primary focus of this research. For the selected peak events, coverage reached approximately 83%. Explicit uncertainty decomposition revealed a predominance of structural uncertainty associated with the hydrological model, ranging from 43% to 99%, with an average contribution of 66%. Structural uncertainty related to the rating curve was also significant, with an average contribution of 30% and a maximum value of 54%.

In contrast, the rainfall-stage model using the prior rating curve could not properly represent the observed stages. Although coverage probabilities increased for the empirical 95% credibility intervals, this increase was primarily due to wider uncertainty bands. For above-average stages, coverage probabilities decreased, and coverage for the selected peak events dropped to 48%. The predominance of structural uncertainty associated with the hydrological model persisted; however, its average contribution reduced to 58%, while the average structural uncertainty related to the rating curve increased to 37%, with a maximum value of 57%. The broadening of rating curve priors led to convergence difficulties, including identifiability issues, as well as substantial deterioration in performance metrics. These results hindered uncertainty propagation through the hydrodynamic model.

For the rainfall-stage model using the estimated rating curve, the so-called true discharges and the rating curve discharges were routed through the hydrodynamic model to assess the impact of explicitly accounting for hydrological model and rating curve uncertainties. The results demonstrate the persistent influence of rating curve uncertainties, across all sections and for all analyzed variables (depth, discharge, and velocity). Uncertainty bands associated with rating curve discharged were, on average, 40% wider for depth, 40% wider for discharges, and 44 % wider for velocity, compared with those obtained from true discharges. This uncertainty affected, for example, the number of sections in which floodplain inundation occurred. These findings highlight the importance of explicitly accounting for rating curve uncertainty. Depth is particularly relevant for defining flood alert system activation criteria; therefore, further research is needed to determine how uncertainty in depth predictions can be operationally incorporated into these criteria.

It should be noted that these conclusions are based on the specific case study analyzed in this work, which is part of a broader research project, and future studies will include the application of the proposed method to urban catchments. Despite the discussed limitations, the proposed modeling framework shows potential when rating curves are well defined. Recommendations for further improving the developed models are presented in Chapter 7.

Overall, the results reinforce the importance of explicitly accounting for rating curve uncertainty, given its substantial contribution to total predictive uncertainty; and the need for discharge measurements, particularly for high flows, to improve rating curve construction where possible. Finally, the study highlights the need to advance the understanding of hydrological processes to improve hydrological model structure and ultimately reduce structural errors, which was identified as the dominant source of uncertainty.

# 7 RECOMMENDATIONS

Based on the results and the discussed limitations, recommendations for future work are presented below and grouped according to the developed modeling components.

Rating-curve model

- Adopt rating curve models that allow for temporal variability, accounting for changes in channel geometry, vegetation, or hydraulic controls over time, as proposed by Mansanarez et al. (2019a) and Eleutério, Silva and Costa (2025). This could improve model performance for low flows, although it could result in higher computational cost;
- Consider alternative residual error models, including autocorrelated structures and flow-dependent error variance, particularly for low-flow conditions;
- Test alternative rating curve formulations, such as polynomial models or hierarchical Bayesian extensions; and
- Analyze the impact of incorporating stage measurement errors.

Rainfall-stage model

- Test alternative hydrological models in addition to GR4H, assessing their sensitivity to uncertainty analysis;
- Consider alternative error models, including non-normal distribution with heavy tails and higher-order autocorrelation structures;
- Explicitly account for uncertainty in input data, such as precipitation and evapotranspiration; and
- Apply the method considering the prior rating curve to a case study with a regular cross-section and available topographic and Manning roughness data.

Hydrodynamic models

- Apply the proposed framework to a case study with available downstream stage data, allowing calibration of the hydrodynamic model, including Manning roughness coefficient and error model parameters;
- Route multiple events in order to evaluate if the observed behavior of the present case study persists;
- Revise the model error formulation, particularly for the rating curve, aiming to obtain hydrographs with more consistent physical behavior. This would allow all hydrograph trajectories to be propagated through the hydrodynamic model with fewer numerical instabilities; and
- Adopt two-dimensional hydrodynamic models, which are more suitable in the case of floodplain activation, provided that input data with compatible spatial and temporal resolution are available.

Finally, future studies should focus on integrating uncertainty-informed hydrological and hydrodynamic predictions into flood alert system activation strategies.

## REFERENCES

AITKEN, A. P. Assessing systematic errors in rainfall-runoff models. **Journal of Hydrology**, v. 20, n. 2, p. 121–136, out. 1973.

AMMANN, Lorenz; FENICIA, Fabrizio; REICHERT, Peter. A likelihood framework for deterministic hydrological models and the importance of non-stationary autocorrelation. **Hydrology and Earth System Sciences**, v. 23, n. 4, p. 2147–2172, 30 abr. 2019.

ANA, Agência Nacional de Águas. **Outros Sistemas Hídricos**. Capa. Disponível em: <https://www.ana.gov.br/sar/outros-sistemas-hidricos/paraopeba/paraopeba>. Acesso em: 29 dez. 2025a.

ANA, Agência Nacional de Águas. **HIDROWEB**. Disponível em: <https://www.snirh.gov.br/hidroweb/apresentacao>. Acesso em: 29 dez. 2025b.

ANA, Agência Nacional de Águas. **ANADEM – Modelo Digital de Terreno para a América do Sul**. Disponível em: <https://metadados.snirh.gov.br/geonetwork/srv/api/records/93664c15-1ff8-4e87-bbed-2bb69d321309>. Acesso em: 29 dez. 2025c.

ARVIZ. **arviz.bfmi — ArviZ 0.23.0 documentation**. Disponível em: <https://python.arviz.org/en/stable/api/generated/arviz.bfmi.html>. Acesso em: 29 dez. 2025.

AYZEL, Georgy; HEISTERMANN, Maik. The effect of calibration data length on the performance of a conceptual hydrological model versus LSTM and GRU: A case study for six basins from the CAMELS dataset. **Computers & Geosciences**, v. 149, p. 104708, abr. 2021.

BAPTISTA, Márcio; LARA, Márcia. **Fundamentos de engenharia hidráulica**. 4ª ed. *[S.l.]*: Editora UFMG, 2016.

BATES, Bryson C.; CAMPBELL, Edward P. A Markov Chain Monte Carlo Scheme for parameter estimation and inference in conceptual rainfall-runoff modeling. **Water Resources Research**, v. 37, n. 4, p. 937–947, abr. 2001.

BENNETT, James C. *et al.* A System for Continuous Hydrological Ensemble Forecasting (SCHEF) to lead times of 9 days. **Journal of Hydrology**, v. 519, p. 2832–2846, nov. 2014.

BETANCOURT, Michael. **A Conceptual Introduction to Hamiltonian Monte Carlo**. arXiv, , 16 jul. 2018. Disponível em: <http://arxiv.org/abs/1701.02434>. Acesso em: 29 dez. 2025

BEVEN, Keith. Changing ideas in hydrology — The case of physically-based models. **Journal of Hydrology**, v. 105, n. 1–2, p. 157–172, jan. 1989.

BEVEN, Keith. Facets of uncertainty: epistemic uncertainty, non-stationarity, likelihood, hypothesis testing, and communication. **Hydrological Sciences Journal**, v. 61, n. 9, p. 1652–1665, 3 jul. 2016a.

BEVEN, Keith. Advice to a young hydrologist. **Hydrological Processes**, v. 30, n. 20, p. 3578–3582, 30 set. 2016b.

BEVEN, Keith; BINLEY, Andrew. The future of distributed models: Model calibration and uncertainty prediction. **Hydrological Processes**, v. 6, n. 3, p. 279–298, jul. 1992.

BOULOMYTIS, Vassiliki Terezinha Galvao *et al.* Estimation and calibration of Manning's roughness coefficients for ungauged watersheds on coastal floodplains. **International Journal of River Basin Management**, v. 15, n. 2, p. 199–206, 3 abr. 2017.

BOX, G. E. P.; COX, D. R. An Analysis of Transformations Revisited, Rebutted. **Journal of the American Statistical Association**, v. 77, n. 377, p. 209–210, mar. 1982.

CAMACHO, René A. *et al.* A Comparison of Bayesian Methods for Uncertainty Analysis in Hydraulic and Hydrodynamic Modeling. **JAWRA Journal of the American Water Resources Association**, v. 51, n. 5, p. 1372–1393, out. 2015.

CARPENTER, Bob *et al. Stan* : A Probabilistic Programming Language. **Journal of Statistical Software**, v. 76, n. 1, 2017.

CARR, Rachel Hogan *et al.* Improving the Use of Hydrologic Probabilistic and Deterministic Information in Decision-Making. **Bulletin of the American Meteorological Society**, v. 102, n. 10, p. E1878–E1896, out. 2021.

CHADWICK, Andrew J.; MORFETT, John C.; BORTHWICK, Martin. **Hydraulics in civil and environmental engineering**. 5th edition ed. Boca Raton London New York: CRC Press, 2013.

CHANCAY, Juseth E.; ESPITIA-SARMIENTO, Edgar Fabian. Improving Hourly Precipitation Estimates for Flash Flood Modeling in Data-Scarce Andean-Amazon Basins: An Integrative Framework Based on Machine Learning and Multiple Remotely Sensed Data. **Remote Sensing**, v. 13, n. 21, p. 4446, 5 nov. 2021.

CHANSON, Hubert. **The hydraulics of open channel flow: an introduction basic principles, sediment motion, hydraulic modelling, design of hydraulic structures**. 2nd ed ed. Amsterdam: Elsevier, 2004.

CHAUDHRY, M. Hanif (ORG.). **Open-Channel Flow**. Boston, MA: Springer Science+Business Media, LLC, 2008.

CHEN, Wei-Bo; LIU, Wen-Cheng. Modeling the Influence of River Cross-Section Data on a River Stage Using a Two-Dimensional/Three-Dimensional Hydrodynamic Model. **Water**, v. 9, n. 3, p. 203, 10 mar. 2017.

CHOW, Ven Te; MAIDMENT, David R.; MAYS, Larry W. **Applied hydrology**. New York: McGraw-Hill, 1988.

CLARK, Martyn P. *et al.* The Abuse of Popular Performance Metrics in Hydrologic Modeling. **Water Resources Research**, v. 57, n. 9, p. e2020WR029001, set. 2021.

COSTA, Veber; FERNANDES, Wilson. Bayesian estimation of extreme flood quantiles using a rainfall-runoff model and a stochastic daily rainfall generator. **Journal of Hydrology**, v. 554, p. 137–154, nov. 2017.

COXON, G. *et al.* A novel framework for discharge uncertainty quantification applied to 500 UK gauging stations. **Water Resources Research**, v. 51, n. 7, p. 5531–5546, jul. 2015.

DAS, Tanmoy; DAS, Subhasish. An integrated Bayesian hydrodynamic framework for quantifying rating curve uncertainty in design flood estimation and flood hazard mapping in a data-scarce urban area. **Water Research**, v. 288, p. 124610, jan. 2026.

DEL GIUDICE, Dario *et al.* Describing the catchment-averaged precipitation as a stochastic process improves parameter and input estimation. **Water Resources Research**, v. 52, n. 4, p. 3162–3186, abr. 2016.

DI BALDASSARRE, G.; MONTANARI, A. Uncertainty in river discharge observations: a quantitative analysis. **Hydrology and Earth System Sciences**, v. 13, n. 6, p. 913–921, 25 jun. 2009.

DI BALDASSARRE, Giuliano; CLAPS, Pierluigi. A hydraulic study on the applicability of flood rating curves. **Hydrology Research**, v. 42, n. 1, p. 10–19, 1 fev. 2011.

DI BALDASSARRE, Giuliano; LAIO, Francesco; MONTANARI, Alberto. Effect of observation errors on the uncertainty of design floods. **Physics and Chemistry of the Earth, Parts A/B/C**, v. 42–44, p. 85–90, 2012.

DOGULU, N. *et al.* Estimation of predictive hydrologic uncertainty using the quantile regression and UNEEC methods and their comparison on contrasting catchments. **Hydrology and Earth System Sciences**, v. 19, n. 7, p. 3181–3201, 23 jul. 2015.

DOMENEGHETTI, A.; CASTELLARIN, A.; BRATH, A. Assessing rating-curve uncertainty and its effects on hydraulic model calibration. **Hydrology and Earth System Sciences**, v. 16, n. 4, p. 1191–1202, 11 abr. 2012.

DOTTO, Cintia B. S. *et al.* Comparison of different uncertainty techniques in urban stormwater quantity and quality modelling. **Water Research**, v. 46, n. 8, p. 2545–2558, maio 2012.

DRUMOND, Marcos Machado. **A Técnica de Traçadores e o seu Potencial para Ampliar o Conhecimento Hidrológico sobre as Bacias Brasileiras: Um Estudo Aplicado à Bacia Representativa de Juatuba-MG**. Belo Horizonte: Universidade Federal de Minas Gerais, 2004.

DUARTE, Juliana Maia; COSTA, Veber Afonso Figueiredo. A metamodel for sensitivity and uncertainty analysis in the modeling of loss of life due to dam failures. **Journal of Hydroinformatics**, v. 26, n. 11, p. 2939–2961, 1 nov. 2024.

ELEUTÉRIO, Iago; SILVA, Francisco; COSTA, Veber. Assessing the stage-period-discharge framework for modeling highly unstable rating curves: a case study at the UHE Peti Carrapato streamflow Gauging Station, Brazil. **Stochastic Environmental Research and Risk Assessment**, v. 39, n. 2, p. 829–845, fev. 2025.

ENGELAND, K.; GOTTSCHALK, L. Bayesian estimation of parameters in a regional hydrological model. **Hydrology and Earth System Sciences**, v. 6, n. 5, p. 883–898, 31 out. 2002.

ESSERY, Richard *et al.* A comparison of 1701 snow models using observations from an alpine site. **Advances in Water Resources**, v. 55, p. 131–148, maio 2013.

EVIN, Guillaume *et al.* Pitfalls and improvements in the joint inference of heteroscedasticity and autocorrelation in hydrological model calibration. **Water Resources Research**, v. 49, n. 7, p. 4518–4524, jul. 2013.

FARZANA, Syeda Zehan. Uncertainty in hydrological modelling: A review. **International Journal of Hydrology Research**, v. 8, n. 1, p. 1–13, 17 fev. 2023.

FENTON, John D. On the generation of stream rating curves. **Journal of Hydrology**, v. 564, p. 748–757, set. 2018.

GARCIA, Rodrigo; COSTA, Veber; SILVA, Francisco. Bayesian Rating Curve Modeling: Alternative Error Model to Improve Low-Flow Uncertainty Estimation. **Journal of Hydrologic Engineering**, v. 25, n. 5, p. 04020012, maio 2020.

HAN, Shasha; COULIBALY, Paulin; BIONDI, Daniela. Assessing Hydrologic Uncertainty Processor Performance for Flood Forecasting in a Semiurban Watershed. **Journal of Hydrologic Engineering**, v. 24, n. 9, p. 05019025, set. 2019.

HAPUARACHCHI, H. A. P.; WANG, Q. J.; PAGANO, T. C. A review of advances in flash flood forecasting. **Hydrological Processes**, v. 25, n. 18, p. 2771–2784, 30 ago. 2011.

HARUNA, Abubakar *et al.* Does Flash Flood Model Performance Increase with Complexity? Signature and Sensitivity-Based Comparison of Conceptual and Process-Oriented Models on French Mediterranean Cases. **Hydrology**, v. 9, n. 8, p. 141, 8 ago. 2022.

HERRERA, Paulo A.; MARAZUELA, Miguel Angel; HOFMANN, Thilo. Parameter estimation and uncertainty analysis in hydrological modeling. **WIREs Water**, v. 9, n. 1, p. e1569, jan. 2022.

HOFFMAN, Matthew D.; GELMAN, Andrew. **The No-U-Turn Sampler: Adaptively Setting Path Lengths in Hamiltonian Monte Carlo**. arXiv, , 2014. Disponível em: <https://arxiv.org/abs/1111.4246>. Acesso em: 29 dez. 2025

HØJBERG, A. L.; REFSGAARD, J. C. Model uncertainty – parameter uncertainty versus conceptual models. **Water Science and Technology**, v. 52, n. 6, p. 177–186, 1 set. 2005.

HORNER, I. *et al.* Impact of Stage Measurement Errors on Streamflow Uncertainty. **Water Resources Research**, v. 54, n. 3, p. 1952–1976, mar. 2018.

HRAFNKELSSON, Birgir *et al.* Modeling discharge rating curves with Bayesian B-splines. **Stochastic Environmental Research and Risk Assessment**, v. 26, n. 1, p. 1–20, jan. 2012.

HRAFNKELSSON, Birgir *et al.* Generalization of the power-law rating curve using hydrodynamic theory and Bayesian hierarchical modeling. **Environmetrics**, v. 33, n. 2, p. e2711, mar. 2022.

HUARD, David; MAILHOT, Alain. A Bayesian perspective on input uncertainty in model calibration: Application to hydrological model “abc”. **Water Resources Research**, v. 42, n. 7, p. 2005WR004661, jul. 2006.

HUARD, David; MAILHOT, Alain. Calibration of hydrological model GR2M using Bayesian uncertainty analysis. **Water Resources Research**, v. 44, n. 2, p. 2007WR005949, fev. 2008.

HULSMAN, Petra; BOGAARD, Thom A.; SAVENIJE, Hubert H. G. Rainfall-runoff modelling using river-stage time series in the absence of reliable discharge information: a case study in the semi-arid Mara River basin. **Hydrology and Earth System Sciences**, v. 22, n. 10, p. 5081–5095, 2 out. 2018.

IBGE, Instituto Brasileiro de Geografia e Estatística. **Malha Municipal | IBGE**. Disponível em: <https://www.ibge.gov.br/geociencias/organizacao-do-territorio/malhas-territoriais/15774-malhas.html>. Acesso em: 29 dez. 2025.

INMET, Instituto Nacional de Meteorologia. **Catálogo de Estações Automáticas**. Disponível em: <https://portal.inmet.gov.br/paginas/catalogoaut#>. Acesso em: 29 dez. 2025.

JAHANDIDEH-TEHRANI, Mahsa *et al.* Hydrodynamic modelling of a flood-prone tidal river using the 1D model MIKE HYDRO River: calibration and sensitivity analysis. **Environmental Monitoring and Assessment**, v. 192, n. 2, p. 97, fev. 2020.

JCGM, Joint Committee for Guides in Metrology. **Evaluation of measurement data — Guide to the expression of uncertainty in measurement**. , 2008.

KASTALI, Abdennour *et al.* Design Flood and Flood-Prone Areas under Rating Curve Uncertainty: Area of Vieux-Ténès, Algeria. **Journal of Hydrologic Engineering**, v. 26, n. 3, p. 05020054, mar. 2021.

KASTALI, Abdennour *et al.* Auto-calibration of HEC-HMS Model for Historic Flood Event under Rating Curve Uncertainty. Case Study: Allala Watershed, Algeria. **KSCE Journal of Civil Engineering**, v. 26, n. 1, p. 482–493, jan. 2022.

KAVETSKI, Dmitri; FRANKS, Stewart W.; KUCZERA, George. Confronting input uncertainty in environmental modelling. *In*: DUAN, Qingyun *et al.* (Orgs.). **Water Science and Application**. Washington, D. C.: American Geophysical Union, 2003a. v. 6 p. 49–68.

KAVETSKI, Dmitri; FRANKS, Stewart W.; KUCZERA, George. Confronting input uncertainty in environmental modelling. *In*: DUAN, Qingyun *et al.* (Orgs.). **Water Science and Application**. Washington, D. C.: American Geophysical Union, 2003b. v. 6 p. 49–68.

KAVETSKI, Dmitri; KUCZERA, George; FRANKS, Stewart W. Bayesian analysis of input uncertainty in hydrological modeling: 1. Theory. **Water Resources Research**, v. 42, n. 3, p. 2005WR004368, mar. 2006.

KIANG, Julie E. *et al.* A Comparison of Methods for Streamflow Uncertainty Estimation. **Water Resources Research**, v. 54, n. 10, p. 7149–7176, out. 2018.

KRUSCHKE, John K.; LIDDELL, Torrin M. Bayesian data analysis for newcomers. **Psychonomic Bulletin & Review**, v. 25, n. 1, p. 155–177, fev. 2018.

KUCZERA, George. Improved parameter inference in catchment models: 1. Evaluating parameter uncertainty. **Water Resources Research**, v. 19, n. 5, p. 1151–1162, out. 1983.

LANG, Michel *et al.* Extrapolation of rating curves by hydraulic modelling, with application to flood frequency analysis. **Hydrological Sciences Journal**, v. 55, n. 6, p. 883–898, 23 ago. 2010.

LANG, Michel *et al.* Accounting for historical data uncertainty in flood frequency analysis: the Upper Rhine River. **Journal of Hydrology**, v. 660, p. 133480, out. 2025.

LE COZ, J. *et al.* Combining hydraulic knowledge and uncertain gaugings in the estimation of hydrometric rating curves: A Bayesian approach. **Journal of Hydrology**, v. 509, p. 573–587, fev. 2014.

LE MOINE, Nicolas; ANDRÉASSIAN, Vazken; MATHEVET, Thibault. Confronting surface- and groundwater balances on the La Rochefoucauld-Touvre karstic system (Charente, France). **Water Resources Research**, v. 44, n. 3, p. 2007WR005984, mar. 2008.

LI, Ming *et al.* Improved error modelling for streamflow forecasting at hourly time steps by splitting hydrographs into rising and falling limbs. **Journal of Hydrology**, v. 555, p. 586–599, dez. 2017.

LIU, Yuqiong; GUPTA, Hoshin V. Uncertainty in hydrologic modeling: Toward an integrated data assimilation framework. **Water Resources Research**, v. 43, n. 7, p. 2006WR005756, jul. 2007.

LUCAS, Mathieu *et al.* Are historical stage records useful to decrease the uncertainty of flood frequency analysis ? A 200-year long case study. **Journal of Hydrology**, v. 624, p. 129840, set. 2023.

MAILHOT, Alain *et al.* Assessment of uncertainties in stage–discharge rating curves: a large-scale application to Quebec hydrometric network. **Hydrology and Earth System Sciences**, v. 29, n. 15, p. 3615–3627, 8 ago. 2025.

MANSANAREZ, V. *et al.* Bayesian analysis of stage-fall-discharge rating curves and their uncertainties. **Water Resources Research**, v. 52, n. 9, p. 7424–7443, set. 2016.

MANSANAREZ, V. *et al.* Shift Happens! Adjusting Stage-Discharge Rating Curves to Morphological Changes at Known Times. **Water Resources Research**, v. 55, n. 4, p. 2876–2899, abr. 2019a.

MANSANAREZ, Valentin *et al.* Rapid Stage-Discharge Rating Curve Assessment Using Hydraulic Modeling in an Uncertainty Framework. **Water Resources Research**, v. 55, n. 11, p. 9765–9787, nov. 2019b.

MARSHALL, Lucy; SHARMA, Ashish; NOTT, David. Modeling the catchment via mixtures: Issues of model specification and validation. **Water Resources Research**, v. 42, n. 11, p. 2005WR004613, nov. 2006.

MASSERONI, Daniele *et al.* A reliable rainfall–runoff model for flood forecasting: review and application to a semi-urbanized watershed at high flood risk in Italy. **Hydrology Research**, v. 48, n. 3, p. 726–740, 1 jun. 2017.

MASSMANN, Carolina. Identification of factors influencing hydrologic model performance using a top-down approach in a large number of U.S. catchments. **Hydrological Processes**, v. 34, n. 1, p. 4–20, jan. 2020.

MATHEVET, Thibault. **Quels modèles pluie-débit globaux au pas de temps horaire ? Développements empiriques et comparaison de modèles sur un large échantillon de bassins versants**. phdthesis—*[S.l.]*: Doctorat spécialité Sciences de l'eau, ENGREF Paris, 4 nov. 2005.

MATOS, Ana Clara De Sousa; SILVA, Francisco Eustáquio Oliveira E. Bayesian estimation of hydrological model parameters in the signature-domain: Aiming for a regional approach. **Journal of Hydrology**, v. 639, p. 131554, ago. 2024.

MATTOS, Tiago Souza *et al.* Towards reducing flood risk disasters in a tropical urban basin by the development of flood alert web application. **Environmental Modelling & Software**, v. 151, p. 105367, maio 2022.

MCMAHON, Thomas A.; PEEL, Murray C.; AMIRTHANATHAN, Gnanathikkam E. Assessing rating curve uncertainty. **Hydrological Sciences Journal**, v. 70, n. 4, p. 687–694, 12 mar. 2025.

MCMILLAN, H. K.; WESTERBERG, I. K. Rating curve estimation under epistemic uncertainty. **Hydrological Processes**, v. 29, n. 7, p. 1873–1882, 30 mar. 2015.

MCMILLAN, Hilary *et al.* Rainfall uncertainty in hydrological modelling: An evaluation of multiplicative error models. **Journal of Hydrology**, v. 400, n. 1–2, p. 83–94, mar. 2011.

MCMILLAN, Hilary *et al.* How uncertainty analysis of streamflow data can reduce costs and promote robust decisions in water management applications. **Water Resources Research**, v. 53, n. 7, p. 5220–5228, jul. 2017.

MCMILLAN, Hilary K.; WESTERBERG, Ida K.; KRUEGER, Tobias. Hydrological data uncertainty and its implications. **WIREs Water**, v. 5, n. 6, nov. 2018.

MERWADE, Venkatesh *et al.* Uncertainty in Flood Inundation Mapping: Current Issues and Future Directions. **Journal of Hydrologic Engineering**, v. 13, n. 7, p. 608–620, jul. 2008.

MOGES, Edom *et al.* Review: Sources of Hydrological Model Uncertainties and Advances in Their Analysis. **Water**, v. 13, n. 1, p. 28, 25 dez. 2020.

MONTANARI, M. *et al.* Calibration and sequential updating of a coupled hydrologic-hydraulic model using remote sensing-derived water stages. **Hydrology and Earth System Sciences**, v. 13, n. 3, p. 367–380, 18 mar. 2009.

MOTA, Tainá *et al.* Combination of the SCS-CN and the GRADEX models to maximum flow estimation. **RBRH**, v. 23, n. 0, 19 jul. 2018.

MOYEED, R. A.; CLARKE, R. T. The use of Bayesian methods for fitting rating curves, with case studies. **Advances in Water Resources**, v. 28, n. 8, p. 807–818, ago. 2005.

NAGHETTINI, Mauro (ORG.). **Fundamentals of Statistical Hydrology**. Cham: Springer International Publishing, 2017.

NGO, Hieu *et al.* Reconstruction of the 1374 Rhine river flood event around Cologne region using 1D-2D coupled hydraulic modelling approach. **Journal of Hydrology**, v. 617, p. 129039, fev. 2023.

OCIO, David *et al.* The role of rating curve uncertainty in real-time flood forecasting. **Water Resources Research**, v. 53, n. 5, p. 4197–4213, maio 2017.

OSORIO, A. L. N. A.; REIS, D. S. A Bayesian Approach for the Evaluation of Rating Curve Uncertainties in Flood Frequency Analyses. *In*: WORLD ENVIRONMENTAL AND WATER RESOURCES CONGRESS 2016. **World Environmental and Water Resources Congress 2016**. West Palm Beach, Florida: American Society of Civil Engineers, 16 maio 2016. Disponível em: <http://ascelibrary.org/doi/10.1061/9780784479858.050>. Acesso em: 27 out. 2025

PANCHANATHAN, Anandharuban *et al.* An overview of approaches for reducing uncertainties in hydrological forecasting: Progress and challenges. **Earth-Science Reviews**, v. 258, p. 104956, nov. 2024.

PAPPENBERGER, F. *et al.* Uncertainty in the calibration of effective roughness parameters in HEC-RAS using inundation and downstream level observations. **Journal of Hydrology**, v. 302, n. 1–4, p. 46–69, fev. 2005.

PATHIRAJA, S. *et al.* Detecting non-stationary hydrologic model parameters in a paired catchment system using data assimilation. **Advances in Water Resources**, v. 94, p. 103–119, ago. 2016.

PELLETIER, Patrice M. Uncertainties in the single determination of river discharge: a literature review. **Canadian Journal of Civil Engineering**, v. 15, n. 5, p. 834–850, 1 out. 1988.

PERRIN, Charles; MICHEL, Claude; ANDRÉASSIAN, Vazken. Improvement of a parsimonious model for streamflow simulation. **Journal of Hydrology**, v. 279, n. 1–4, p. 275–289, ago. 2003.

PETERSEN-ØVERLEIR, Asgeir. Accounting for heteroscedasticity in rating curve estimates. **Journal of Hydrology**, v. 292, n. 1–4, p. 173–181, jun. 2004.

PETERSEN-ØVERLEIR, Asgeir; REITAN, Trond. Bayesian analysis of stage–fall–discharge models for gauging stations affected by variable backwater. **Hydrological Processes**, v. 23, n. 21, p. 3057–3074, 15 out. 2009.

PETERSEN-ØVERLEIR, Asgeir; SOOT, André; REITAN, Trond. Bayesian Rating Curve Inference as a Streamflow Data Quality Assessment Tool. **Water Resources Management**, v. 23, n. 9, p. 1835–1842, jul. 2009.

PINHEIRO, Viviane Borda; NAGHETTINI, Mauro; PALMIER, Luiz Rafael. Uncertainty estimation in hydrodynamic modeling using Bayesian techniques. **RBRH**, v. 24, p. e38, 2019.

PONCE, Victor Miguel. **Engineering Hydrology, Principles and Practices**. *[S.l.]*: Prentice Hall, 2014.

PORTO, Rodrigo de Melo. **Hidráulica básica**. 4. ed. rev ed. São Carlos: EESC, 2006.

QIU, Jiangchao *et al.* Combining a segmentation procedure and the BaRatin stationary model to estimate nonstationary rating curves and the associated uncertainties. **Journal of Hydrology**, v. 597, p. 126168, jun. 2021.

RDOCUMENTATION. **MCSE function - RDocumentation**. Disponível em: <https://www.rdocumentation.org/packages/LaplacesDemon/versions/16.1.6/topics/MCSE>. Acesso em: 29 dez. 2025.

REIS, Guilherme Da Cruz Dos *et al.* Analysis of the Uncertainty in Estimates of Manning's Roughness Coefficient and Bed Slope Using GLUE and DREAM. **Water**, v. 12, n. 11, p. 3270, 21 nov. 2020.

REITAN, Trond; PETERSEN-ØVERLEIR, Asgeir. Bayesian methods for estimating multi-segment discharge rating curves. **Stochastic Environmental Research and Risk Assessment**, v. 23, n. 5, p. 627–642, 2008.

RENARD, Benjamin *et al.* Understanding predictive uncertainty in hydrologic modeling: The challenge of identifying input and structural errors. **Water Resources Research**, v. 46, n. 5, maio 2010.

RODRIGUES DO AMARAL, Francisco *et al.* Technical note: Operational calibration and performance improvement for a 1D hydrodynamic model in a data-scarce coastal area. **Hydrology and Earth System Sciences**, v. 29, n. 17, p. 4327–4340, 12 set. 2025.

SAADI, Mohamed; FURUSHO-PERCOT, Carina. Which range of streamflow data is most informative in the calibration of an hourly hydrological model? **Hydrological Sciences Journal**, v. 69, n. 1, p. 1–20, 2 jan. 2024.

SAADI, Mohamed; OUDIN, Ludovic; RIBSTEIN, Pierre. Physically consistent conceptual rainfall–runoff model for urbanized catchments. **Journal of Hydrology**, v. 599, p. 126394, ago. 2021.

SAMADI, S.; TUFFORD, D. L.; CARBONE, G. J. Estimating hydrologic model uncertainty in the presence of complex residual error structures. **Stochastic Environmental Research and Risk Assessment**, v. 32, n. 5, p. 1259–1281, maio 2018.

SCHAEFLI, Bettina; TALAMBA, Daniela Balin; MUSY, André. Quantifying hydrological modeling errors through a mixture of normal distributions. **Journal of Hydrology**, v. 332, n. 3–4, p. 303–315, jan. 2007.

SCHOUPS, Gerrit; VRUGT, Jasper A. A formal likelihood function for parameter and predictive inference of hydrologic models with correlated, heteroscedastic, and non-Gaussian errors. **Water Resources Research**, v. 46, n. 10, out. 2010.

SEMAD, Secretaria de Estado de Meio Ambiente e Desenvolvimento Sustentável. **Geovisualizador IDE-Sisema/MG**. Disponível em: <https://visualizador.idesisema.meioambiente.mg.gov.br/>. Acesso em: 29 dez. 2025.

SIKORSKA, A. E. *et al.* Considering rating curve uncertainty in water level predictions. **Hydrology and Earth System Sciences**, v. 17, n. 11, p. 4415–4427, 8 nov. 2013.

SIKORSKA, Anna E.; RENARD, Benjamin. Calibrating a hydrological model in stage space to account for rating curve uncertainties: general framework and key challenges. **Advances in Water Resources**, v. 105, p. 51–66, jul. 2017.

SILVA, Francisco Eustáquio Oliveira e. **AVALIAÇÃO DE MÉTODOS DE PROPAGAÇÃO DE VAZÕES EM CURSOS D'ÁGUA NATURAIS COM ÊNFASE EM ASPECTOS DA GEOMORFOLOGIA FLUVIAL**. Master—*[S.l.]*: Universidade Federal de Minas Gerais, 2006.

SILVA, Francisco; NAGHETTINI, Mauro; FERNANDES, Wilson. Avaliação bayesiana das incertezas nas estimativas dos parâmetros de um modelo chuva-vazão conceitual. **Revista Brasileira de Recursos Hídricos**, v. 19, n. 4, p. 148–159, 2014.

SINGH, V. P. (ORG.). **Computer models of watershed hydrology**. Rev. ed ed. Highlands Ranch, Colo: Water Resources Publications, 1995.

SMITH, Tyler *et al.* Development of a formal likelihood function for improved Bayesian inference of ephemeral catchments. **Water Resources Research**, v. 46, n. 12, p. 2010WR009514, dez. 2010.

SMITH, Tyler Jon; MARSHALL, Lucy Amanda. Bayesian methods in hydrologic modeling: A study of recent advancements in Markov chain Monte Carlo techniques. **Water Resources Research**, v. 44, n. 12, p. 2007WR006705, dez. 2008.

SOROOSHIAN, Soroosh; DRACUP, John A. Stochastic parameter estimation procedures for hydrologie rainfall-runoff models: Correlated and heteroscedastic error cases. **Water Resources Research**, v. 16, n. 2, p. 430–442, abr. 1980.

SOROOSHIAN, Soroosh; GUPTA, Vijai Kumar. The Analysis of Structural Identifiability: Theory and Application to Conceptual Rainfall-Runoff Models. **Water Resources Research**, v. 21, n. 4, p. 487–495, abr. 1985.

STAN. **MCMC Sampling**. Disponível em: <https://mc-stan.org/docs/reference-manual/mcmc.html>. Acesso em: 29 dez. 2025a.

STAN. **How to Diagnose and Resolve Convergence Problems**. Disponível em: <https://mc-stan.org/learn-stan/diagnostics-warnings.html>. Acesso em: 29 dez. 2025b.

STAN. **Posterior Analysis**. Disponível em: <https://mc-stan.org/docs/reference-manual/analysis.html>. Acesso em: 29 dez. 2025c.

STAN. **Program Execution**. Disponível em: <https://mc-stan.org/docs/reference-manual/execution.html#initialization>. Acesso em: 29 dez. 2025d.

STAN, Stan Development. Stan Reference Manual. 2025e.

STEINBAKK, G. H. *et al.* Propagation of rating curve uncertainty in design flood estimation. **Water Resources Research**, v. 52, n. 9, p. 6897–6915, set. 2016.

SUN, Ruochen; YUAN, Huiling; LIU, Xiaoli. Effect of heteroscedasticity treatment in residual error models on model calibration and prediction uncertainty estimation. **Journal of Hydrology**, v. 554, p. 680–692, nov. 2017.

SUN, W. C.; ISHIDAIRA, H.; BASTOLA, S. Towards improving river discharge estimation in ungauged basins: calibration of rainfall-runoff models based on satellite observations of river flow width at basin outlet. **Hydrology and Earth System Sciences**, v. 14, n. 10, p. 2011–2022, 22 out. 2010.

SUN, Wenchao; ISHIDAIRA, Hiroshi; BASTOLA, Satish. Prospects for calibrating rainfall-runoff models using satellite observations of river hydraulic variables as surrogates for in situ river discharge measurements. **Hydrological Processes**, v. 26, n. 6, p. 872–882, 15 mar. 2012a.

SUN, Wenchao; ISHIDAIRA, Hiroshi; BASTOLA, Satish. Calibration of hydrological models in ungauged basins based on satellite radar altimetry observations of river water level. **Hydrological Processes**, v. 26, n. 23, p. 3524–3537, 15 nov. 2012b.

TIMBADIYA, P. V.; PATEL, P. L.; POREY, P. D. A 1D–2D Coupled Hydrodynamic Model for River Flood Prediction in a Coastal Urban Floodplain. **Journal of Hydrologic Engineering**, v. 20, n. 2, p. 05014017, fev. 2015.

TUCCI, Carlos Eduardo Morelli. **Hidrologia: Ciência E Aplicação**. 4ª edição ed. *[S.l.]*: Editora da UFRGS, 2007.

UHLENBECK, G. E.; ORNSTEIN, L. S. On the Theory of the Brownian Motion. **Physical Review**, v. 36, n. 5, p. 823–841, 1 set. 1930.

USACE, Hydrologic Engineering Center. **Introduction to HEC-RAS**. Disponível em: <https://www.hec.usace.army.mil/confluence/rasdocs/rasum/6.1/introduction-to-hec-ras>. Acesso em: 6 fev. 2026.

VAN ESSE, W. R. *et al.* The influence of conceptual model structure on model performance: a comparative study for 237 French catchments. **Hydrology and Earth System Sciences**, v. 17, n. 10, p. 4227–4239, 29 out. 2013.

VEHTARI, Aki *et al.* Rank-Normalization, Folding, and Localization: An Improved Rˆ for Assessing Convergence of MCMC (with Discussion). **Bayesian Analysis**, v. 16, n. 2, 1 jun. 2021.

VIEIRA, Luan Marcos Da Silva *et al.* Assessing the effects of rating curve uncertainty in flood frequency analysis. **RBRH**, v. 27, p. e11, 2022.

VIJAY, Ritesh; SARGOANKAR, Aabha; GUPTA, Apurba. Hydrodynamic Simulation of River Yamuna for Riverbed Assessment: A Case Study of Delhi Region. **Environmental Monitoring and Assessment**, v. 130, n. 1–3, p. 381–387, jul. 2007.

VRUGT, Jasper A. *et al.* Treatment of input uncertainty in hydrologic modeling: Doing hydrology backward with Markov chain Monte Carlo simulation. **Water Resources Research**, v. 44, n. 12, p. 2007WR006720, dez. 2008.

WARMINK, Jord J. *et al.* Identification and Quantification of Uncertainties in a Hydrodynamic River Model Using Expert Opinions. **Water Resources Management**, v. 25, n. 2, p. 601–622, jan. 2011.

WESTERBERG, Ida K. *et al.* Uncertainty in hydrological signatures for gauged and ungauged catchments. **Water Resources Research**, v. 52, n. 3, p. 1847–1865, mar. 2016.

WESTERBERG, Ida K. *et al.* Hydrological model calibration with uncertain discharge data. **Hydrological Sciences Journal**, v. 67, n. 16, p. 2441–2456, 10 dez. 2022.

WILBY, Robert L. *et al.* The 'dirty dozen' of freshwater science: detecting then reconciling hydrological data biases and errors. **WIREs Water**, v. 4, n. 3, p. e1209, maio 2017.

WRIEDT, G.; RODE, M. Investigation of parameter uncertainty and identifiability of the hydrological model WaSiM-ETH. **Advances in Geosciences**, v. 9, p. 145–150, 26 set. 2006.

WSC, Water Survey of Canada. **Measuring Discharge with FlowTracker Acoustic Doppler Velocimeters**. , 2015. Disponível em: <https://publications.gc.ca/collections/collection_2022/eccc/En56-301-2015-eng.pdf>

YANG, Jing; REICHERT, Peter; ABBASPOUR, Karim C. Bayesian uncertainty analysis in distributed hydrologic modeling: A case study in the Thur River basin (Switzerland). **Water Resources Research**, v. 43, n. 10, p. 2006WR005497, out. 2007.

ZEROUAL, Ayoub; MEDDI, Mohamed; ASSANI, Ali A. Artificial Neural Network Rainfall-Discharge Model Assessment Under Rating Curve Uncertainty and Monthly Discharge Volume Predictions. **Water Resources Management**, v. 30, n. 9, p. 3191–3205, jul. 2016.

*APPENDIX A – Rating curve code*

```
// Rating curve model
data {

  // time series data
  int<lower = 0> N;  // sample size to calibrate model
  vector[N] y;       // observed stages
  vector[N] q;       // observed streamflow

  // parameters of prior distributions
  real<lower = 0> S_lwr;      // lower bound of uniform prior distribution of S
  real<lower = 0> S_upr;      // upper bound of uniform prior distribution of S

  real<lower = 0> nc_lwr;      // upper bound of uniform prior distribution of nc
  real<lower = 0> nc_upr;      // upper bound of uniform prior distribution of nc
  real<lower = 0> nc_mean;      // mean prior distribution of nc
  real<lower = 0> np_lwr;      // upper bound of uniform prior distribution of np
  real<lower = 0> np_upr;      // upper bound of uniform prior distribution of np
  real<lower = 0> np_mean;      // mean prior distribution of np

  real<lower = 0> B1_lwr;     // lower bound of uniform prior distribution of B1
  real<lower = 0> B1_upr;     // upper bound of uniform prior distribution of B1
  real<lower = 0> B2_lwr;     // lower bound of uniform prior distribution of B2
  real<lower = 0> B2_upr;     // upper bound of uniform prior distribution of B2

  // related to the rating curve (first control)
  real mu_b1;                 // mean of the normal prior distribution of b1
  real<lower = 0> sigma_b1;   // standard deviation of the normal prior distribution of b1
  real<lower = 0> mu_c1;      // mean of the normal prior distribution of c1
  real<lower = 0> sigma_c1;   // standard deviation of the normal prior distribution of c1

  //                        (second control)
  real mu_k2;                 // mean of the normal prior distribution of k2
  real<lower = 0> sigma_k2;   // standard deviation of the normal prior distribution of k2
```

```
  real<lower = 0> mu_c2;      // mean of the normal prior distribution of c2
  real<lower = 0> sigma_c2;   // standard deviation of the normal prior distribution of c2

  // measurement error
  real<lower = 0> sigma_q;  // standard deviation of the normal prior distribution of qq
}

transformed data{
  real y_min = min(y);
  real nc_sd =  (nc_upr - nc_mean) / (1.959963985);  // standard deviation of the manning coefficient
  real np_sd =  (np_upr - np_mean) / (1.959963985);  // standard deviation of the manning coefficient
  real var_nc =  pow(nc_sd, 2);                      // variance of the manning coefficient
  real var_np =  pow(np_sd, 2);                      // variance of the manning coefficient

  real var_S = (S_upr - S_lwr)^2 / 12;
  real var_B1 = (B1_upr - B1_lwr)^2 / 12;
  real var_B2 = (B2_upr - B2_lwr)^2 / 12;
  real mu_S = (S_upr + S_lwr)/2;
  real mu_B1 = (B1_upr + B1_lwr)/2;
  real mu_B2 = (B2_upr + B2_lwr)/2;
  real mu_nc = (nc_upr + nc_lwr)/2;
  real mu_np = (np_upr + np_lwr)/2;

  // standard deviation (square root of the variace) of rating curve's coefficient "a1"

  real sd_a1 = ((- mu_B1 * sqrt(mu_S) / mu_nc^2)^2 *  var_nc +
                (sqrt(mu_S)/mu_nc)^2 * var_B1 +
                (mu_B1 / (2 * mu_nc * sqrt(mu_S)))^2 * var_S) ^ 0.5;

  real sd_a2 = ((- mu_B2 * sqrt(mu_S) / mu_np^2)^2 *  var_np +
                (sqrt(mu_S)/mu_np)^2 * (var_B2 + var_B1) +
                (mu_B2 / (2 * mu_np * sqrt(mu_S)))^2 * var_S) ^ 0.5;

  real mean_a1 = (1/mu_nc)*mu_B1*sqrt(mu_S);
```

```
  real mean_a2 = (1/mu_np)*mu_B2*sqrt(mu_S);

}

parameters {

  // hydraulic characteristics
  real<lower = nc_lwr, upper = nc_upr>nc;        // main channel's manning
  real<lower = np_lwr, upper = np_upr>np;        // flood plain's manning
  real<lower = S_lwr, upper = S_upr> S;          // slope of river bed (m/m)
  real<lower = B1_lwr, upper = B1_upr> B1;       // channel's width (m)
  real<lower = B2_lwr, upper = B2_upr> B2;       // flood plain's width (m)

  // rating curve - first control (main channel)
  real<lower = 0> a1;         // a coefficient of the rating curve
  real<upper = y_min> b1;     // b coefficient of the rating curve
  real<lower = 0> c1;         // c coefficient of the rating curve

  // rating curve - second control (flood plain)
  real<lower = 0> a2;         // a coefficient of the rating curve
  real<lower = b1> k2;        // elevation at the ativation of the second stage of the rating curve
  real<lower = 0> c2;         // c coefficient of the rating curve

  // model error
  real<lower=0, upper = 1> beta0;       // intercept of the error model
  real<lower=0, upper = 1> beta1;       // slope of the error model
}

transformed parameters{

    real b2 = k2;
}

model {
```

```
  vector[N] qfit;                    // estimated flow with the rating curve
  vector[N] sd_q = sigma_q * q;      // standard deviation of the measured flows due to measurement uncertainty
  real error;

  // prior distributions
  nc ~ normal(nc_mean, nc_sd);
  np ~ normal(np_mean, np_sd);

  a1 ~ normal(mean_a1, sd_a1);
  b1 ~ normal(mu_b1, sigma_b1);
  c1 ~ normal(mu_c1, sigma_c1);

  a2 ~ normal(mean_a2, sd_a2);
  k2 ~ normal(mu_k2, sigma_k2);
  c2 ~ normal(mu_c2, sigma_c2);

  beta0 ~ lognormal(1, 1);
  beta1 ~ lognormal(0.5, 1);

  for (i in 1:N) {
    if (y[i] > k2) {
      qfit[i] = a2 * (y[i] - k2)^c2 + a1 * (y[i] - b1)^c1;
    } else {
      qfit[i] = a1 * (y[i] - b1)^c1;
    }

    error = beta0 + beta1 * qfit[i];
    q[i] ~ normal(qfit[i], sqrt((error^2 + sd_q[i]^2)));
  }
}
```

*APPENDIX B – Rainfall-stage code*

```
functions {
  // Hydrological model - GR4H
  vector frun_gr4h(vector P, vector E, vector Param_hm){

  int N = rows(P);          // full time series length
  vector[N] S;              // production store
  vector[N] R;              // routing store
  vector[N] Pn;             // net precipitation
  vector[N] En;             // net evapotranspiration capacity
  vector[N] Ps;             // part of Pn that fills the production store
  vector[N] Es;             // part of En that will evaporate from the store
  vector[N] Perc;           // percolation leakage from the production store
  vector[N] Pr;             // water that reaches the routing functions
  vector[N] F;              // groundwater exchange term
  vector[N] Q9;             // flow component from UH1
  vector[N] Q1;             // flow component from UH2
  vector[N] Qr;             // flow component from UH1 after groundwater exchange
  vector[N] Qd;             // flow component from UH2 after groundwater exchange
  vector[N] qhm;            // simulated flow
  real x1 = Param_hm[1];
  real x2 = Param_hm[2];
  real x3 = Param_hm[3];
  real x4 = Param_hm[4];

  int n = 20;
  int m = 40;
  vector[n+1] SH1;          // S curve 1
  vector[m+1] SH2;          // S-curve 1
  vector[n] UH1;            // ordinates from unit hydrograph 1
  vector[m] UH2;            // ordinates from unit hydrograph 2

  if (x1 < 0.01) x1 = 0.01;
  if (x3 < 0.01) x3 = 0.01;
```

```
if (x4 < 0.5) x4 = 0.5;

// initial conditions
S[1] = 0.3 * x1;
R[1] = 0.5 * x3;

//Net Precipitation and Evaporation
vector[N] P_minus_E = P - E;
Pn = fmax(0, P_minus_E);
En = fmax(0, -P_minus_E);

//Production Store
for (t in 1:N) {
  if (t > 1) S[t] = S[t-1];
  Ps[t] = (x1 * (1 - (S[t] / x1)^2) * tanh(Pn[t] / x1)) /
          (1 + S[t] / x1 * tanh(Pn[t] / x1));
  Es[t] = (S[t] * (2 - S[t]/x1) * tanh(En[t] / x1)) /
          (1 + (1 - S[t]/x1) * tanh(En[t] / x1));
  S[t] += Ps[t] - Es[t];
  Perc[t] = S[t] * (1 - pow(1 + pow(4.0/21.0 * S[t] / x1, 4), -0.25));
  S[t] -= Perc[t];
  Pr[t] = Perc[t] + Pn[t] - Ps[t];
}

//UH Calculation
SH1[1] = 0;
SH2[1] = 0;
for (i in 1:(n+1)) SH1[i] = i < x4 ? pow(i / x4, 1.25) : 1;
for (i in 1:(m+1))
  SH2[i] = i < x4 ? 0.5 * pow(i / x4, 1.25)
         : i < 2 * x4 ? 1 - 0.5 * pow(2 - i / x4, 1.25)
         : 1;

UH1[1] = SH1[1];
```

```
for (i in 2:n) UH1[i] = SH1[i] - SH1[i-1];
UH2[1] = SH2[1];
for (i in 2:m) UH2[i] = SH2[i] - SH2[i-1];

//Convolution with UH
for (t in 1:N) {
  Q9[t] = 0;
  Q1[t] = 0;
  for (j in 1:min(n, t)) Q9[t] += 0.9 * Pr[t - j + 1] * UH1[j];
  for (j in 1:min(m, t)) Q1[t] += 0.1 * Pr[t - j + 1] * UH2[j];
}

// Routing
for (t in 1:N) {
  if (t > 1) R[t] = R[t-1];
  F[t] = x2 * pow(R[t]/x3, 3.5);
  R[t] = fmax(0, R[t] + Q9[t] + F[t]);
  Qr[t] = R[t] * (1 - pow(1 + pow(R[t]/x3, 4), -0.25));
  R[t] -= Qr[t];
  Qd[t] = fmax(0, Q1[t] + F[t]);
  qhm[t] = (Qr[t] + Qd[t])*(113./3.6); //revisar
}

return qhm;
}

//Rating curve
vector rating_curve(vector h, vector Param_rc){

int N = rows(h);            // full time series length
real a1 = Param_rc[1];
real b1 = Param_rc[2];
real c1 = Param_rc[3];
real a2 = Param_rc[4];
```

```
real b2 = Param_rc[5];
real c2 = Param_rc[6];
vector[N] qrc;

for (t in 1:N) {
  qrc[t] = h[t] < b2
  ? a1 * pow((h[t] - b1), c1)
  : a1 * pow((h[t] - b1), c1) + a2 * pow((h[t] - b2), c2);
}
    return qrc;
}

// Jacobian
real log_det_jacob(int N, vector h, vector Param) {
  real a1 = Param[1];
  real b1 = Param[2];
  real c1 = Param[3];
  real a2 = Param[4];
  real b2 = Param[5];
  real c2 = Param[6];
  real total = 0;
  for (t in 1:N) {
    real deriv = h[t] < b2
      ? a1 * c1 * pow(h[t] - b1, c1 - 1)
      : a1 * c1 * pow(h[t] - b1, c1 - 1) + a2 * c2 * pow(h[t] - b2, c2 - 1);
    total += log(abs(deriv));
  }
  return total;
}

// funcao auxiliar 1 - Calcula o log-determinante de uma matriz simétrica tridiagonal positiva definida
// via fatoração de Cholesky. A complexidade é O(N)
real log_det_cholesky_tridiagonal(vector diag_M, vector off_diag_M) {
    int N = rows(diag_M);
```

```
  vector[N] log_diag_L;
  if (diag_M[1] <= 0) {
    reject("A matriz M não é positiva definida. Elemento diagonal 1 é ", diag_M[1]);
  }
  log_diag_L[1] = 0.5 * log(diag_M[1]);
  real last_diag_L_sq = diag_M[1];
  for (i in 2:N) {
    real val = diag_M[i] - (off_diag_M[i-1]^2) / last_diag_L_sq;
    if (val <= 0) {
      reject("A matriz M não é positiva definida. Falha no passo ", i, " com valor ", val);
    }
    last_diag_L_sq = val;
    log_diag_L[i] = 0.5 * log(last_diag_L_sq);
  }
  return 2 * sum(log_diag_L);
}

// Funcaoo Auxiliar 2 - Soluciona um sistema linear tridiagonal simétrico M*x = b usando a fatoração de Cholesky (M=LLT).
// @return O vetor solução x.
vector solve_cholesky_tridiagonal_system(vector diag_M, vector off_diag_M, vector b) {
  int N = rows(diag_M);
  vector[N] x;
  vector[N] y;

  // Fator de Cholesky L (bidiagonal inferior)
  // diag_L: diagonal principal de L
  // off_diag_L: sub-diagonal de L
  vector[N] diag_L;
  vector[N-1] off_diag_L;

  // 1. Calcular o fator de Cholesky L
  if (diag_M[1] <= 0) reject("Matrix M is not positive-definite.");
  diag_L[1] = sqrt(diag_M[1]);
  for (i in 2:N) {
```

```
    off_diag_L[i-1] = off_diag_M[i-1] / diag_L[i-1];
    real diag_sq = diag_M[i] - off_diag_L[i-1]^2;
    if (diag_sq <= 0) reject("Matrix M is not positive-definite.");
    diag_L[i] = sqrt(diag_sq);
  }

  // 2. Resolver L*y = b (Forward substitution)
  y[1] = b[1] / diag_L[1];
  for (i in 2:N) {
    y[i] = (b[i] - off_diag_L[i-1] * y[i-1]) / diag_L[i];
  }

  // 3. Resolver LT*x = y (Backward substitution)
  x[N] = y[N] / diag_L[N];
  for (i in reverse(linspaced_int_array(N-1, 1, N-1))) {
    x[i] = (y[i] - off_diag_L[i] * x[i+1]) / diag_L[i];
  }

  return x;
}

//Função Principal Likelihood
real stan_loglikOU(vector qrc, vector qsim,
                   real lbd1, real lbd2,
                   real phi1, real phi2,
                   real gam1, real gam2) {
  int N = rows(qrc);
  if (rows(qsim) != N) {
    reject("qrc e qsim devem ter o mesmo comprimento");
  }

  vector[N] dvec;
  for (i in 1:N) {
    dvec[i] = qsim[i];
```

```
}

real rho = exp(-1.0 / phi2);
real sigma2 = phi1^2;
if (rho >= 1.0 || rho <= -1.0) reject("Parâmetro rho fora do intervalo (-1, 1): ", rho);

vector[N-1] off_Q;
vector[N] main_Q;
real inv_1_minus_rho2_div_sigma2 = 1.0 / ((1.0 - rho^2) * sigma2);
off_Q = rep_vector(-rho * inv_1_minus_rho2_div_sigma2, N - 1);
main_Q = rep_vector((1.0 + rho^2) * inv_1_minus_rho2_div_sigma2, N);
main_Q[1] = inv_1_minus_rho2_div_sigma2;
main_Q[N] = inv_1_minus_rho2_div_sigma2;

vector[N] Rdiag = (gam1 + gam2 * qsim) .* (gam1 + gam2 * qsim);

real log_det_Sigma;
real quad_form;
vector[N] v = qrc - qsim;

if (sum(Rdiag) < 1e-12) {
  // Caso especial (sem alteração)
  real log_det_S = N * log(sigma2) + (N - 1) * log(1 - rho^2);
  log_det_Sigma = log_det_S + 2 * sum(log(dvec));
  vector[N] u = v ./ dvec;
  quad_form = main_Q[1] * u[1]^2;
  for (i in 2:N) {
    quad_form += main_Q[i] * u[i]^2 + 2 * off_Q[i-1] * u[i] * u[i-1];
  }
} else {
  // Caso geral
  vector[N] Rinv_diag;
  for(i in 1:N) { Rinv_diag[i] = 1.0 / (Rdiag[i] + 1e-12); }
```

```
        real log_det_R = sum(log(Rdiag));
        real log_det_S = N * log(sigma2) + (N - 1) * log(1 - rho^2);

        vector[N] main_M = main_Q + (dvec .* dvec .* Rinv_diag);

        real log_det_M = log_det_cholesky_tridiagonal(main_M, off_Q);
        log_det_Sigma = log_det_R + log_det_S + log_det_M;

        vector[N] Rinv_v = Rinv_diag .* v;
        vector[N] DRinv_v = dvec .* Rinv_v;

        vector[N] z = solve_cholesky_tridiagonal_system(main_M, off_Q, DRinv_v);

        quad_form = dot_product(Rinv_v, v) - dot_product(DRinv_v, z);
      }

      return -0.5 * (N * log(2 * pi()) + log_det_Sigma + quad_form); // revisar
    }
}


data {
  // Hydrological model
  int<lower=0> N;            // length of data
  int<lower=0> N_run;        // number of elements in PeriodRun
  vector[N] P;               // measured precipitation
  vector[N] E;               // potential evaporation
  vector[N] h;               // measured water level
  array[N_run] int<lower=1, upper=N> PeriodRun;  // indices to use
  real lbd1;
  real lbd2;
}

transformed data {
```

```
  real h_min = min(h);
}

parameters {
  // Hydrological model
  real <lower=1, upper=2000> x1;
  real <lower=-1, upper=0.3> x2;
  real <lower=0, upper=500> x3;
  real <lower=0, upper=10> x4;

  real<lower=0, upper = 0.15> sigma_ar;
  real<lower=0, upper = 200> phi_ar;

  // Rating curve
  real<lower=3.03178, upper= 3.88526> a1;
  real<lower=0.80562, upper= 0.85415> b1;
  real<lower=1.61634, upper= 1.71563> c1;
  real<lower=1.64763, upper= 12.28405> a2;
  real<lower=2.60955, upper= 3.19340> b2;
  real<lower=1.61550, upper= 1.71758> c2;
  real<lower=0.00524, upper= 0.05118> beta0;
  real<lower=0.14536, upper= 0.26119> beta1;

}

model {
  // priors
  x1 ~ lognormal(3.80045122977104, 1.93900572947502);
  x3 ~ lognormal(0.80471895621705, 2.76014752153324);
  x4 ~ lognormal (-1.15129254649702, 1.7621824691281);

  phi_ar ~ lognormal(3.91202300542815, 1);
```

```
  a1 ~ normal(3.45852, 0.21337);
  b1 ~ normal(0.82988, 0.01213) T[ , h_min];
  c1 ~ normal(1.66599, 0.02482);
  a2 ~ normal(6.96584, 2.65910);
  b2 ~ normal(2.90147, 0.14596) T[b1, ];
  c2 ~ normal(1.66654, 0.02552);
  beta0 ~ normal(0.02821, 0.01148);
  beta1 ~ normal(0.20327, 0.02896);

  vector[N] qhm_full = frun_gr4h(P, E, to_vector({x1, x2, x3, x4}));
  vector[N] qrc_full = rating_curve(h, to_vector({a1, b1, c1, a2, b2, c2}));

  vector[N_run] qhm_run = qhm_full[PeriodRun];
  vector[N_run] qrc_run = qrc_full[PeriodRun];
  vector[N_run] h_run = h[PeriodRun];

  // likelihood
  target += stan_loglikOU(qrc_run, qhm_run, lbd1, lbd2, sigma_ar, phi_ar, beta0, beta1)
          + log_det_jacob(N_run, h_run, to_vector({a1, b1, c1, a2, b2, c2}));
}
```